

**WL-TR-96-4082**



**PROCESSING OF  
INTERCONNECTED GLASS AND  
CERAMIC COMPOSITES FOR  
ELECTRONIC PACKAGING**

**PRASHANT N. KUMTA**  
Department of Materials Science and Engineering  
Carnegie Mellon University  
Pittsburgh PA 15213

DECLASSIFIED

**JULY 9, 1996**

**FINAL REPORT FOR JULY 27, 1994 - APRIL 26, 1996**

**19960813 001**

**Approved for public release; distribution unlimited**


**MATERIALS DIRECTORATE  
WRIGHT LABORATORY  
AIR FORCE MATERIEL COMMAND  
WRIGHT-PATTERSON AIR FORCE BASE, OH 45433-7734**

## NOTICE

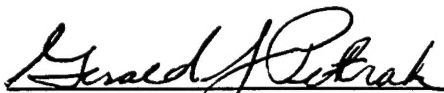
WHEN GOVERNMENT DRAWINGS, SPECIFICATIONS, OR OTHER DATA ARE USED FOR ANY PURPOSE OTHER THAN IN CONNECTION WITH A DEFINITELY GOVERNMENT-RELATED PROCUREMENT, THE UNITED STATES GOVERNMENT INCURS NO RESPONSIBILITY OR ANY OBLIGATION WHATSOEVER. THE FACT THAT THE GOVERNMENT MAY HAVE FORMULATED OR IN ANY WAY SUPPLIED THE SAID DRAWINGS, SPECIFICATIONS, OR OTHER DATA, IS NOT TO BE REGARDED BY IMPLICATION OR OTHERWISE IN ANY MANNER CONSTRUED, AS LICENSING THE HOLDER OR ANY OTHER PERSON OR CORPORATION, OR AS CONVEYING ANY RIGHTS OR PERMISSION TO MANUFACTURE, USE, OR SELL ANY PATENTED INVENTION THAT MAY IN ANY WAY BE RELATED THERETO.

THIS REPORT IS RELEASABLE TO THE NATIONAL TECHNICAL INFORMATION SERVICE (NTIS). AT NTIS, IT WILL BE AVAILABLE TO THE GENERAL PUBLIC, INCLUDING FOREIGN NATIONS.

THIS TECHNICAL REPORT HAS BEEN REVIEWED AND IS APPROVED FOR PUBLICATION.



PAUL D. JERO, Project Engineer  
Materials Development Branch  
Metals and Ceramics Division



GERALD J. PETRAK, Actg Chief  
Materials Development Branch  
Metals and Ceramics Division



WALTER M. GRIFFITH, Asst Chief  
Metals and Ceramics Division  
Materials Directorate

IF YOUR ADDRESS HAS CHANGED, IF YOU WISH TO BE REMOVED FROM OUR MAILING LIST, OR IF THE ADDRESSEE IS NO LONGER EMPLOYED BY YOUR ORGANIZATION, PLEASE NOTIFY, WL/MLLM, WRIGHT-PATTERSON AFB OH 45433-7817 TO HELP US MAINTAIN A CURRENT MAILING LIST.

COPIES OF THIS REPORT SHOULD NOT BE RETURNED UNLESS RETURN IS REQUIRED BY SECURITY CONSIDERATIONS, CONTRACTUAL OBLIGATIONS, OR NOTICE ON A SPECIFIC DOCUMENT.

# REPORT DOCUMENTATION PAGE

Form Approved  
OMB No. 0704-0188

Public reporting burden for this collection of information is estimated to average 1 hour per response, including the time for reviewing instructions, searching existing data sources, gathering and maintaining the data needed, and completing and reviewing the collection of information. Send comments regarding this burden estimate or any other aspect of this collection of information, including suggestions for reducing this burden, to Washington Headquarters Services, Directorate for Information Operations and Reports, 1215 Jefferson Davis Highway, Suite 1204, Arlington, VA 22202-4302, and to the Office of Management and Budget, Paperwork Reduction Project (0704-0188), Washington, DC 20503.

1. AGENCY USE ONLY (Leave blank)		2. REPORT DATE 07/09/96	3. REPORT TYPE AND DATES COVERED Final 07/27/94 - 04/26/96	
4. TITLE AND SUBTITLE Processing of Interconnected Glass and Ceramic Composites for Electronic Packaging			5. FUNDING NUMBERS C: F33615-94-5217 PE: 6201F PR: 2420 TA: 51 WU: S3	
6. AUTHOR(S) Prashant N. Kumta				
7. PERFORMING ORGANIZATION NAME(S) AND ADDRESS(ES) Carnegie Mellon 5000 Forbes Avenue Pittsburgh, PA 15213			8. PERFORMING ORGANIZATION REPORT NUMBER 1-52203	
9. SPONSORING/MONITORING AGENCY NAME(S) AND ADDRESS(ES) Materials Directorate Wright Laboratory Air Force Materiel Command WPAFB OH 45433-7734 POC: Paul D. Jero, WL/MLLM, 513-255-9818			10. SPONSORING/MONITORING AGENCY REPORT NUMBER WL-TR-96-4082	
11. SUPPLEMENTARY NOTES				
12a. DISTRIBUTION/AVAILABILITY STATEMENT Approved for public release; Distribution unlimited			12b. DISTRIBUTION CODE	
13. ABSTRACT (Maximum 200 words)  Glasses and glass-ceramics are well known for their low dielectric constant ( $\epsilon \approx 3-5$ ) at 1MHz which make them useful substrate materials for high speed electronic packaging. On the other hand, crystalline ceramics such as AlN have moderate dielectric constants ( $\epsilon \approx 9-12$ ) at 1MHz and high thermal conductivity useful for high power packages. Porous and glass infiltrated ceramic composites with interconnected high thermal conductivity phases therefore, have the potential of possessing optimum dielectric constant ( $\approx 5$ ) and thermal conductivity ( $\approx 20-60$ W/m-K) for substrate applications. This report discusses the results of the work conducted in processing interconnected porous composites of AlN, and also low dielectric constant glasses and glass-ceramics in the $B_2O_3-P_2O_5-SiO_2$ system. A systematic investigation has been conducted to study the effect of pre-treatment of AlN powders in ammonia on their sinterability. At the same time, the combined effects of this pretreatment and the influence of volume fraction on thermal conductivity has been studied. Similarly, studies have been conducted to understand the structure of the oxide glasses, their sinterability, and the effect of nitrogen substitution on their dielectric constant.				
14. SUBJECT TERMS Glass and Ceramic Composites, Processing			15. NUMBER OF PAGES 92	
			16. PRICE CODE	
17. SECURITY CLASSIFICATION OF REPORT Unclassified	18. SECURITY CLASSIFICATION OF THIS PAGE Unclassified	19. SECURITY CLASSIFICATION OF ABSTRACT Unclassified	20. LIMITATION OF ABSTRACT SAR	

	<b>TABLE OF CONTENTS</b>	<b>PAGE</b>
Abstract		1
1. Introduction		2
2. Concept and Methodology		3
3. Research Objectives		12
<b>Part I</b>		
I-1. Experimental Procedure		13
I-2. Results and Discussion		18
I-3. Conclusions		28
I-4. Future Work		29
4. References		33
<b>Appendix</b>		
<b>Part II</b>		
A. Development of Glasses and Glass-Ceramics in the $B_2O_3$ - $P_2O_5$ - $SiO_2$ System		34
II-1. Experimental Procedure		34
II-2. Results and Discussion		41
II-3. Conclusions		64
II-4. References		66



<b>B .</b>	<b>Effect of Incorporation of Nitrogen on the Structure and Dielectric Properties of MOSP Derived Borosilicate Glasses and Glass-Ceramics</b>	<b>67</b>
III-1.	Experimental Procedure	67
III-2.	Results and Discussion	71
III-3.	Conclusions	89
III-4.	References	92

## PROCESSING AND CHARACTERIZATION OF INTERCONNECTED GLASS AND CERAMIC COMPOSITES FOR ELECTRONIC PACKAGING

### Abstract

Glasses and glass-ceramics are well known for their low dielectric constants ( $\epsilon \approx 3-5$ ) at 1MHz which make them useful candidate materials as substrates for high speed electronic packaging. On the other hand crystalline non-oxide ceramics such as AlN and SiC have moderate dielectric constants ( $\epsilon \approx 9-12$ ) at 1MHz but display excellent thermal conductivity values useful for high power packages. Porous and glass infiltrated ceramic composites with interconnected high thermal conductivity phases therefore, have the potential of possessing optimum dielectric ( $\approx 5$ ) and thermal conductivities ( $\approx 20-60$  W/m-K) which could make them useful as substrates for electronic packaging. Experiments were conducted at Wright Patterson during the summer of 1993 to assess the feasibility of fabrication of such composites. Preliminary densification studies conducted on AlN powders showed the formation of porous ceramics ( $\approx 28\%$  porosity) with contiguous pores. These composites therefore appear to be very promising for substrate applications.

The present report describes the results of the work conducted on the development of glasses, glass-ceramics, and 3-D interconnected porous composites. The work during the last year and a half has focused in two directions. One, to process 3-D interconnected porous composites of AlN and evaluate these composites for their thermal conductivity. Second, to develop new and inexpensive sol-gel processes to synthesize glasses and glass-ceramics in the  $B_2O_3$ - $P_2O_5$ - $SiO_2$  system that display dielectric constant of 3.9-4.5 @ 1MHz and at room temperature. A systematic investigation has been conducted to understand the structure of these glasses, their sinterability, and the effect of nitrogen substitution on the dielectric constant of these glasses. Similarly, detailed analyses have been conducted to study the effect of pre-treatment of the AlN powders in ammonia on their sinterability. At the same time, the combined effects of this pretreatment and the influence of volume fraction on thermal conductivity has been studied. The results of these studies have been discussed in the report keeping in mind the potential application of these composites as substrates for electronic packaging.

## 1. Introduction

Integrated circuit technology has advanced considerably in recent years. As a result, there has been significant improvements made in fabrication of devices. Consequently, there is an increasing demand towards processing and integration of high power devices on a single silicon chip. The main objective of such advances is the miniaturization of devices with corresponding increase in the device density. The devices need to generate high power and also operate at high switching speed. This has placed stringent requirements on the substrate technology. Substrates therefore need to be fabricated and designed so that heat removal and signal propagation are both achieved in an efficient manner. The high density of devices leads to generation of considerable amount of heat that has to be dissipated without causing degradation of the device. At the same time, the switching speed of the circuits has to be optimum so that signals can be propagated with minimum delay. The main heat dissipation mechanism is by thermal conduction, while signal propagation is based on the velocity of the electric signal given by

$$v = \sqrt{\frac{1}{\mu\epsilon}}$$

where ' $\mu$ ' is the relative magnetic permeability and ' $\epsilon$ ' is the relative dielectric permittivity of the material. The substrate materials therefore need to possess excellent thermal conductivity and minimum dielectric constant. The choice of materials satisfying these criteria is mainly restricted to ceramics and polymers. The role of ceramic materials as substrates in several packages such as dual-in-line packages, chip carriers, and pin grid arrays is well known and ceramic packaging is becoming one of the most actively pursued areas of research [1-6].

### 1.1 Ceramics, Glasses and Glass-Ceramics: - Candidate Substrate Materials

Ceramics have dielectric constants ranging from 4 to 10,000, thermal expansion coefficients matching silicon ( $30 \times 10^{-7} / ^\circ\text{C}$ ), and display a range of thermal conductivity making them one of the best insulators and heat conductors. They even exhibit better heat conduction than aluminum metal. They are also highly refractory with excellent temperature stability making them good materials for hermetic applications. The main drawback of ceramic materials with respect to packaging is their moderate to high dielectric constant and the high processing temperatures. Research in the development of materials for packaging application has been focused at achieving objectives which include lower dielectric constant, lower processing temperatures, thermal expansion match to silicon, improved thermal conductivity, improved techniques of power dissipation, multilayer processing and high mechanical strength. The materials that have been identified for these purposes have been AlN, BeO, SiC, cubic BN and diamond among the ceramic materials, while glasses and

glass-ceramics have also been investigated for packaging applications because of their low dielectric constant[7-16]. Table 1 lists the crystalline ceramic materials of interest for electronic packaging. Heat dissipation in devices implementing crystalline ceramics is mainly from the bottom of the device through the substrate itself as shown in Figure 1.

### 1.2 Glass-Ceramics

Glass-ceramics with their dielectric constant around 5 and their excellent thermal expansion match with silicon coupled with the ability to co-sinter with copper, or gold make them potentially one of the best candidate materials for high-performance multilayer ceramic substrates[17]. In addition, thin film metallization and dielectric material could be easily deposited onto the surface of these substrates, therefore making them amenable for high performance application. The major disadvantage of glass-ceramics are their low thermal conductivity which make them poor materials for heat dissipation in packaging application where the chip is bonded face-in in the cavity up configuration. However, in the case of the application where the heat dissipation occurs from the back of the chip, this limitation is largely overcome by external vias and water cooling mechanism as in the thermal conduction module of IBM[18] (Figure 2).

Much of the heat is removed from the back of the silicon chip (flip-chip) by implementing expensive external cooling modes rather than the substrate itself and hence glass-ceramics with their lower dielectric constants serve as better materials than the other covalently bonded ceramics. Their lower dielectric constants has attracted considerable research in this class of materials. Table 2 lists several low dielectric constant glass, glass-ceramic, and several glasses added to various low dielectric constant ceramics. From the above it can be seen that there are basically two different types of packaging technologies to cope with the substrate material limitations. One geared towards high power devices employing by and large crystalline ceramics and the other directed towards high speed devices utilizing glass-ceramics. Considerable expenses are therefore incurred for implementing different package designs and fabrication technologies to maintain high quality performance. The need for these two technologies could be obviated by processing a composite with suitable thermal and dielectric properties[18].

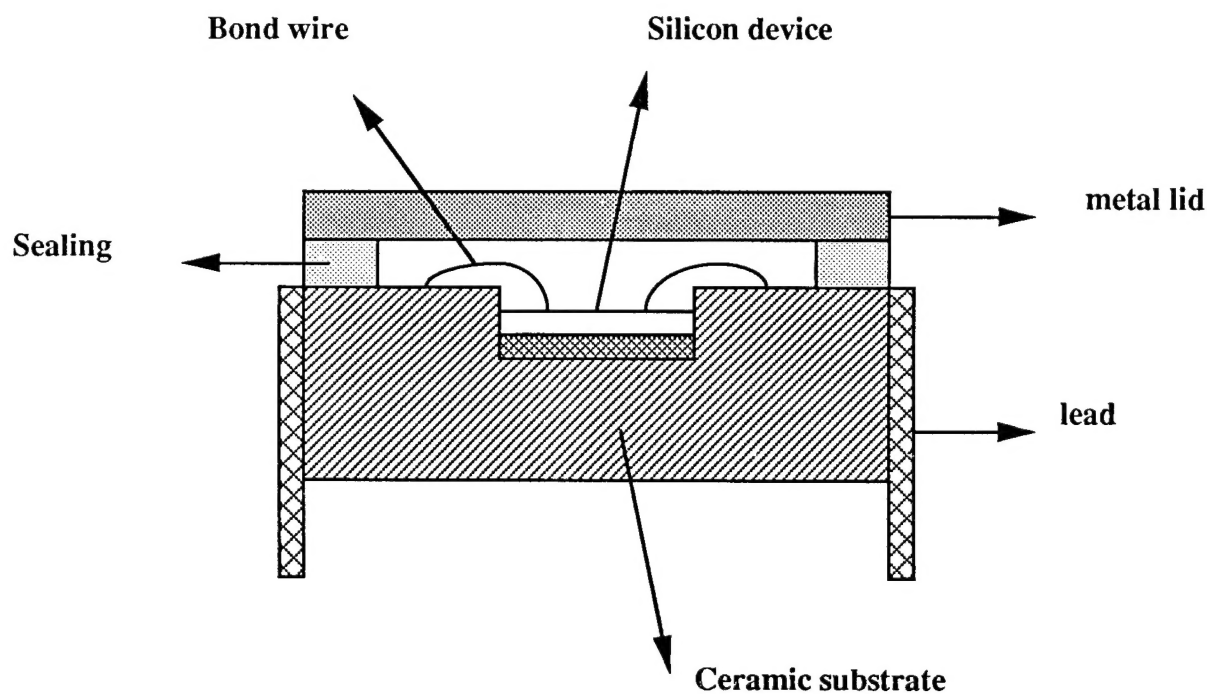
## **2. Concept and Methodology**

### 2.1 Concept idea

The success of such a composite possessing the desired optimum thermal and dielectric properties will depend upon the selection of the individual phases and a suitable microstructural design to obtain an interconnected microstructure. This is because as will be explained in the later section, thermal conductivity and dielectric constant in a particular direction are influenced more by connected rather than dispersed phases. Thus, the potential success of a composite as a substrate

Table 1. Properties of Selected Ceramic Substrate Materials.

Substrate Properties	AlN	SiC	BeO	Glass-Ceramics	90% Alumina	cubic BN	Diamond
Thermal Conductivity (W/m-K)	230	270	290	5	25	250	2000
Coefficient of Thermal expansion (20-200 C) ( $\times 10^{-7}/^{\circ}\text{C}$ )	43	37	68	30-42	67	48	35
Dielectric Constant at 1 MHz	8.9	42	6.8	5.0	9.4	7.1	5.6
Flexural Strength (MPa)	350	420	250	210	280	-	-



**Ceramic - Package Outline**

Figure 1. Schematic illustration showing the package structural elements. The ceramic package has the device bonded to the ceramic substrate through which most of the heat generated by the device is dissipated. The thermal conductivity of the substrate is extremely important for these packages. See text for further details.

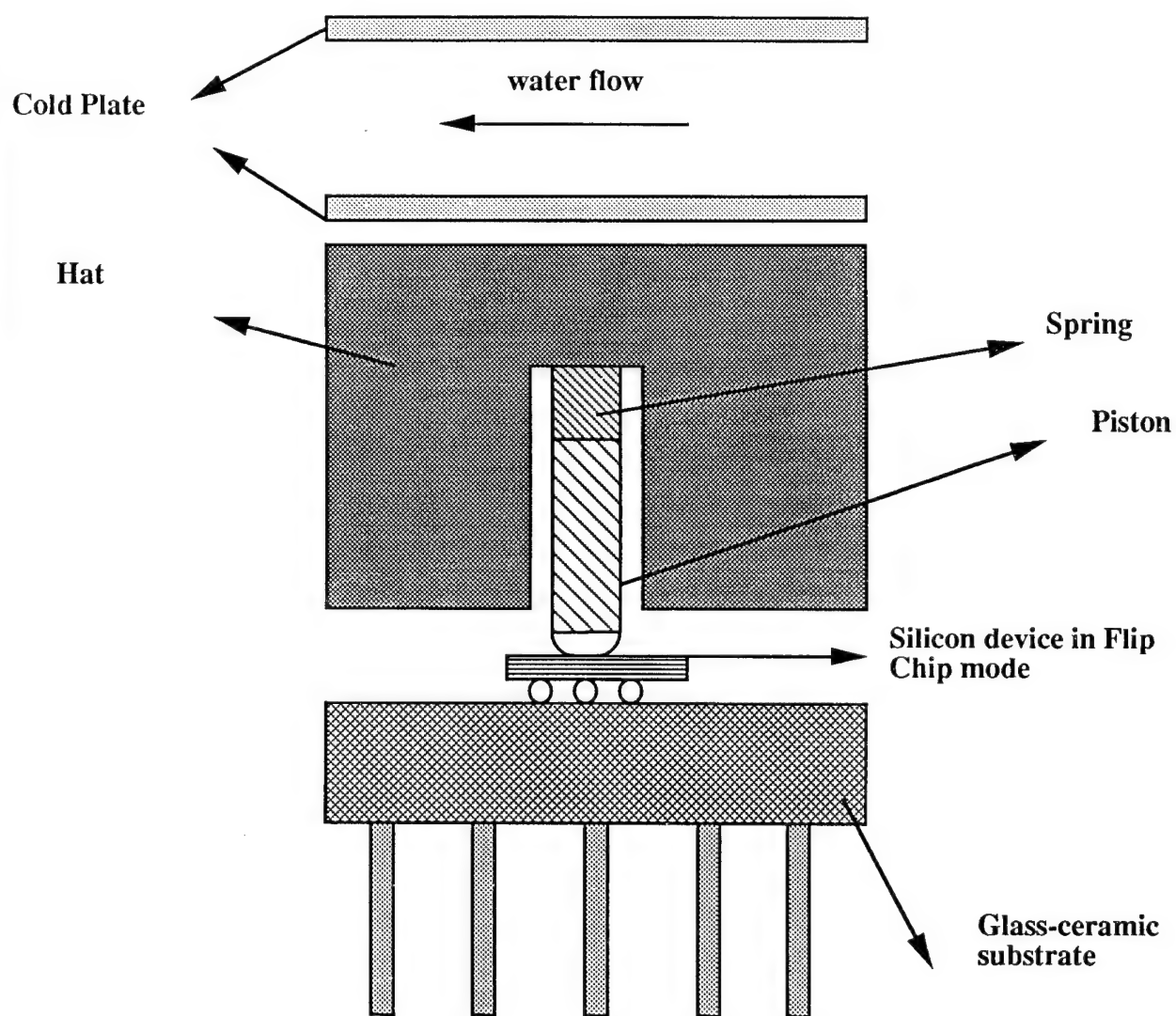


Figure 2. Cross section of the multilayer ceramic package developed by IBM. A schematic of the cooling path and the components that contribute to the thermal resistance of the module is shown. As can be seen the chip is mounted face down on the substrate and much of the heat is removed from the back of the chip through the piston and the water cooled plates attached to the hat connecting to the piston. See text for more details.

Table 2. Properties of Glasses, Glass + Ceramics, and Glass-Ceramics.

Materials	Dielectric Constant	Coefficient of Thermal Expansion $10^{-7}/^{\circ}\text{C}$
<b>Glasses</b>		
$\text{B}_2\text{O}_3\text{-SiO}_2\text{-Al}_2\text{O}_3\text{-Na}_2\text{O}$	4.1	32
<b>Glass + Ceramics</b>		
$\text{PbO} + \text{B}_2\text{O}_3 + \text{SiO}_2 + (\text{Al}_2\text{O}_3)$	7.5	42
$\text{MgO} + \text{Al}_2\text{O}_3 + \text{SiO}_2 + \text{B}_2\text{O}_3 + \text{Al}_2\text{O}_3$	4.5	30
$\text{B}_2\text{O}_3 + \text{SiO}_2 + (\text{Al}_2\text{O}_3)$	5.6	45
$2\text{MgO} \cdot 2\text{Al}_2\text{O}_3 \cdot 5\text{SiO}_2 + (\text{Al}_2\text{O}_3)$	5.5	30
$\text{CaO} + \text{Al}_2\text{O}_3 + \text{SiO}_2 + \text{B}_2\text{O}_3 + (\text{Al}_2\text{O}_3)$	7.7	55
$\text{Li}_2\text{O} + \text{SiO}_2 + \text{MgO} + \text{Al}_2\text{O}_3 + \text{SiO}_2 + (\text{Al}_2\text{O}_3)$	7.3	59
$\text{Li}_2\text{O} + \text{Al}_2\text{O}_3 + \text{SiO}_2 + (\text{Al}_2\text{O}_3)$	7.8	30
<b>Glass-Ceramics</b>		
$\text{MgO-Al}_2\text{O}_3\text{-SiO}_2\text{-B}_2\text{O}_3\text{-P}_2\text{O}_5$	5.0	30
$\text{Li}_2\text{O-Al}_2\text{O}_3\text{-SiO}_2\text{-B}_2\text{O}_3$	6.5	25

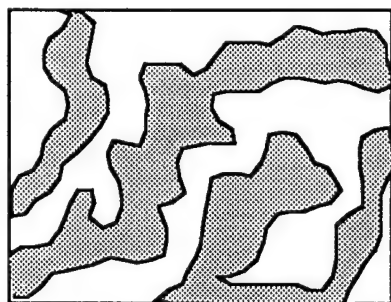


material possessing optimum dielectric and thermal conductivity is very largely dependent on the attainment of an interconnected microstructure. In this context, ceramic fibers are very attractive since their geometry can be adjusted to achieve the desired interconnectivity in the composite, while glass with its low dielectric constant serves as an excellent second phase material. The thermal conductivity of the commercially available fibers however, are too low in the range of 12 W/m-K. Thus, only moderate improvements in thermal conductivity could be visualized in the case of glass and fiber composites. On the other hand, the formation of a porous high thermal conductivity ceramic with contiguous pores is an attractive concept for a composite for substrate applications. The presence of contiguous pores results in an interconnected microstructure of the high thermal conductivity crystalline material forming one phase and the pores forming the second phase. The interconnectivity of the pores and the thermally conducting solid phase would lead to composites with optimum dielectric and thermal conductivity. The presence of pores would be undesirable from the point of view of hermeticity of the package. However, this could be easily prevented by partial infiltration of glass into the pores, thus preventing moisture from entering the pores. Figure 3 shows a schematic of the proposed composite and hermetic seal concept.

This rationale formed the basis for the preliminary experiments performed at the Wright Patterson Air Force Base which have been published elsewhere[19,20]. The present work is an extension of this idea and is aimed at developing low dielectric constant glasses and glass-ceramics as well as processing 3-D interconnected porous ceramic composites. The work is also focused on identifying new economical approaches for synthesizing the glasses and relating their structure to the electrical properties. Similarly, the goal of the work is also to study the effect of processing conditions on the microstructure and thermal properties of the composite.

## 2.2 Materials Selection

The formation of the composite is contingent on the selection of matrix phase and the addition of second phase material to form the continuous interconnected phases. The choice of selection is very strongly dependent on the dielectric and thermal conductivity values of the materials. It is therefore desirable to select two materials, one with the lowest dielectric constant and the other having a high thermal conductivity. Thus, in this context porous ceramic composites are very appealing since the pores would be essentially filled with air of dielectric constant ( $\epsilon = 1$ ). From the list provided in Table 1, the choice of electrically insulating materials exhibiting high thermal conductivity are limited to AlN, SiC, BeO and diamond. AlN is an extremely good choice over beryllia for high performance packages. Diamond on the other hand is an excellent material but the difficulty in synthesizing fine particles and obtaining a continuous phase limits its choice. Silicon carbide as seen from Table 1 has a thermal conductivity of 270 W/m-K, but much higher dielectric



Filled region corresponds to the pores and the infilled region corresponds to the high thermal conductivity phase

Figure 3. Concept idea of interconnected pores and continuous solid phase of high thermal conductivity material. Such composites exhibit the potential for displaying optimum thermal conductivity and dielectric constant.

constant in comparison to the others. Aluminum nitride is therefore an ideal candidate and is the material selected for the present studies.

There are also a number of glasses and glass-ceramic materials as indicated above which have low dielectric values as choice materials for encapsulation of the pores. Among the materials cordierite, borosilicate glasses and glass-ceramics of these two systems have received the most attention for high speed packaging. Other glasses such as the borophosphosilicate have also been developed by MacDowell and Beall [21,22] which show potentially lower dielectric constants (3.8-4.5) and loss tangents which are below  $10^{-3}$  above 1 kHz and up to 200°C. Borosilicate glasses have been well studied and considerable information is available in the literature in regard to the processing, electrical and thermal properties. Thus, these two glass systems have been selected for the present studies.

### 2.3 Theoretical and Empirical Models

As discussed above, the main goal of the study was to fabricate composites with optimum thermal conductivity and dielectric constant for applications as substrates in electronic packaging. The properties of such a composite can be predicted to some extent based on certain mathematical models. There are several models that exist, the one that is most well known is the volume fraction model[23-25]. There are four basic rules which are well known, a)Series, (b)Parallel, (c) Lichtenecker's Logarithmic, and Maxwell's Mixing rules. The series and parallel rules apply for a composite that has alternating layers of materials with different material constants, the implementation of the exact form would however depend upon the direction of application of the electric field. Figure 4 shows a schematic geometric arrangement of the composites. The logarithmic rule and Maxwell's rules are known to give better values for systems in which neither parallel nor series mixing is strongly preferred. Similar rules seem to work for both thermal conductivity and dielectric constant. This is because the dielectric constant for a capacitor is analogous to thermal conductivity in heat conduction. The logarithmic and Maxwell's rules give values intermediate between those for the series and parallel configurations. The logarithmic rule is given by:

$$\ln \epsilon_m = \sum_i^n V_{fi} \ln \epsilon_i$$

where ' $\epsilon_m$ ' is the effective dielectric constant, ' $V_{fi}$ ' is the volume fraction of the individual phases and ' $\epsilon_i$ ' is the dielectric constant of the individual distinct phases. The Maxwell's rule is given by:

$$\epsilon_m = \epsilon_2 \left\{ 1 + \frac{3V_f(\epsilon_1 - \epsilon_2)}{\epsilon_1 + 2\epsilon_2 - V_f(\epsilon_1 - \epsilon_2)} \right\}$$

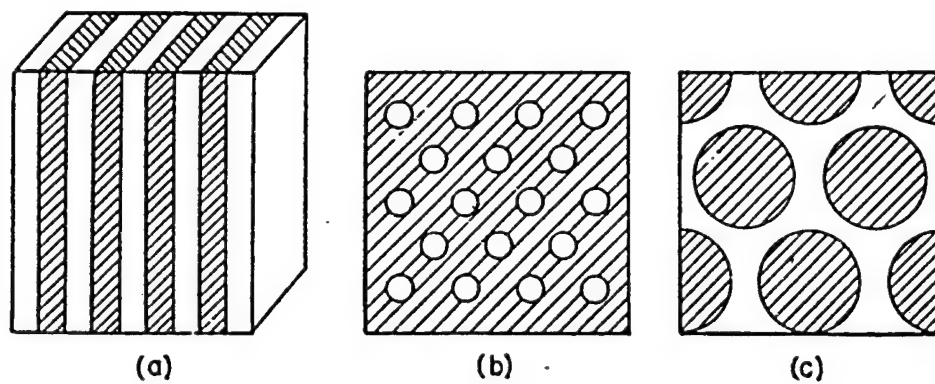


Figure 4. Schematic idealized arrangements of phases for application of the mixing rules. (a) Parallel; (b) Continuous major phase; (c) Continuous minor phase.

where ' $V_f$ ' is the volume fraction occupied by the dispersed particles and ' $\epsilon_1$ ' and ' $\epsilon_2$ ' are the dielectric constants of the two different materials. Based on these empirical rules, it can be seen that a certain volume fraction of two different phases could result in an optimum thermal conductivity and dielectric constant. However, what is important for thermal conductivity is the interconnectivity which the models do not take into account. Thermal conductivity and dielectric constants in a particular direction are influenced more by connected rather than dispersed phases and the effective values of each property are more realistically predicted by the percolation theory and the effective medium theory[26].

In regard towards connectivity, therefore, the use of thermally conducting aluminum nitride as a composite material is very attractive if it is possible to deliberately introduce a continuous porous phase. Thus, this would essentially involve fabrication of a two phase material, the first phase constituting interconnected pores while the second phase is comprised of the thermally conducting aluminum nitride. Ceramists have always been interested in densification of powders to obtain materials with densities close to the theoretical values. It is known that to achieve densities close to theoretical values, normally both vapor transport and surface diffusion are undesirable as they lead to necking and particle coarsening with no apparent contribution to densification. In fact, Kuczynski and Kingery [27] have examined vapor transport as a mechanism which contributes to neck growth in the initial stages of sintering without leading to any substantial shrinkage. These ideas have been demonstrated in sphere-to-sphere experiments on NaCl and ZnO indicating the effects of vapor transport on particle coarsening with lack of densification.

Initial experiments on sintering of aluminum nitride conducted by Prochazka et al.[28] have also indicated that during heat treatment of the green bodies of these covalent ceramics there is essentially coarsening in absence of densification. This suggests that the geometry of the interconnected structure remains unchanged while the scale of the grains increases with temperature. They also performed surface area measurements which indicate an effective surface to surface transport process operating at relatively low temperatures. Their preliminary studies clearly indicate that during sintering of these covalent ceramics, vapor transport is significantly more rapid than boundary diffusion resulting in neck growth producing porous elongated microstructures. This dominance of vapor transport over boundary diffusion could be exploited to generate porous AlN ceramics. Preliminary experiments conducted at Wright-Patterson clearly demonstrated this concept. The results of this work have already been published[19,20].

### 3. Research Objectives

The objectives of the present work conducted in this report follow from the preliminary results discussed above. Accordingly, the research plan has comprised of two parts. The first part is

focused on the processing porous AlN composites and evaluating its thermal conductivity and the second part is aimed at development of low dielectric constant glasses and glass-ceramics. The objectives of the work for the two parts are given below:

**Part I:**

1. To process porous AlN composites and evaluate their thermal conductivity.
2. To systematically investigate the effect of pretreatment on the microstructure and thermal conductivity of the composite.
3. To systematically evaluate the effect of sintering time and temperature on the microstructure and its impact on the thermal conductivity of these composites.

**Part II:**

1. To develop economical sol-gel processes to synthesize glass-ceramics in the borophosphosilicate system.
2. To study the structure of these glasses, assess their sinterability and investigate their dielectric properties.
3. To study the influence of nitrogen on the structure and dielectric properties of the borosilicate glasses.

Part II did not really constitute a major portion of the tasks to be conducted in the present work but the results are certainly relevant to the present study. Hence, the results of Part II are included as an appendix in this report.

**Part I**

In this section results of the studies conducted on the development of porous 3-D interconnected AlN composites are described. Commercial AlN powders were obtained from Dow chemicals. These powders were then subjected to different pre-treatments, sintering temperature and sintering hold time in order to observe the effects of volume fraction, and surface oxygen contents on the thermal conductivity. The results of these studies are described and discussed in the following section.

**Processing of Porous Aluminum Nitride Composites for Electronic Packaging**

**I-1. Experimental Procedure**

***I-1.1. Processing of Porous AlN composites***

Preliminary experiments conducted at Wright Patterson had demonstrated the concept of formation of a 3-D interconnected porous AlN composite[19]. However, the thermal conductivity of the composite is a very strong function of the purity of the AlN powder itself. One could process the high purity powders or obtain them commercially. The latter option was chosen due to the preliminary nature of the work. Accordingly, powders were obtained from Dow Chemicals.

The specific surface area of the powder is  $2.81 \text{ m}^2/\text{g}$ . The impurity level of the powder is listed in Table I-1. This powder contains 0.86 wt% oxygen and 0.04 wt% carbon. The level of metal impurity is less than 100 ppm. The procedure consisted of fabrication of compacts of the powder which were then sintered. The compaction pressure, volume fraction of AlN and the sintering time were parameters that were varied in the study. Similarly, attempts were made to purify the material further and remove the surface oxide that formed on the AlN particles. The presence of this surface oxide layer plays a very detrimental role on the thermal conductivity. Figure I-1 shows the flow chart indicating the procedure followed to fabricate the porous AlN composites.

The as-received powders were mixed with acetone and cold pressed to form pellets ( $\approx 0.5''$  thick and  $0.5''$  in diameter) by application of  $\approx 1000$  psi pressure. The cold-pressed pellets were dried in vacuum overnight and then isostatically cold-pressed employing a pressure of either 10,000 or 35,000 psi to change the initial volume fraction. The pellets were then pre-treated in  $\text{NH}_3$  at  $1350^\circ\text{C}$  for 48 hours to remove the surface oxygen layer and initiate necking of the oxide-free particles. Argon heat treatments were also attempted at  $1350^\circ\text{C}$  for 48 hours to analyze the effect of ammonia pre-treatment on the thermal conductivity of the resultant partially sintered porous AlN composite. These treatments were conducted in order to obtain a comparison of the presence of surface oxide on the thermal conductivity. The pellets that were pre-treated in either  $\text{NH}_3$  or Ar were then placed in a closed graphite crucible covered with loose AlN powder and sintered in vacuum at  $1900^\circ\text{C}$  for 10 minutes or 2 hours to control the contact area between particles as well as shrinkage of the pellets due to the densification process. The full heat-treatment profile and the nomenclature followed for naming each heat-treated sample is shown in Table I-2. Accordingly, ammonia and argon pre-heat treated samples are denoted as ' $\text{NH}_3$ ' and 'Ar', respectively. The numbers to the right of these letters correspond to the hold time at the final temperature employed for the heat treatment. The number '1' corresponds to a hold time of 10 minutes while the number '2' corresponds to a hold time of 2 hours. The letters 'HP' and 'LP' represent the 'High CIP Pressure (35,000 psi)' and 'Low CIP Pressure (10,000 psi)' respectively. These different pressure settings were used as the parameter to control the volume fraction of the solid material. It should be noted that both samples processed using a high and low CIP pressure were subjected to pre-treatment in ammonia.

### I-1.2. Materials Characterization

Scanning electron microscopy (SEM) was conducted to analyze the microstructure of the sintered samples. The SEM study was conducted using a CamScan scanning electron microscope. SEM analysis was performed on the fracture surface of the sintered samples to observe the contact area and porosity between the particles, and thereby evaluate the connectivity between aluminum

Table I-1. Impurity contents of AlN powder obtained from Dow Chemicals\* used for processing porous AlN composite

Oxygen (wt%)	Carbon (wt%)	Fe (ppm)	Ca (ppm)	Si (ppm)
0.86	0.04	30	64	<25

\*Dow Chemicals Co., Midland, MI 48574



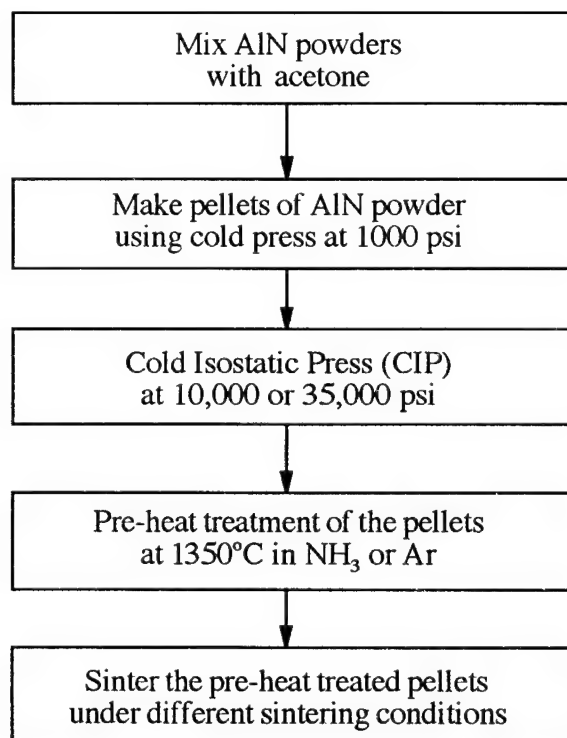


Figure I-1. Flow sheet showing the procedure used to process 3-D interconnected porous AlN composites.

Table I-2 Heat-treatment schedule that was implemented for processing the porous AlN composites

Sample*	Temperature (°C) / Duration (atmosphere)	
HP-NH <sub>3</sub> -1350	1350/48h (NH <sub>3</sub> )	-
LP-NH <sub>3</sub> -1350	1350/48h (NH <sub>3</sub> )	-
HP-NH <sub>3</sub> -1900-1	1350/48h (NH <sub>3</sub> )	1900/10min (Vacuum)
LP-NH <sub>3</sub> -1900-1	1350/48h (NH <sub>3</sub> )	1900/10min (Vacuum)
HP-NH <sub>3</sub> -1900-2	1350/48h (NH <sub>3</sub> )	1900/2h (Vacuum)
LP-NH <sub>3</sub> -1900-2	1350/48h (NH <sub>3</sub> )	1900/2h (Vacuum)
HP-Ar-1350	1350/48h (Ar)	-
LP-Ar-1350	1350/48h (Ar)	-
HP-Ar-1900-1	1350/48h (Ar)	1900/10min (Vacuum)
LP-Ar-1900-1	1350/48h (Ar)	1900/10min (Vacuum)
HP-Ar-1900-2	1350/48h (Ar)	1900/2h (Vacuum)
LP-Ar-1900-2	1350/48h (Ar)	1900/2h (Vacuum)

\*HP : cold isostatic press at 35,000 psi \*\*LP : cold isostatic press at 10,000 psi ; See text for details on sample nomenclature.

nitride particles in the sintered microstructure. Sintered samples were then subjected to thermal diffusivity measurement. Thermal diffusivity of sintered samples was measured using the Laser Flash Technique. The description of the instrument and the technique can be found in the literature [29] This measurement was conducted by Professor D.P.H. Hasselman at Virginia Polytechnic Institute, Blacksburg, Virginia. The thermal conductivity ( $k$ ) was calculated from thermal diffusivity ( $\alpha$ ) using following equation:

$$k_c = 0.01 \cdot \alpha_c \cdot c_c \cdot \rho_c$$

where ' $k_c$ ' is the thermal conductivity of the composite (W/m-K), ' $\alpha_c$ ' is the thermal diffusivity of the composite ( $\text{cm}^2/\text{s}$ ), ' $c_c$ ' is the specific heat capacity of the composite (J/K-g), ' $\rho_c$ ' is the density of the composite ( $\text{g}/\text{cm}^3$ ), and 0.01 is the conversion factor for  $\text{cm}^{-1}$  to  $\text{m}^{-1}$ .

In a porous composite, density and heat capacity of the composite can be expressed by following relation:

$$\rho_c = \rho_{\text{AIN}} v_{\text{AIN}} + \rho_{\text{air}} (1 - v_{\text{AIN}}) \approx \rho_{\text{AIN}} v_{\text{AIN}} \quad (\text{g}/\text{cm}^3)$$

$$c_c = c_{\text{AIN}} = 0.8236 \text{ (J/K-g) [30]}$$

where ' $v_{\text{AIN}}$ ' is the volume fraction of aluminum nitride.

The thermal conductivity of the porous aluminum nitride composite was therefore calculated from the thermal diffusivity using the following relation:

$$k_c = 0.01 \cdot \alpha_c \cdot c_{\text{AIN}} \cdot \rho_{\text{AIN}} v_{\text{AIN}}$$

## I-2. Results and Discussion

### I-2.1. Effect of ammonia pre-treatment on thermal conductivity

The samples after pretreatment in argon and ammonia, and after sintering were measured for their volume fraction, thermal diffusivity and thermal conductivity. These values are listed in Table I-3. The volume fraction of the samples prepared using a pressure of 35,000 psi (HP samples) is in the range of 0.614 to 0.674. The maximum shrinkage in volume was estimated to be about 23%. This was obtained by comparing the highest estimated volume fraction of the sintered sample (0.674) with volume fraction of the green pellet (0.518) prior to densification. In the case of the samples prepared using a lower pressure of 10,000 psi (LP samples), the volume fraction was estimated to be in the range of 0.573 to 0.633. The samples that were pre-treated in  $\text{NH}_3$  densified to a lower extent than the Ar pre-treated samples when sintered at  $1900^\circ\text{C}$  for 2 hours. This can be seen from the estimated volume fractions tabulated in Table I-3 for both, the HP and LP samples that were heat treated in  $\text{NH}_3$  and Ar prior to sintering at  $1900^\circ\text{C}$  for 2 hours. The HP sample that was pre-treated in ammonia prior to sintering at  $1900^\circ\text{C}$  for 2 hours revealed a volume fraction of 0.662 after the sintering treatment. On the other hand, the argon treatment of HP samples revealed

Table I-3. Thermal conductivity data obtained on sintered AlN composites

Sample*	Volume fraction of AlN**	Thermal diffusivity ( $\times 10^{-2} \text{ cm}^2/\text{s}$ )	Thermal conductivity (W/m-K)	Increase in thermal conductivity by $\text{NH}_3$ pre-treatment (%)
HP-Ar-1350	0.615	3.26	5.38	31.3
HP-NH <sub>3</sub> -1350	0.614	4.30	7.07	
HP-Ar-1900-1	0.641	6.97	12.00	23.0
HP-NH <sub>3</sub> -1900-1	0.633	8.68	14.75	
HP-Ar-1900-2	0.674	10.06	18.21	18.1
HP-NH <sub>3</sub> -1900-2	0.662	12.10	21.51	
LP-Ar-1350	0.573	2.43	3.74	28.0
LP-NH <sub>3</sub> -1350	0.573	3.11	4.79	
LP-Ar-1900-1	0.603	6.22	10.07	14.7
LP-NH <sub>3</sub> -1900-1	0.596	7.22	11.55	
LP-Ar-1900-2	0.633	9.17	15.59	7.4
LP-NH <sub>3</sub> -1900-2	0.623	10.01	16.74	

\* See text for details on the nomenclature of samples.

\*\* Volume fraction of AlN was determined from sample dimension.

a volume fraction of 0.674. Similarly, the LP samples that were pre-treated in ammonia and argon revealed a volume fraction of 0.623 and 0.633 respectively. Thus, in both cases irrespective of the pressure employed for cold isostatic pressing, reduction of the surface oxide layer limits the reduction in volume fraction by at least 1.6-1.8%. On the other hand, the influence of pre-treatment on sintering seems to be negligible for samples sintered at 1350°C for 48 hours employing both high and low pressures for cold isostatic pressure treatments. This is once again visible from the values of the volume fraction estimated for both HP (0.614 for ammonia pre-treatment vs 0.615 for argon treatments) and LP (0.573 for both ammonia and argon treatments) samples. The lower volume fraction and consequently, a lower extent of shrinkage observed in ammonia pre-treated samples would be mainly due to the removal of surface oxide layer, thereby limiting densification and promoting more grain coarsening.

Thermal conductivity measurements conducted on these samples indicate very interesting results pertaining to reduction in surface oxide, densification and particle-particle contact area. These results can be discussed in two sections corresponding to the use of high and low pressures during cold isostatic pressing.

#### I. Cold isostatically pressed samples employing high pressure (35000 psi) HP:

The results obtained for all these samples are tabulated in Table I-3. In all, six samples were analyzed for thermal conductivity and these values have been tabulated with the corresponding volume fractions that were estimated after the sintering treatments. Two different sintering treatments were initiated to the samples that were subjected to either ammonia or argon pre-treatments at 1350°C. The two sintering treatments varied with respect to the hold times at 1900°C which were 10 minutes and 2 hours respectively. The samples that were subjected to identical cold isostatic pressing treatments and pre-treated in argon and ammonia at 1350°C showed negligible variation in volume fraction ( $\approx 0.16\%$ ). However, there was a marked difference in the thermal conductivity. An increase of  $\approx 31.3\%$  was observed in the thermal conductivity for the samples pre-treated in ammonia with negligible variation in volume fraction. This result clearly indicates the profound influence of ammonia pre-treatments. The same samples that were pre-treated in ammonia and argon were sintered at 1900°C for 10 minutes and 2 hours. The results of thermal conductivity measured for the sample sintered at 1900°C for only 10 minutes tends to show a decreasing influence of ammonia pre-treatments. This decrement also appears to be enhanced as the sintering time at 1900°C is further increased to 2 hours. As can be seen with increase in sintering temperature and time, there is a significant increase in the volume fraction of the argon treated samples. This is mainly because of the extended necking and sintering that is facilitated by the probable presence of the surface oxide layer. Consequently, there is a  $\approx 4.2\%$  increase in the

volume fraction of the solid that is observed in the samples that were treated in argon prior to sintering at 1900°C for 10 minutes. Accordingly, there is a significant increase in the thermal conductivity corresponding to  $\approx 120\%$ . This increase is obviously due to the densification that occurs because of the presence of the surface oxide. The ammonia pre-treated samples on the other hand exhibit only a 3% increase in volume fraction after undergoing the sintering treatment at 1900°C for 10 minutes. This small reduction in the volume fraction corresponding to a lower densification is obviously a reflection of the ammonia pre-treatments causing for a reduction in the surface oxide. This removal of the surface oxide layer limits the densification kinetics due to the poor diffusion of nitrogen leading to poor mass transport as is well known. Thus, only a 23% increase in thermal conductivity is seen for the sample that was pre-treated in ammonia prior to being subjected to a sintering treatment at 1900°C for 10 minutes in comparison to the argon treated sample. This increase is even lowered further at longer hold times of 2 hours for the two samples. Accordingly, only 18% increase in thermal conductivity is seen for the ammonia pre-treated sample after the sintering treatment at 1900°C for 2h. Once again this reduction in the increase in thermal conductivity is due to the enhanced densification seen in the argon treated samples due to the surface oxide layer which off-sets the increase in thermal conductivity that should have been expected for the ammonia pre-treated samples after being sintered at 1900°C. Nevertheless, if one compares the thermal conductivity values for the ammonia pre-treated samples after the treatment at 1350°C and after the sintering treatment at 1900°C for 2h, it can be seen that there is a phenomenal increase corresponding to  $\approx 200\%$ . Although the absolute value of thermal conductivity is not yet in the vicinity of what one might expect for pure AlN, the trend seen in the study helps in deriving some important conclusions. This accelerated increase in thermal conductivity obviously suggests that there could be other factors related to the microstructure affecting the thermal conductivity in addition to increase in volume fraction due to sintering. This can also be seen from the theoretical value of thermal conductivity that is predicted by the Maxwell's relation[23].

Maxwell's relation as is well known only incorporates the effect of volume fraction in predicting the effective thermal conductivity ( $k_{eff}$ ). Since the thermal conductivity of the continuous phase which is AlN, ' $k_c$ ' is greater than the thermal conductivity of the discrete phase constituted by pores, the Maxwell's relation reduces to

$$k_{eff} = k_c [1 - v_d / 1 + v_d]$$

where ' $v_d$ ' is the volume fraction of the discrete phase. The value for the thermal conductivity of the continuous phase is dictated by the purity of AlN. It has been reported in the literature that single crystal AlN containing 0.8wt% oxygen exhibited a thermal conductivity of 80W/mK[31]. In

the present work the AlN powders contain 0.86wt% oxygen and hence the thermal conductivity has been assumed to be 60W/mK which appears plausible based on the above reported values. Using this relation for the two samples, HP-NH<sub>3</sub>-1350 and HP-NH<sub>3</sub>-1900-2, and incorporating the corresponding volume fraction of the solid continuous phase namely, 0.614 and 0.662, the effective thermal conductivity is obtained as 26.6 W/mK and 29.7 W/mK. This result therefore suggests that upon increasing the sintering temperature to 1900°C and holding the sample for 2h, the effective thermal conductivity as predicted by Maxwell's relation should have increased by only 11.6%. However, the experimental results indicate an almost 200% increase in thermal conductivity. This therefore suggests that the increase in thermal conductivity during sintering is mainly due to the increase in the contact area between AlN particles rather than increase in volume fraction. This increase in thermal conductivity brought about by increase in the contact area is also reflected in the argon treated samples as well. The presence of the surface oxide helps in the densification and the corresponding rise in the thermal conductivity to a value of 18.21 W/mK from 5.38 W/mK which is the value obtained after the argon treatment at 1350°C. This increase in thermal conductivity lowers the difference between the thermal conductivity of ammonia and argon treated samples after sintering at 1900°C for 2h to only 18% as opposed to what was 31% that was seen after the pretreatment at 1350°C.

## II. Cold isostatically pressed samples employing low pressure (10,000 psi) LP:

The samples that were subjected to cold isostatic pressing treatment at low pressures indicate a similar trend as the HP samples except that the increase in thermal conductivity is lower. The difference between argon and ammonia treated samples at 1350°C is only 28% as opposed to 31% in the HP samples. This lower value could be expected because of a lower volume fraction of the solid suggesting more porosity in the samples. However, what is interesting is the 7.4% increase in thermal conductivity that is seen in the ammonia treated samples after sintering at 1900°C for 2h in comparison to argon treated samples. The difference in volume fraction between the two samples is 1.6% which is not significantly different from 1.8% difference seen in the HP samples.

The lower percentage increase is therefore probably caused by other factors. A probable explanation could be reoxidation of the surface of the samples after ammonia pre-treatment. This is quite possible especially due to the continuous characteristic of the pores. The samples sintered in ammonia at 1350°C have oxide free regions which undergo necking which is the main path for the heat propagation. Hence, considerable improvement in the thermal conductivity is seen for these samples (31.3% increase for HP samples and 28% increase for LP samples). Subsequent sintering at high temperatures could have involved reoxidation of the surface of the AlN in the pores. This could have occurred during handling of the samples. The consequence of this is the formation of

new oxide surfaces while the oxide-free particle boundary remains the same. There is growth of the contact area between the oxidized particles which does not help in improving the thermal conductivity as is the case in comparison to the HP samples. The samples prepared using a lower pressure of 10,000 psi show a greater decrease in the effect of  $\text{NH}_3$  pre-treatment in comparison to the samples prepared using a higher pressure of 35,000 psi during cold isostatic pressing. It is possible that the samples prepared using a lower pressure of 10,000 psi, have considerably less number of oxide-free necked regions in comparison to the samples prepared using a higher pressure of 35,000 psi. This decrease in the oxide-free necked region is because of the lower volume fraction of the solid in the case of the LP samples (0.614 for HP- $\text{NH}_3$ -1350 and 0.573 for LP- $\text{NH}_3$ -1350) when pre-treated in  $\text{NH}_3$  at 1350°C. Analysis of the total oxygen and the lattice oxygen contents as well as the surface oxygen would help in providing more quantitative information and justify the above possibilities. These studies are proposed to be conducted in future to help improve the thermal conductivity of the composites further. Such a study would involve the use of hot gas extraction analysis to analyze the lattice oxygen while the use of Auger analysis would provide information on the surface oxygen[32]. Similarly, the use of electron energy loss spectroscopy (EELS) would help in providing some understanding of the role of oxygen at the grain boundaries.

### I-2.2. Microstructural Analysis

Scanning electron microscopy was used to observe the microstructure of the fracture surfaces of all the samples that were used for this study. Accordingly, both samples that were sintered employing a high pressure of 35,000 psi as well as a low pressure of 10,000 psi were used for microstructural analysis. The results of the analysis are discussed in two sections.

#### I. Cold isostatic pressed samples employing high pressure (35,000 psi)

In order to observe the effect of the heat treatment at 1350°C, both the argon and ammonia treated samples were observed under the SEM. Figures I-2(a) and I-2(b) show the fracture surfaces of these two samples. Both the samples show significant necking to have occurred between the particles. However, based on the SEM images alone it is very difficult to identify the differences due to ammonia treatments. The fact that is very clear is that the AlN particles are very fine and are in the sub-micron range ranging from 0.1 to 0.5  $\mu\text{m}$ . There does not appear to be any significant growth of the particles during ammonia treatment. This is to be expected since the ammonia treatments only help in inducing the  $\text{O} \rightarrow \text{N}$  exchange reaction without producing any change in the morphology as we have seen in our studies on nitridation of borosilicate glasses discussed in part II in the appendix of this report. Subsequent heat treatment and sintering of both the argon and ammonia samples at 1900°C for 10 minutes however induces significant changes.



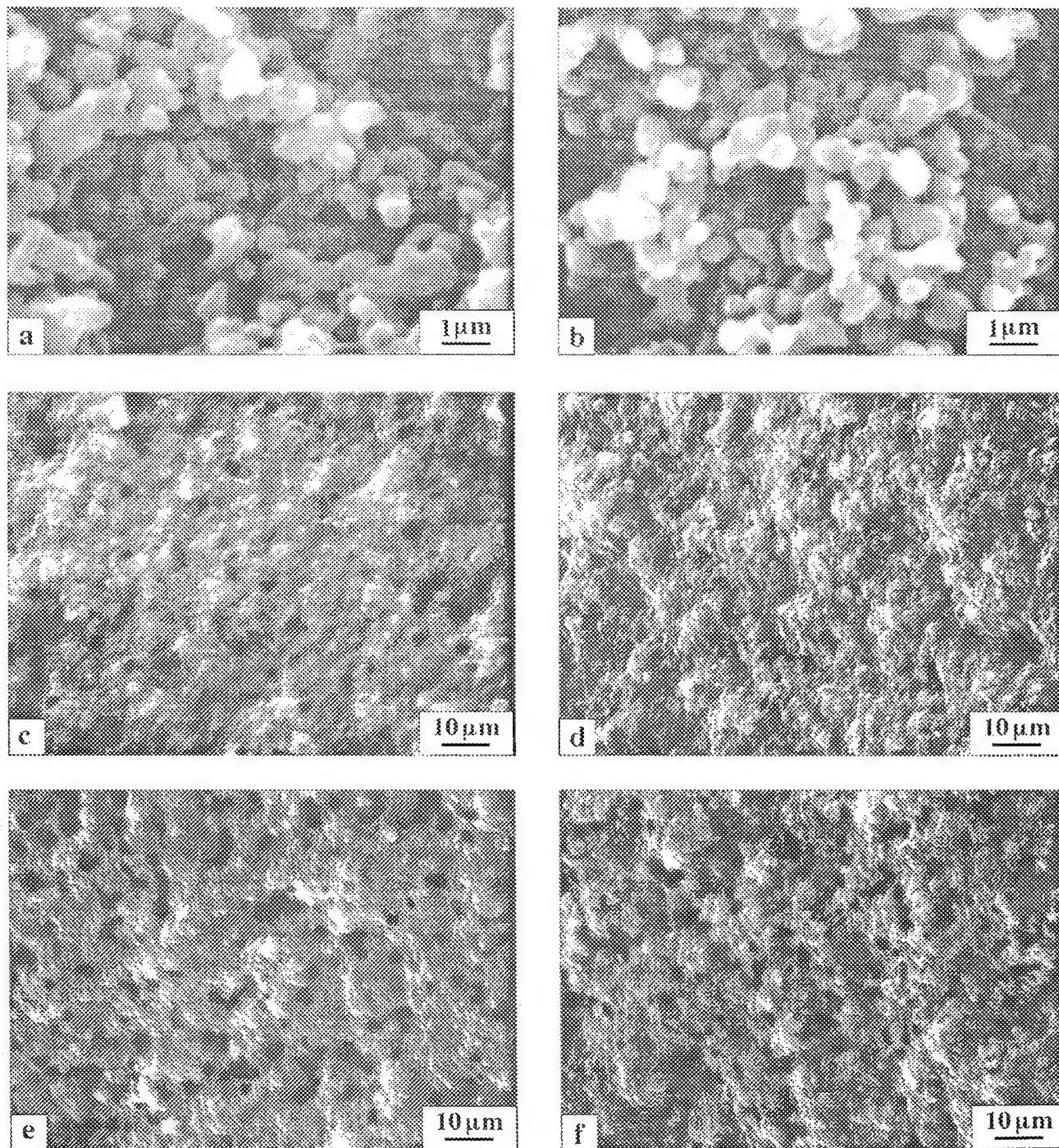


**Figure I-2.** SEM micrographs showing the fracture surface of sintered samples prepared using a pressure of 35,000 psi during cold isostatic pressing; (a) HP-Ar-1350, (b) HP-NH<sub>3</sub>-1350, (c) HP-Ar-1900-1, (d) HP-NH<sub>3</sub>-1900-1, (e) HP-Ar-1900-2, and (f) HP-NH<sub>3</sub>-1900-2. See text for details on sample nomenclature.

The fracture surfaces of these samples were once again observed under the SEM and are shown in Figures I-2(c) and I-2(d). As can be seen from the micrographs, both the argon and ammonia treated samples after sintering at 1900°C for 10 minutes seem to show signs of coalescence of the particles.

It is interesting to note that there is very little porosity that is seen in both these samples after sintering at 1900°C for 10 minutes. This is surprising particularly, since measurements indicate that both these samples have at least  $\approx 35\%$  porosity. It was therefore decided to observe the surface of the HP-Ar-1900-1 sample more closely. Figure I-4 is a higher magnification micrograph taken over a region shown in Figure I-2(c) of the HP-Ar-1900-1 sample. The micrograph clearly shows sintered regions comprised of  $1\mu\text{m}$  size grains. However, in addition to a large interconnected pore that is  $\approx 3\mu\text{m}$  in diameter there are several pin-hole type micropores. This therefore suggests that sintering at 1900°C for 10 minutes probably initiates the coalescence of the particles with the formation of micropores that are well distributed. Continued sintering of the samples at 1900°C for 2h seemed to have helped in increasing the extent of coalescence of the particles thereby transforming the micropores to well formed interconnected porous channels 2-10  $\mu\text{m}$  in diameter. Figures I-2(e) and I-2(f) show the fracture surfaces of both argon and ammonia treated samples after they have undergone sintering at 1900°C for 2h. It should be noted that even though the ammonia treated samples i.e. HP-NH<sub>3</sub>-1900-2 have a lower (1.8%) volume fraction of solids in comparison to the HP-Ar-1900-2 sample, the nature and size of the porous channels are very similar in both cases.

## II. Cold isostatic pressed samples employing low pressure (10,000 psi)

Scanning electron microscopy was used to observe the microstructure of the fracture surfaces of all the samples that were cold isostatically pressed employing low pressure of 10,000 psi similar to the high pressure samples. All the samples were cold isostatically pressed and were treated in argon and ammonia after which they were subjected to sintering treatments. Similar to the case of the high pressure samples, both argon and ammonia pre-treated samples at 1350°C were observed under the SEM to identify any changes due to the treatments. The micrographs are shown in Figures I-3(a) and I-3(b). The micrographs are very similar to the high pressure analogs. Extensive necking is seen in both the cases and it is extremely difficult to identify the influence ammonia treatments at this stage. The use of Auger electron microscopy and depth profiling would perhaps provide more information on the changes occurring in the oxygen contents on the surface. These studies will be conducted in the future. The grain sizes in both samples are very similar to those described in section I above and are in the range of 0.1-0.5  $\mu\text{m}$ . Similar to section I above, both the argon and ammonia treated samples were subjected to sintering at 1900°C for 10 minutes.

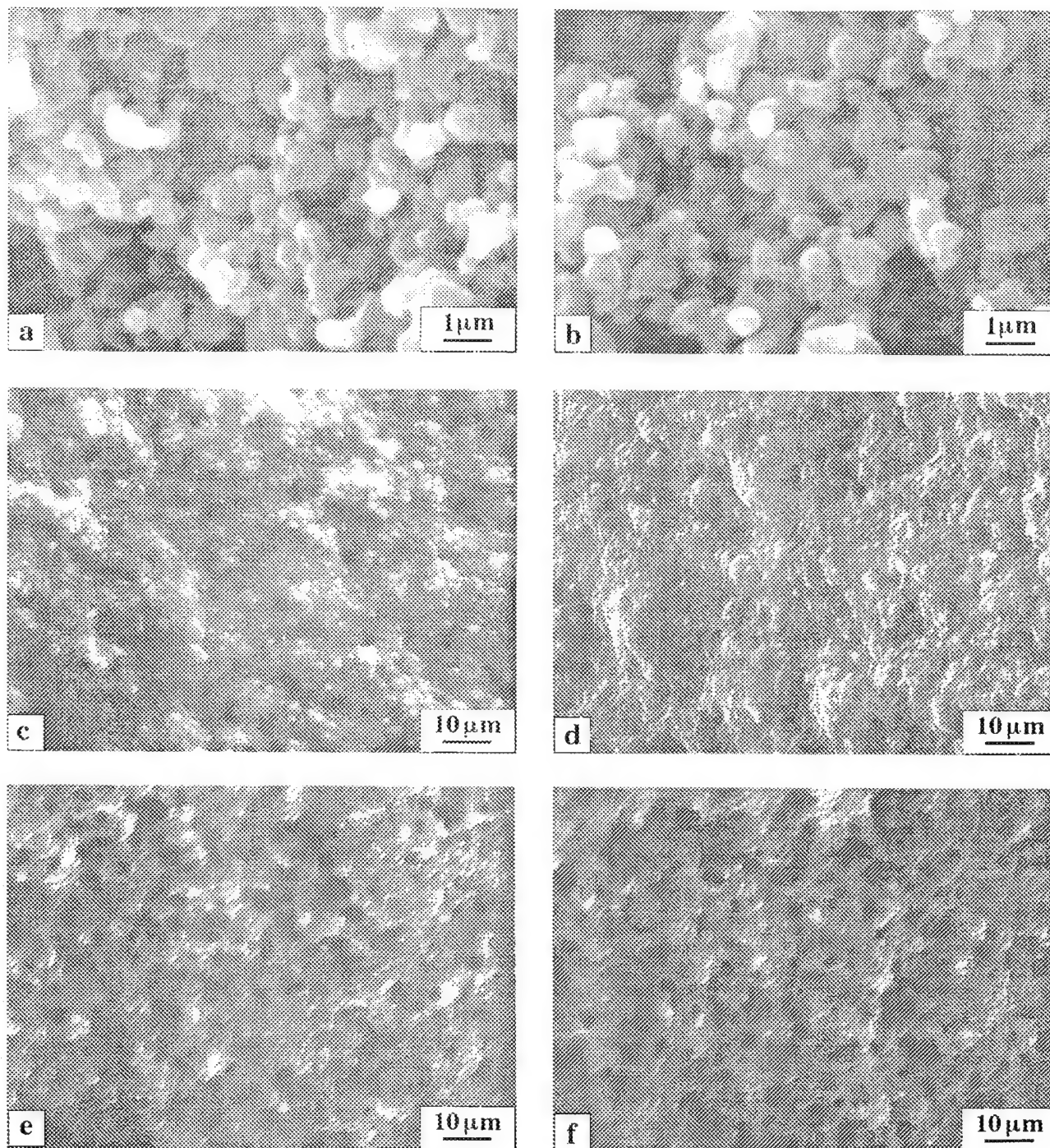


**Figure I-3.** SEM micrographs showing the fracture surface of sintered samples prepared using a pressure of 10,000 psi during cold isostatic pressing; (a) LP-Ar-1350, (b) LP-NH<sub>3</sub>-1350, (c) LP-Ar-1900-1, (d) LP-NH<sub>3</sub>-1900-1, (e) LP-Ar-1900-2, and (f) LP-NH<sub>3</sub>-1900-2. See text for details on sample nomenclature.



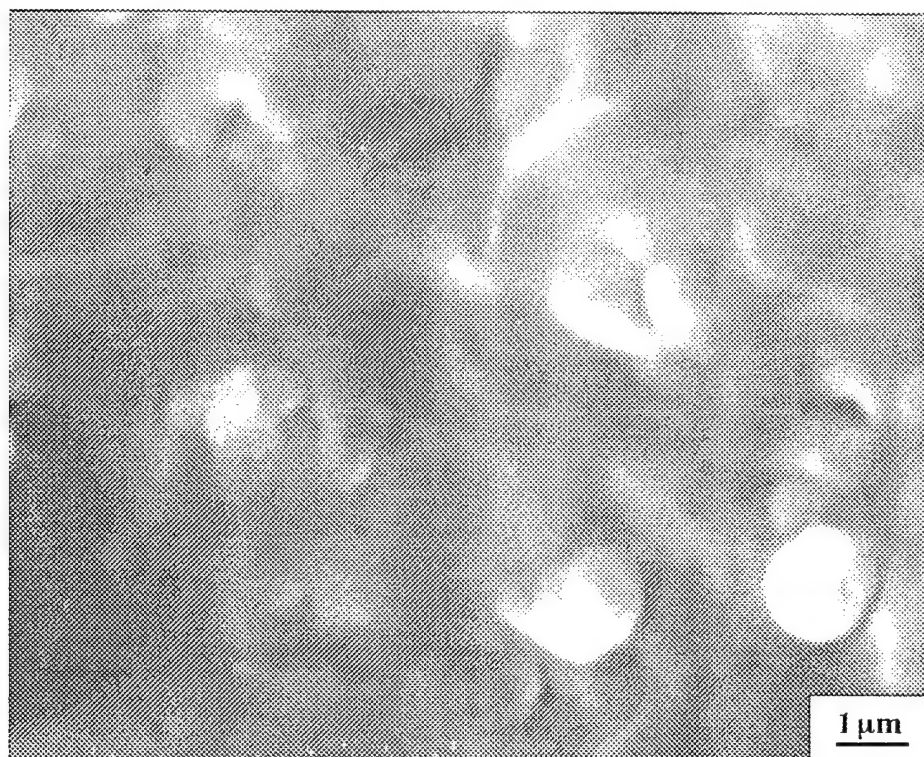


**Figure I-4.** SEM micrograph showing a magnified region of sintered sample (HP-Ar-1900-1). The micrograph shows the presence of micropores distributed between the fine particles.

Figures I-3(c) and I-3(d) show the micrographs of the two samples treated in argon and ammonia prior to sintering at 1900°C for 10 minutes. The micrographs show the same features as in the case of the HP samples. There is very little porosity seen in the micrographs since the very fine AlN particles are in the process of undergoing coalescence. The time is too short to induce any vapor transport and hence there is very little driving force for the growth and formation of large connected pores. Most of the porosity which is  $\approx 40\%$  at this stage exists mainly in the form of micropores. The extent of coalescence due to diffusion processes is only facilitated when the samples are sintered at 1900°C for 2 hours. The micrographs of the fracture surfaces in both samples as shown in Figures I-3(e) and I-3(f) show formation of considerable amount of interconnected porosity. The pores are large in both the samples and range in size from 2-10 $\mu\text{m}$  in diameter. The fact that the AlN particles are very fine ( $\approx 0.1\text{-}0.5\ \mu\text{m}$ ) probably helps in enhancing their sinterability but at the same time makes them very susceptible to oxidation. The small particle size also facilitates the rapid initiation of necking leading to coalescence of the particles and the formation of micropores. These micropores are very detrimental and lead to poor thermal conductivity. Thus, both the LP and HP samples sintered at 1900°C for only 10 minutes exhibit much lower thermal conductivity (12 W/mK and 14.75 W/mK for HP and, 10.07 W/mK and 11.55 W/mK for LP samples) in comparison to the samples that are sintered at 1900°C for 2h even though the difference in volume fraction is very negligible in comparison to the difference in thermal conductivity. It is also possible that these micropores are retained in the samples that are sintered at 1900°C for 2h and hence the thermal conductivity of these samples could in fact be higher.

### I-3. Conclusions

The work conducted on processing of 3-D interconnected porous AlN composites shows that it is possible to initiate interconnectivity between the particles and obtain increments in thermal conductivity. The pre-treatments in ammonia was found to be essential to increase the thermal conductivity due to the removal of the surface oxygen which inhibits the thermal conduction process. This increase was found to be substantial at low temperatures. Subsequent increase in the sintering time and temperature helps to have a less impact on the thermal conductivity although, there is an overall improvement in the thermal conductivity of the ammonia treated samples. The increase is however not commensurate with the volume fraction but is however significantly higher than the thermal conductivity obtained at lower temperatures of 1350°C. The highest value of thermal conductivity obtained in the present study is 21.51 W/mK. This increment is caused by increase in the contact area between the particles which leads to improved thermal conduction. Further improvements in the thermal conductivity can be achieved if the purity of AlN can be

increased and the lattice oxygen can be further lowered. This forms a part of the future studies. These initial studies conducted show that the approach has promise and it is possible to obtain composites whose thermal conductivity can be optimized by controlling the process parameters such as sintering time and the pressure used during cold isostatic pressing. It should be mentioned that although the maximum thermal conductivity obtained in the present approach is only 21.5 W/mK which is comparable to alumina, the interconnected porosity of the composite will definitely lower the dielectric constant to values better than dense alumina and aluminum nitride. Thus, the AlN composite obtained in the present study could act as a substrate whose performance would rate better than glass-ceramic in terms of heat dissipation while exhibiting the same high speed propagation characteristics.

#### **I-4. Future Work**

Based on the above results, it can be seen that there is considerable potential for the development of this approach to process porous AlN composites. The work in the future will be concentrated on improving the thermal conductivity to at least 40 or 50W/mK while maintaining the dielectric constant to  $\approx 5$  at 1 MHz. The present studies seem to indicate that the main cause for attainment of low thermal conductivity lies in the purity of the AlN particles. The presence of lattice oxygen and micropores are the two factors that lead to poor values. It is hoped that by increasing the sintering time, the particles could coarsen further thereby eliminating any micropores. It is also hoped that addition of very small amounts ( $< 1\text{wt}\%$ ) of sintering aids will help in gettering the oxygen and still retain the porosity that is essential for lowering the dielectric constant. The present studies were also focused on using very fine particles which are very conducive to reoxidation and formation of micropores which are both detrimental to the thermal conductivity. Future studies will concentrate on using high purity particles which are atleast  $10\text{ }\mu\text{m}$  in size. Thus, the future studies will concentrate on optimizing the processing conditions while also using characterization techniques such as hot gas extraction and Auger analysis to evaluate variation in the surface oxygen, the total and lattice oxygen. At the same time, electron microscopy will be used to understand the variation of oxygen levels across the grain boundary. These studies will be conducted in addition to evaluating the thermal conductivity and dielectric constant. All these studies will form a part of the studies that will be conducted in the future.

#### 4. References

1. 'Microelectronic Packaging Handbook', Edited by R.R. Tummala and E.J. Rymaszewski, Van Nostrand Reinhold, New York , (1989).
2. G. Geiger, Bulletin American Ceramic society, 69, (1990) 1131.
3. E.M. Rabinovich, J. Electronic Packaging, 111, (1989) 183.
4. R.R. Tummala and R.B. Shaw, High Tech Ceramics, Ed. P. Vincenzini, Elsevier Science Publishers B.V. Amsterdam, (1987) 75.
5. J.L. Sprague, IEEE Transactions on Components, Hybrids, and Manufacturing Technology, 13, (1990) 390.
6. K.R. Kinsman, J. Metals, 6, (1988) 7.
7. N. Kuramoto, H. Taniguchi and I. Aso, Ceramic Bulletin, 68, NO. 4, (1989) 883.
8. N. Kuramoto and H. Taniguchi, J. Mater. Sci. Lett.,3, (1984) 471.
9. T.B. Troczynski and P.S. Nickolson, J. Amer. Ceram. Soc., 72 [8] (1989) 1488-1491.
10. N.S. Van Damme, S.M. Richard and S.R. Wizer, J. Am. Ceram. Soc., 72 [8] (1989) 1409-1414.
11. A. Hai, T. Shi, K. Wakimura, Sennan, M. Tonaka. Shimonoseki, Mitsui Toatsu Chem. Inc. Tokyo. Japan, "Method For Preparing Aluminum Nitride And Its Sintering". U.S. Patent No. 4869925, (1989).
12. U. Klabunde, W. Chester, E.J. Newitt, C. Ford, F.N. Tebbe, H. Del. E.I. DuPont de Nemours & Co. Wilmington, Delaware, "Gas Phase Preparation of Aluminum Nitride", U.S. Patent No. 4865830, (1989).
13. S.L. Dole, R.H. Arendt, W.D. Pasco, General Electric Co., Schnectady, N.Y., "Alkaline Earth Fluoride Additive For Sintering Aluminum Nitride", U.S. Pat. No. 4843042, (1989).
14. S. Kuratani, K. Uno, S. Mizuno, H. Sakuramoto, and S. Nishiyama, Narumichina Corp., Nagoya, Japan, "Black Sintered Body of Aluminum Nitride And Process For Producing the Same", U.S. Pat. No. 4843038, (1989).
15. S. Mizuno, S. Kuratani, K. Uno, H. Sakuramoto, and S. Nishiyama, Narumochina Corp., Nagoya, Japan, "Sintered Body of Aluminum Nitride", U.S. Pat. No. 4833108, (1989).
16. A. Ikegami and T. Yasuda, "High Thermal Conductive SiC Substrate and Its Applications", 5th European Hybrid Microelectronics Conference, (1985) 465.
17. R.R. Tummala, J. Am. Ceram. Soc. 74 (1991) 895.

18. A.J. Blodgett, Jr., *Scientific American*, 249 (1983) 2.
19. P.N. Kumta, T. Mah, P.D. Jero, R.J. Kerans, *Mat. Lett.* 21 (1994) 329.
20. P.N. Kumta, 'Processing Aspects of Glass-Nicalon Fiber and Interconnected Porous Aluminum Nitride Glass and Ceramic Composites' *J. Mat. Sc.* (in Press).
21. J.F. MacDowell, G.H. Beall, *Proc. of the 1st International Science and Technology Conference, "Materials and Processes for Microelectronic Systems"*, Ceramic Transactions, Ed. K.M. Nair, R.Pohanka and R.C. Buchanan, Vol. 15 (1989) 259.
22. J.F. MacDowell and G.H. Beall, *Mat. Res. Soc. Symp. Proc.*, "Advanced Electronic Packaging Materials", Ed. A.T. Barfknecht, J.P. Partridge, C.J. Chen and Che-Yu Li, Vol. 167 (1989).
23. W.D. Kingery, H.K. Bowen and D.R. Uhlmann, 'Introduction to Ceramics', John Wiley & Sons, Second Edition, (1976) 635.
24. A.J. Moulson and J.M. Herbert, 'Electroceramics, Materials, Properties and Applications', Chapman and Hall (1990) 79.
25. L.E. Cross and T.R. Gururaja, *Mat. Res. Soc. Symp.*, "Electronic Packaging Materials Science II", Eds. K.A. Jackson, R.C. Pohanka, D.R. Uhlmann and D.R. Ulrich, Vol. 72 (1986).
26. D.P. Button, B.A. Yost, R.H. French, W.Y. Hsu, J.D. Bolt, M.A. Subramanian, H.M. Zhang, R.E. Giedd, A.J. Whitaker and D.G. Onn, *Advances in Ceramics*, Vol. 26, "Ceramic Substrates and Packages for Electronic Applications", Eds. M.F. Yan, K. Niwa, H.M. O'Bryan, Jr., and W.S. Young, American Ceramic Society (1989) 87-105.
27. D.W. Readey, J. Lee, and T. Quadir in, 'Sintering and Heterogeneous Catalysis', Eds. G.C. Kuczynski, A.E. Miller and G.A. Sargent, *Materials Science Research*, Vol. 16, *Proceedings of the International Conference on Sintering and Related Phenomena* (Plenum Press, 1984) 115.
28. S. Prochazka and C.F. Bobik, *Materials Science Research*, Vol. 13, "Sintering Processes", Ed. G.C. Kuczynski, *Proc. 5th Intl. Conference on Sintering and Related Phenomena*, (1979) 321.
29. D.P.H. Hasselman and K.Y. Donaldson, *International Journal of Thermophysics*, Vol. 11. No. 3 (1990) 573.
30. *CRC Materials Science and Engineering handbook*, 2nd Ed., edited by J.F. Shackelford, (CRC press, Boca Raton, 1994) p. 263.



31. D.D. Marchant and T.E. Nemecek, Ceramic Substrates and Packages for Electronic Applications, edited by M.F. Yan, K.Niwa, H.M. O'Bryan, Jr., and W.S. Young, Advances in Ceramic Vol. 26, (The American Ceramic Society, Westerville, OH) p.19.
32. G. Gorzawski, M. Sternitzke, W.F. Müller, A. Berger, and G. Müller, J. European Ceramic Society, 15 (1995) 95.

## APPENDIX

### Part II

- (A) Development of glasses and glass-ceramics in the  $B_2O_3$ - $P_2O_5$ - $SiO_2$  system
- (B) Effect of incorporation of nitrogen on the structure and dielectric properties of modified oxide sol-precipitated borosilicate glasses and glass-ceramics

## Part II

### (A) Development of glasses and glass-ceramics in the $B_2O_3$ - $P_2O_5$ - $SiO_2$ system

Typical sol-gel processes consist of using metal alkoxides which undergo hydrolysis and condensation reactions in the presence of a common organic solvent. The use of metal alkoxides render the process expensive and air sensitive. In the present approach, an economical modified oxide sol-gel process was developed based on the use of metal oxides which can be reacted with alcohol to generate the metal alkoxide in-situ. Once the alkoxide is synthesized in-situ, it can then undergo hydrolysis and condensation reactions similar to the traditional sol-gel process. The kinetics of the reaction can be controlled very similar to the conventional sol-gel process to generate both a gel or a powder. Accordingly, two processes called modified oxide sol-gel (MOSG) and modified oxide sol-precipitation (MOSP) processes were studied in the present work.

#### II-1. Experimental Procedure

##### II-1.1. Synthesis of Borophosphosilicate Glass

Borophosphosilicate glasses were synthesized using both modified oxide sol-gel (MOSG) and modified oxide sol-precipitation (MOSP) processes employing commercially obtained boron oxide (99.98 %, Johnson Matthey) and phosphorus pentoxide (99.998 %, Aldrich), while using tetraethylorthosilicate (TEOS; 99.999 %, Aldrich) for silicon. Stoichiometric quantities of the oxides and TEOS were reacted in the ratio of  $B_2O_3:P_2O_5:SiO_2 = 1:1:4$  and  $1:1:8$  respectively.

The MOSG process consisted of mixing equimolar amounts of  $B_2O_3$  and  $P_2O_5$  in a Nalgene beaker. All the necessary materials were then placed in a glove bag filled with nitrogen in order to create an inert atmosphere. This was necessary to prevent the volatilization of boron alkoxide and the subsequent formation of crystalline boron oxide as a discrete phase. The glove bag was sealed and the remainder of the experiment was conducted inside the bag itself. The oxide powders ( $B_2O_3$  and  $P_2O_5$ ) were then dissolved in 100 ml of alcohol. The beaker was covered with parafilm, and the contents were stirred for 10 minutes in order to dissolve the powders. At this stage, TEOS was added to the beaker containing  $B_2O_3$  and  $P_2O_5$ , and the solution was mixed for 15 minutes. Water was then added to the resulting solution in two stages. The initial stage consisted of adding 16 ml and stirring the solution for 45 minutes at  $50^\circ C$ . The final stage consisted of adding a basic solution of water (16 ml) containing 10 drops of (14.8 N) ammonium hydroxide. The entire solution was then mixed for 2 hours at  $50^\circ C$ . Gelation of the solution occurred after a period of 6 days. Figure II-1 shows a schematic of the procedure followed to synthesize the borophosphosilicate gels using the MOSG process.

The procedure followed in the MOSP approach is very similar to the MOSG process except that precipitation is induced by rapid kinetics of the sol-gel reaction. To induce precipitation, excess

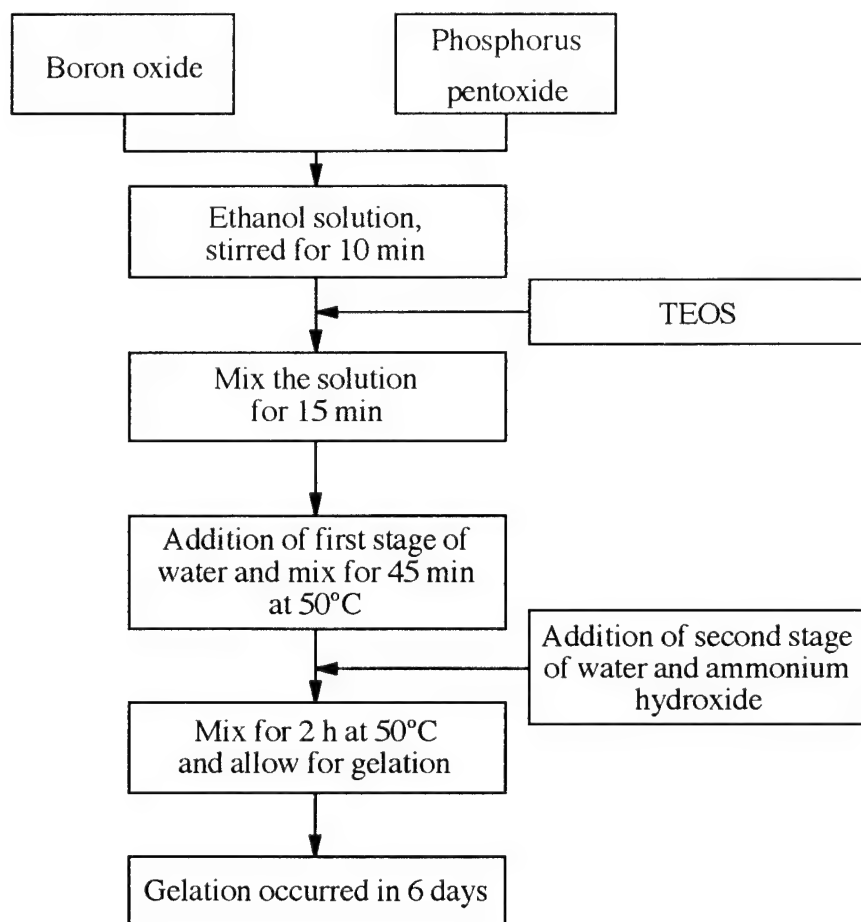


Figure II-1. Flow sheet showing the procedure followed in the MOSG process for synthesizing borophosphosilicate gels.

ammonium hydroxide was mixed with the water that was added at the final stage (25 ml of (14.8 N) ammonium hydroxide and 16 ml of water). After the precipitation reaction, precipitates were collected using a centrifugal separator and dried in air at 150 °C for 2h. A schematic of the procedure used in the MOSP process is shown in Figure II-2.

In order to compare the molecular and crystal structure of the crystalline  $\text{BPO}_4$  phase present in the synthesized borophosphosilicate gels, borophosphate gels were also prepared using a similar procedure published earlier. Accordingly, stoichiometric amounts of  $\text{B}_2\text{O}_3$  and  $\text{P}_2\text{O}_5$  in the ratio of 1:1 were dissolved in a solution of alcohol acidified with HCl, and the mixture was stirred at room temperature for 5-6 hours in a beaker provided with a parafilm seal. Water was then added corresponding to a 'r' ratio of 20 and the mixture stirred for approximately 8h until the solution became increasingly viscous. The viscous solution was poured into a petridish and heated to approximately 70°C until it transformed to a dry xerogel. Finally, the xerogel was then heat-treated at 800°C for 24 h to form the crystalline  $\text{BPO}_4$  phase.

#### II-1.2. Heat treatment

Heat treatment was performed based on the DTA results as shown in Figure II-3. Accordingly, the heat treatments were conducted in air at 450°C, 500°C and 800°C for both MOSG and MOSP derived samples to investigate the following three processes. First, to understand the structural changes occurring in the glasses. Second, to identify the crystallization of  $\text{BPO}_4$ , and third, to analyze the removal of residual carbon. According to the DTA results, the glass transition temperature ( $T_g$ ) of the borophosphosilicate gel corresponding to  $\text{B}_2\text{O}_3:\text{P}_2\text{O}_5:\text{SiO}_2 = 1:1:4$  stoichiometry and the temperature of crystallization ( $T_c$ ) of  $\text{BPO}_4$  are 430°C and 490°C, respectively. Thus, both the gels and precipitated powders were subjected to identical heat treatments in air up to 400°C as shown in Table II-1 before being heat-treated at 450°C and 500°C for 24 h, respectively. The heat treatment procedures at 800°C were however, conducted in a slightly different manner for the samples obtained using the two processes. In the case of the MOSG process, the gel powders were heat-treated at 800°C and reground several times in order to remove the carbon entirely, and to induce crystallization of the borophosphate phase. Hence, the total time for heat-treatment at 800°C was 96 hours. In the case of the MOSP process, the precipitates were crushed with a mortar and pestle and heat-treated up to 800°C for 24 h. The full heat-treatment profile and the nomenclature followed for naming each heat-treated sample are shown in Table II-1. Accordingly, the modified oxide sol-gel and sol-precipitation derived samples are denoted as 'SG' and 'SP', respectively. The numbers to the left and right of these letters correspond to the stoichiometry of the samples and the heat treatment condition employed,

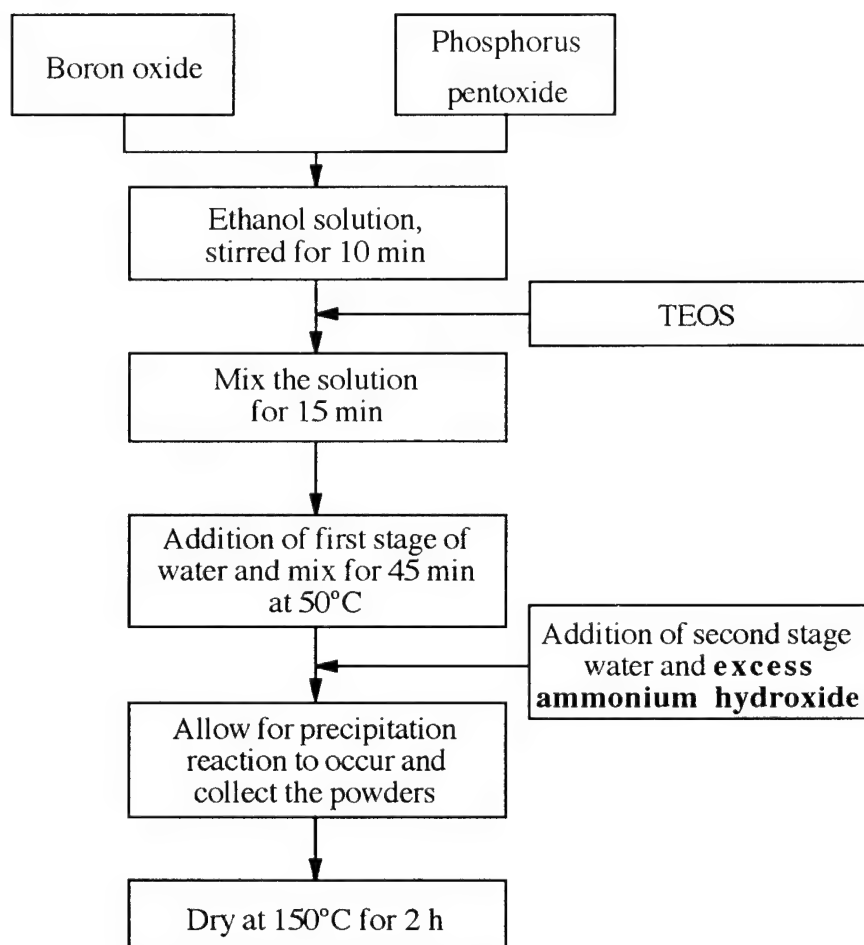


Figure II-2. Flow sheet showing the procedure followed in the MOSP process for synthesizing borophosphosilicate gels.

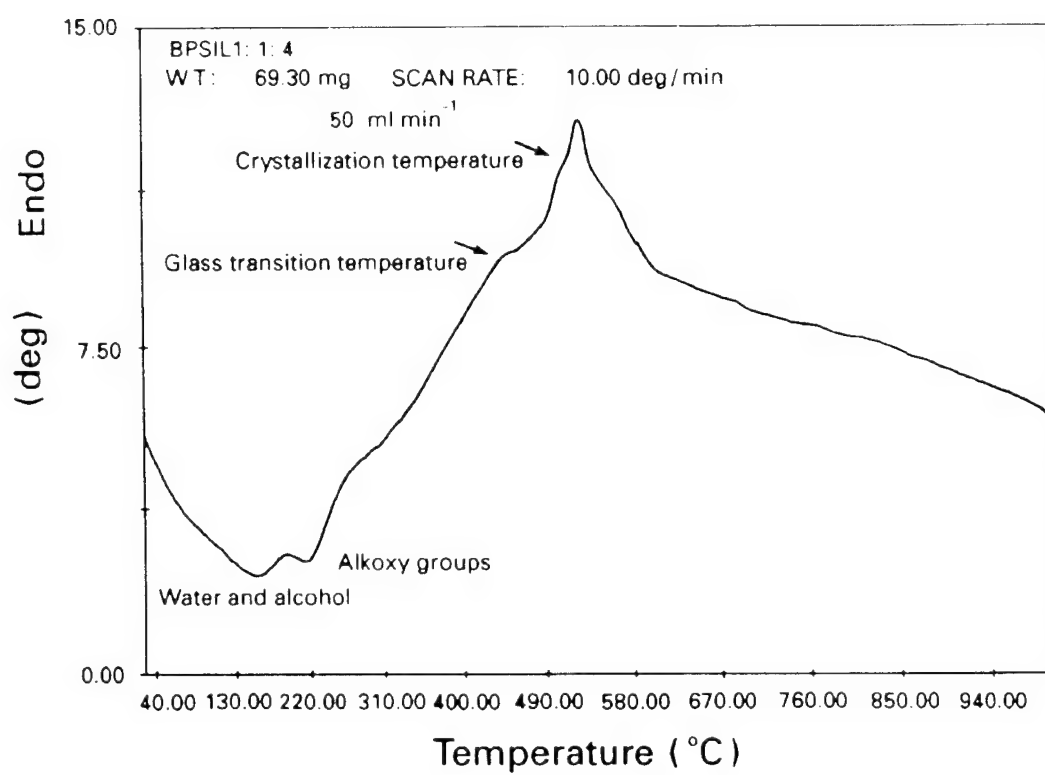


Figure II-3. Differential thermal analysis plot obtained on the borophosphosilicate glasses heated in air at 10°C/min.

Table II-1 Heat-treatment schedule that was followed for processing borophosphosilicate glass-ceramics

Temperature (°C)	Duration (hours)			
	114SG-450 and 114SP-450	114SG-500 and 114SP-500	114SG-800 and 118SG-800	114SP-800 and 118SP-800
150	5	5	5	5
200	5	5	5	5
300	10	10	10	10
400	10	10	10	10
450	24	N	N	N
500	N	24	N	N
800	N	N	96 (regrinding twice)	24

\* 114 and 118 indicate the stoichiometric ratio of  $B_2O_3$ ,  $P_2O_5$  and  $SiO_2$ .

\*\* SG and SP are referred to as Sol-Gel samples and Sol-Precipitated samples, respectively.

\*\*\* 450, 500 and 800 indicate the final temperature of heat-treatment.

\*\*\*\* Heating rate was set at 1°C/min for all heat-treatments.



respectively. The letters 'AP' represent the as-prepared state of the powders obtained via both processes.

The heat-treated powders derived using the MOSG process were sintered with and without pressure. The heat-treated powders were cold isostatically pressed (CIP) as well as cold-pressed into pellets using a pressure of either 40,000 psi or 10,000 psi. The sample that was cold isostatically pressed employing a pressure of 40,000 psi was then sintered initially at 1000°C for 24 h followed by further sintering at 1100°C for 72 h, while the sample cold-pressed with a pressure of 10,000 psi was sintered at 1100°C for 144 h. Some of the heat-treated powder was also hot-pressed using a 10 ton Electrofuel (Toronto, Canada) hot-press at 1200°C for 1 h employing a pressure of 4,500 psi in an argon atmosphere.

The calcined powders derived using the MOSP process were cold-pressed into pellets using a pressure of approximately 10,000 psi. The cold-pressed pellets were then sintered in air at a temperature of 1000°C for 72 h.

### II-1.3. Materials Characterization

X-ray Diffraction using a Rigaku  $\theta/\theta$  diffractometer was performed on the as-prepared and heat-treated gels to identify the presence of any crystalline phases. The molecular linkages of the various components in the heat-treated and the as-prepared powders were investigated using a Fourier Transform Infrared Spectrometer (Galaxy Series FTIR 5000, ATI Mattson). Infrared spectra were collected on the powders using the KBr pressed-pellet method in the spectral range of 400 - 4000  $\text{cm}^{-1}$ . The gel powders prepared using both processes were chemically analyzed for H, C and N contents while MOSP derived gels were also analyzed for their metal contents (Galbraith laboratories, Knoxville, TN). Scanning electron microscopy (SEM) analysis was performed on the sintered samples to observe the microstructure using a CamScan scanning electron microscope.

Dielectric measurements were also conducted on the sintered samples. Samples for dielectric measurements were prepared by grinding them into the approximate shape of a rectangular plate, and applying silver electrodes to the sample faces. The capacitance ' $C_m$ ' and the loss tangent were measured using an HP 4275A multifrequency LCR meter. The edge effect for capacitance, ' $C_e$ ', was estimated using the following formula based on the earlier work reported by Field [1] and later modified by Subramanian *et al.* [2].

$$C_e = \left[ 0.019 \cdot \ln\left(\frac{P}{t}\right) - 0.043 \right] \cdot P$$

where 'P' is the sample perimeter and 't' is the sample thickness.

The corrected capacitance for the sample, 'C', was then determined using the following relation.

$$C = C_m - C_c$$

Dielectric constants were calculated using the corrected capacitance in the following relationship:

$$\kappa = \left( \frac{C}{\epsilon_0} \right) \cdot \left( \frac{t}{A} \right)$$

where ' $\kappa$ ' is the dielectric constant, ' $\epsilon_0$ ' is the permittivity of vacuum, and 'A' is the area.

## II-2. Results and Discussion

### II-2.1. X-ray Analyses

Borophosphosilicate gels were prepared using both modified oxide sol-gel (MOSG) and modified oxide sol-precipitation (MOSP) processes. The resultant gels and heat-treated powders were first characterized for the presence of crystalline  $\text{BPO}_4$  phase using X-ray diffraction. The as-prepared borophosphate gel powders showed the presence of single phase crystalline  $\text{BPO}_4$  after heat-treatment at  $800^\circ\text{C}$  for 24 h in air (see Figure II-4). Figure II-5 shows the XRD traces obtained on the gel samples derived using the MOSG process. XRD profiles obtained on the as-prepared powders with  $\text{B}_2\text{O}_3:\text{P}_2\text{O}_5:\text{SiO}_2=1:1:4$  stoichiometry and  $\text{B}_2\text{O}_3:\text{P}_2\text{O}_5:\text{SiO}_2=1:1:8$  stoichiometry indicate the typical amorphous nature characteristic of the gel powders (see Figs. II-5(a) and (e)). The gel powders heat-treated at  $450^\circ\text{C}$ , below the crystalline temperature of  $490^\circ\text{C}$ , still show the amorphous nature (Figure II-5(b)), while the sample heat-treated at  $500^\circ\text{C}$ , which is just above crystallization temperature, shows the formation of crystalline  $\text{BPO}_4$  (Fig. II-5(c)). When the gel powders were heat-treated to a higher temperature of  $800^\circ\text{C}$  (Fig. II-5(d)), the peak intensities corresponding to the  $\text{BPO}_4$  phase are observed to increase in the samples corresponding to a stoichiometry of  $\text{B}_2\text{O}_3:\text{P}_2\text{O}_5:\text{SiO}_2=1:1:4$  (114SG-800). The gel samples corresponding to  $\text{B}_2\text{O}_3:\text{P}_2\text{O}_5:\text{SiO}_2=1:1:8$  stoichiometry (118SG-800) on the other hand, exhibit decreasing intensities of  $\text{BPO}_4$  phase compared to the gel samples of  $\text{B}_2\text{O}_3:\text{P}_2\text{O}_5:\text{SiO}_2=1:1:4$  stoichiometry (114SG-800) due to the presence of a relatively smaller volume fraction of available  $\text{B}_2\text{O}_3$  and  $\text{P}_2\text{O}_5$  (refer to Figs. II-5(d) and (f)).

The XRD traces obtained on the MOSP derived samples are presented in Figure II-6. The MOSP derived samples also exhibit a similar trend with respect to the formation of the  $\text{BPO}_4$  phase as the MOSG derived samples. However, there is a distinct difference in the peak intensities of the  $\text{BPO}_4$  phase observed in the MOSG (114SG-500) and MOSP (114SP-500) derived samples corresponding to the  $\text{B}_2\text{O}_3:\text{P}_2\text{O}_5:\text{SiO}_2=1:1:4$  stoichiometry heat-treated at  $500^\circ\text{C}$  (see Figs. II-5(c) and II-6(c)). The MOSG derived sample shows more intense peaks corresponding to the  $\text{BPO}_4$  phase than the MOSP derived sample when the as-prepared powders are heat-treated at  $500^\circ\text{C}$  for

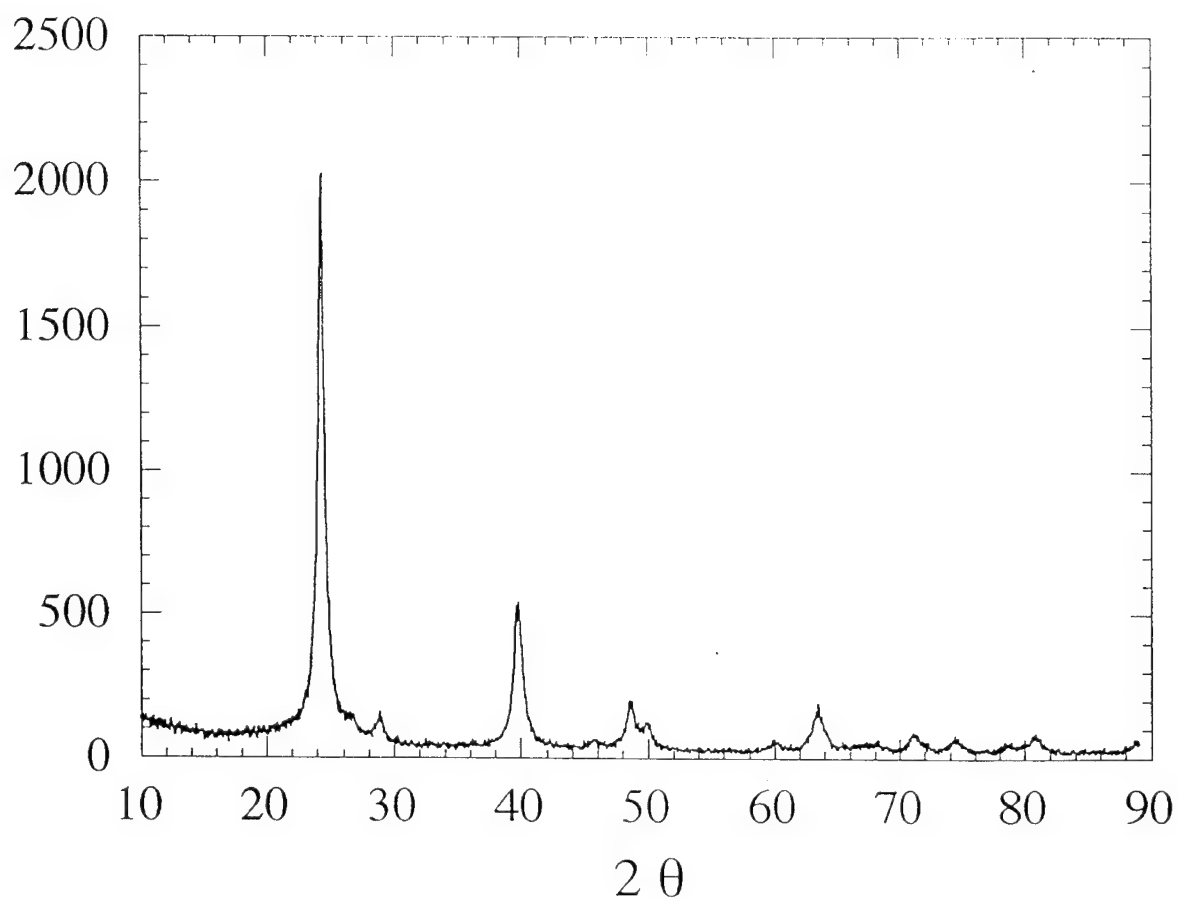


Figure II-4. X-ray diffraction trace of borophosphate gels heat-treated at 800°C for 24 hours indicating the formation of crystalline  $\text{BPO}_4$  phase.

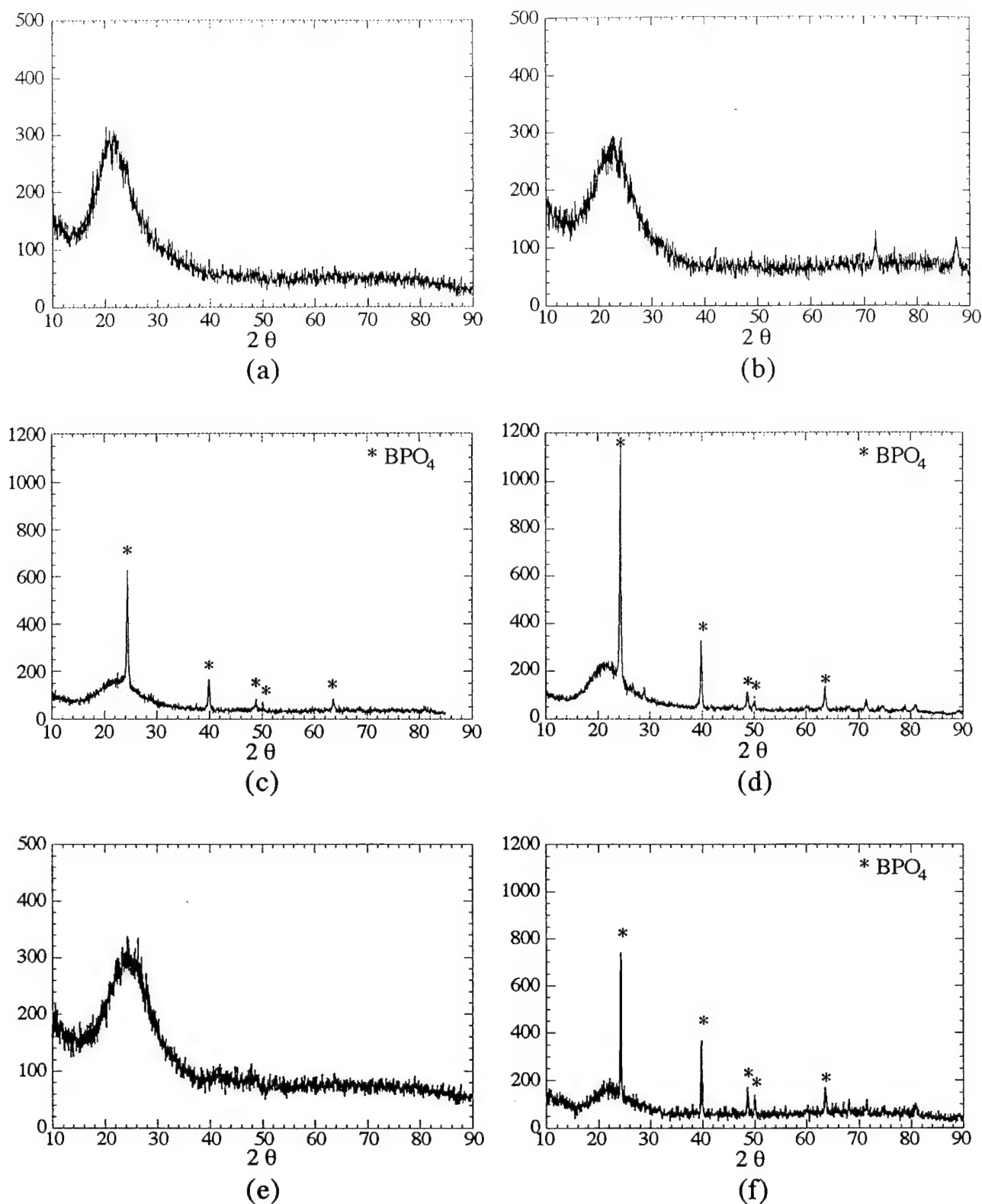


Figure II-5. X-ray diffraction traces of as-prepared and heat-treated borophosphosilicate gel powders derived using the MOSG process; (a) 114SG-AP, (b) 114SG-450, (c) 114SG-500, (d) 114SG-800, (e) 118SG-AP and (f) 118SG-800. See text for details on the nomenclature.

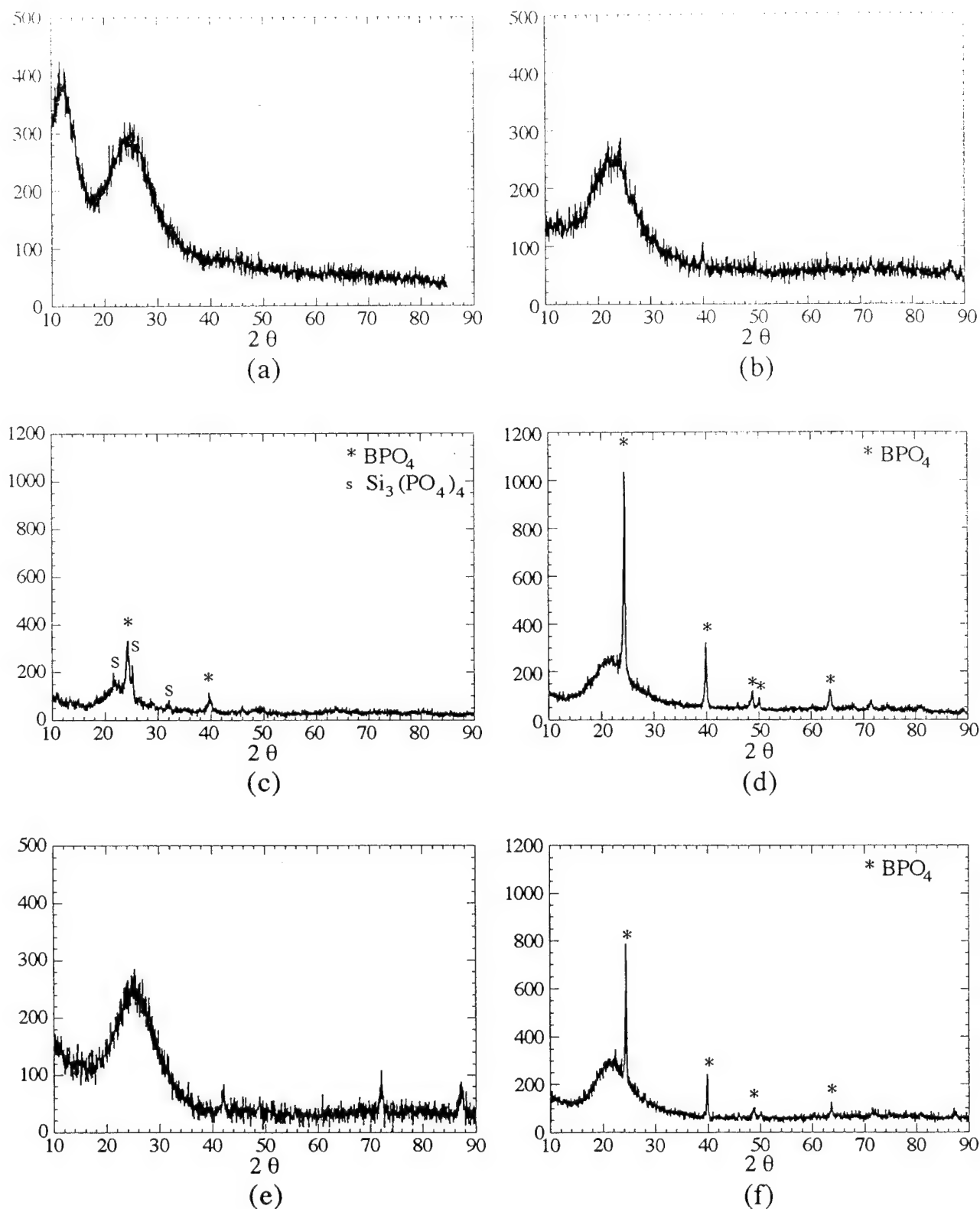


Figure II-6. X-ray diffraction traces of as-prepared and heat-treated borophosphosilicate precipitated powders derived using the MOSP process; (a) 114SP-AP, (b) 114SP-450, (c) 114SP-500, (d) 114SP-800, (e) 118SP-AP and (f) 118SP-800. See text for details on the nomenclature.

24 hours. This result indicates that the MOSG derived as-prepared powders corresponding to the  $B_2O_3:P_2O_5:SiO_2 = 1:1:4$  stoichiometry contain more B-O-P linkages than the MOSP derived sample representing an identical composition of  $B_2O_3$ ,  $P_2O_5$  and  $SiO_2$ . The other important difference between the MOSG and MOSP derived samples corresponding to the  $B_2O_3:P_2O_5:SiO_2 = 1:1:4$  stoichiometry is the appearance of  $Si_3(PO_4)_4$  phase in the MOSP derived sample (114MOSP-500) when heat-treated at  $500^\circ C$ . This phase is not observed in the corresponding MOSG derived sample heat-treated at  $500^\circ C$ . The formation of silicon phosphate could be explained based on the fact that although the starting composition ( $B_2O_3 : P_2O_5 = 1:1$ ) was selected to correspond to formation of  $BPO_4$ , there is loss of boron due to the possible presence of unreacted alkoxide that remains dissolved in the extracted liquid. The origin for this is the incomplete bridging of boron to silicon or phosphorus via formation of B-O-Si or B-O-P molecular linkages. As a result, the sol-precipitated powder is noticeably deficient in boron content. The results of chemical analyses conducted on the as-prepared powders derived using the MOSP process confirm the deficiency of boron compared to phosphorous (refer to Table II-2). Here, the molar ratio of  $B_2O_3$  to  $P_2O_5$  is 0.6:1, although the starting composition of  $B_2O_3$  to  $P_2O_5$  was selected corresponding to a 1:1 ratio. Thus, there is a 40% loss of boron in the MOSP derived gel powders. Nevertheless, the silicon phosphate phase appears to be consumed into the glass phase during heat treatment of the gel powders to  $800^\circ C$  leading to the formation of only  $BPO_4$  as the crystalline phase (see Figure II-6(d)). The excess P therefore remains probably bonded to silicon in the glass phase.

### II-2.2. IR Spectra Analyses

To investigate the structure of the glasses synthesized using different approaches, the gel powders were characterized for their molecular linkages using FTIR. The IR spectra collected on the as-prepared powders synthesized using both MOSG and MOSP processes corresponding to  $B_2O_3:P_2O_5:SiO_2=1:1:4$  stoichiometry are presented in Figure II-7. The assignment for the various peaks observed in the spectra are listed in Table II-3. The as-prepared gel powders derived from both the MOSG and MOSP processes show intense peaks corresponding to Si-O-Si ( $466\text{ cm}^{-1}$ ), O-Si-O ( $800\text{ cm}^{-1}$ ), Si-O ( $1100\text{ cm}^{-1}$ ), B-O ( $1400\text{ cm}^{-1}$ ), C-O ( $1630\text{ cm}^{-1}$ ) and  $NH_2$  ( $3210\text{ cm}^{-1}$ ) linkages, and weak peaks corresponding to B-OH ( $560\text{ cm}^{-1}$ ), B-O-Si ( $670\text{ cm}^{-1}$ ), B-O-B ( $720\text{ cm}^{-1}$ ) and  $CH_3$  ( $1193$ ,  $1450$  and  $2960\text{ cm}^{-1}$ ) linkages. In addition, there is a wide band spanning the  $3300\text{ cm}^{-1}$  to  $3700\text{ cm}^{-1}$  wave number range which could be related to unreacted Si-OH, P-OH and B-OH groups [11]. It should be noted that in comparison with the as-prepared powders derived using the MOSG process, the as-prepared powders synthesized using the MOSP process

Table II-2 Chemical analyses showing the B, P and Si contents in the as-prepared powders synthesized using the MOSP processes corresponding to the stoichiometry of  $\text{B}_2\text{O}_3:\text{P}_2\text{O}_5:\text{SiO}_2=1:1:4$

Sample	Boron*	Phosphorus*	Silicon*
MOSP	2.28	10.53	17.61

\*All the analyses are in wt%.

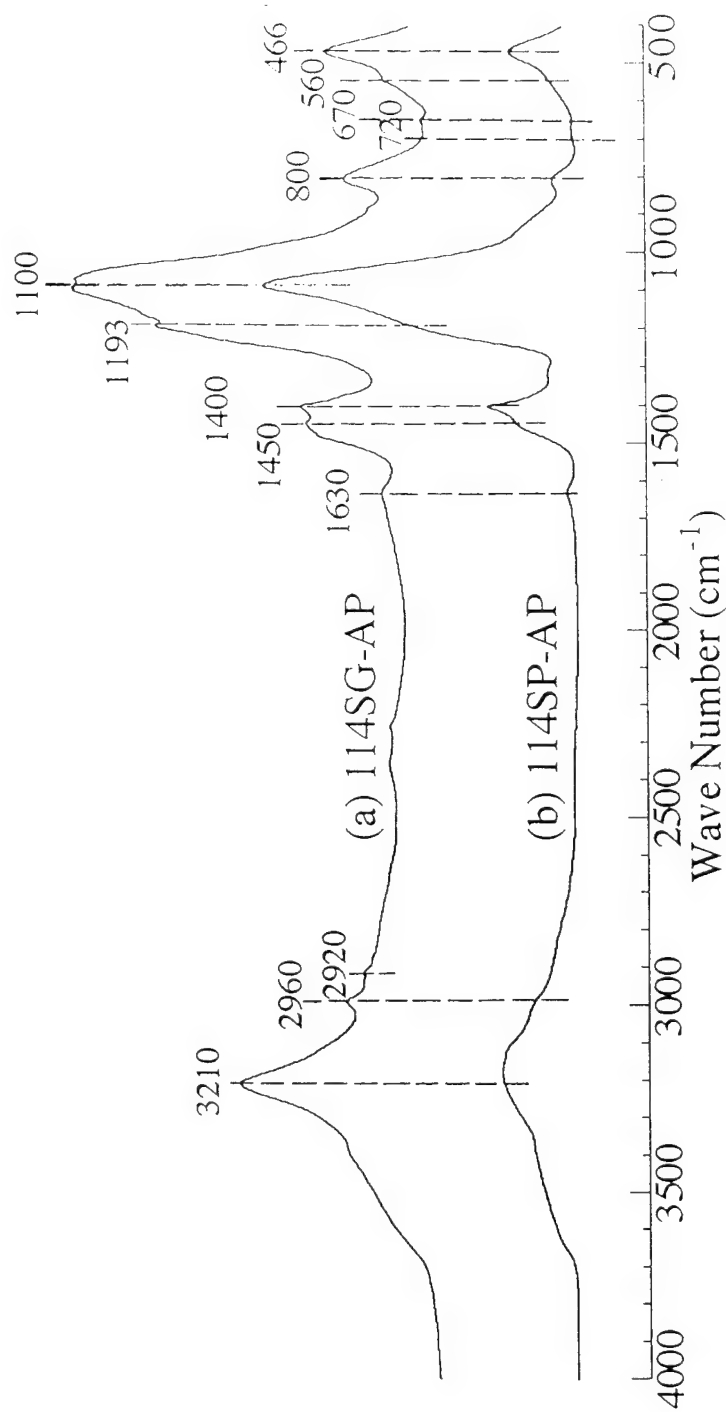


Figure II-7. Infrared absorption spectra collected on the as-prepared borophosphosilicate powders synthesized using the MOSG and MOSP processes; (a) 114SG-AP and (b) 114SP-AP. The sample nomenclature is given in the text.



Table II-3 Assignment of peaks observed in the IR spectra obtained for the as-prepared powders derived using the MOSG and MOSP processes

Wave Number (cm <sup>-1</sup> )	Assignment	114MOSG-AP	114MOSP-AP	Ref.
466	Si-O-Si (bending)	s	s	3, 4
560	B-OH	w	vw (shoulder)	5, 6
670	B-O-Si (symmetric stretch)	w	w	3, 4 5, 6
720	B-O-B	w	w	6, 7
800	O-Si-O (bending)	s	s	3, 4
1100	Si-O (stretch)	s	s	3, 4 7, 8
1193	CH <sub>3</sub> (rocking)	w	vw (shoulder)	5
1400	B-O (stretch)	s	s	4, 5 7
1450	CH <sub>3</sub> (asymmetric bending)	s	vw (shoulder)	8
1630	C-O (stretch)	w	w	9
2920	C-H (stretch)	w	N	8
2960	CH <sub>3</sub> and CH <sub>2</sub>	w	vw (shoulder)	8
3210	NH <sub>2</sub> (symmetric stretch)	s	s	10
3300-3700 (wide band)	(possibly due to residual) P-OH (3300), Si-OH	vw (shoulder)	vw (shoulder)	11

s : strong intensity   w : weak intensity   vw : very weak intensity   N : no intensity

exhibit much less intense peaks corresponding to  $\text{CH}_3$  ( $1193$ ,  $1450$  and  $2965\text{ cm}^{-1}$ ) vibrations. All the peaks related to the  $\text{CH}_3$  group appear very broad and are shown as shoulders. This result implies that the as-prepared powders corresponding to the  $\text{B}_2\text{O}_3:\text{P}_2\text{O}_5:\text{SiO}_2=1:1:4$  stoichiometry derived using the MOSP process contain a lower carbon content than the gel samples of the same stoichiometry derived using the MOSG process. Results of chemical analyses conducted on the as-prepared gel powders do confirm the above result (refer to Table II-4).

It can be seen from Table II-4 that the MOSP derived sample shows significantly reduced amounts of carbon and hydrogen compared to the MOSG derived sample. However, the MOSP derived samples contain more nitrogen due to ammonium hydroxide, which was added in excess to induce precipitation. The main reason for the MOSP derived sample to have a lower carbon content is because of the precipitation reaction, which forces the separation of residual water and alcohol from the condensed alkoxide units. The other distinct difference between the as-prepared powders derived using both processes is the intensity of the peak observed at  $560\text{ cm}^{-1}$  due to the presence of unreacted B-OH groups. The as-prepared powders derived using the MOSG process exhibit a more intense peak at this wave number compared to the MOSP derived sample. This is an indication that more unreacted B-OH groups remain in the gel samples derived using the MOSG process. This distinction is quite important since the presence of unreacted B-OH groups in the as-prepared powder could induce significant changes in the gel structure after heat-treatment.

Figure II-8 shows the IR spectra collected on the MOSG derived gel powders corresponding to  $\text{B}_2\text{O}_3:\text{P}_2\text{O}_5:\text{SiO}_2=1:1:4$  stoichiometry, heat-treated at  $450^\circ\text{C}$ ,  $500^\circ\text{C}$  and  $800^\circ\text{C}$ , respectively. The Figure also shows for comparison, the IR spectra collected on the borophosphate gel powders heat-treated at  $800^\circ\text{C}$  for 24 hours in air. The borophosphate gel powders, which indicated the presence of crystalline  $\text{BPO}_4$  phase in the X-ray diffraction analysis (Figure II-4), shows intense peaks corresponding to  $\text{BO}_4$  groups ( $490\text{ cm}^{-1}$ ) [12], B-O-P ( $624\text{ cm}^{-1}$ ) [13], and P-O-P ( $952$  and  $1149\text{ cm}^{-1}$ ) [12, 14] (see Figure II-8(d)). All heat-treated powders derived using the MOSG process show Si-O-Si ( $466\text{ cm}^{-1}$ ), B-O-P ( $624\text{ cm}^{-1}$ ), O-Si-O ( $800\text{ cm}^{-1}$ ), B-O-Si ( $930\text{ cm}^{-1}$ ) [3, 7, 14], Si-O ( $1100\text{ cm}^{-1}$ ), B-O-B ( $1350\text{ cm}^{-1}$ ) [14] and B-O ( $1400\text{ cm}^{-1}$ ) linkages. In addition, there is a wide band spanning  $3300$  to  $3600\text{ cm}^{-1}$  for gel samples heat-treated up to  $500^\circ\text{C}$ , which may be related to the presence of unreacted Si-OH, P-OH, or B-OH groups [11]. This band disappears in the sample which was heat-treated at  $800^\circ\text{C}$  (see Figure II-8(a)). The peak corresponding to B-O-P ( $624\text{ cm}^{-1}$ ) linkage is seen to appear as the  $\text{BPO}_4$  phase forms, and the intensity of the peak continues to increase with the corresponding increase in the heat-treatment

Table II-4 Chemical analyses showing the C, H and N contents in the as-prepared powders synthesized using the MOSG and MOSP processes corresponding to the stoichiometry of  $\text{B}_2\text{O}_3:\text{P}_2\text{O}_5:\text{SiO}_2=1:1:4$

Sample	Carbon*	Hydrogen*	Nitrogen*
MOSG	7.75	3.27	0.57
MOSP	0.65	2.26	4.35

\*All the analyses are in wt%

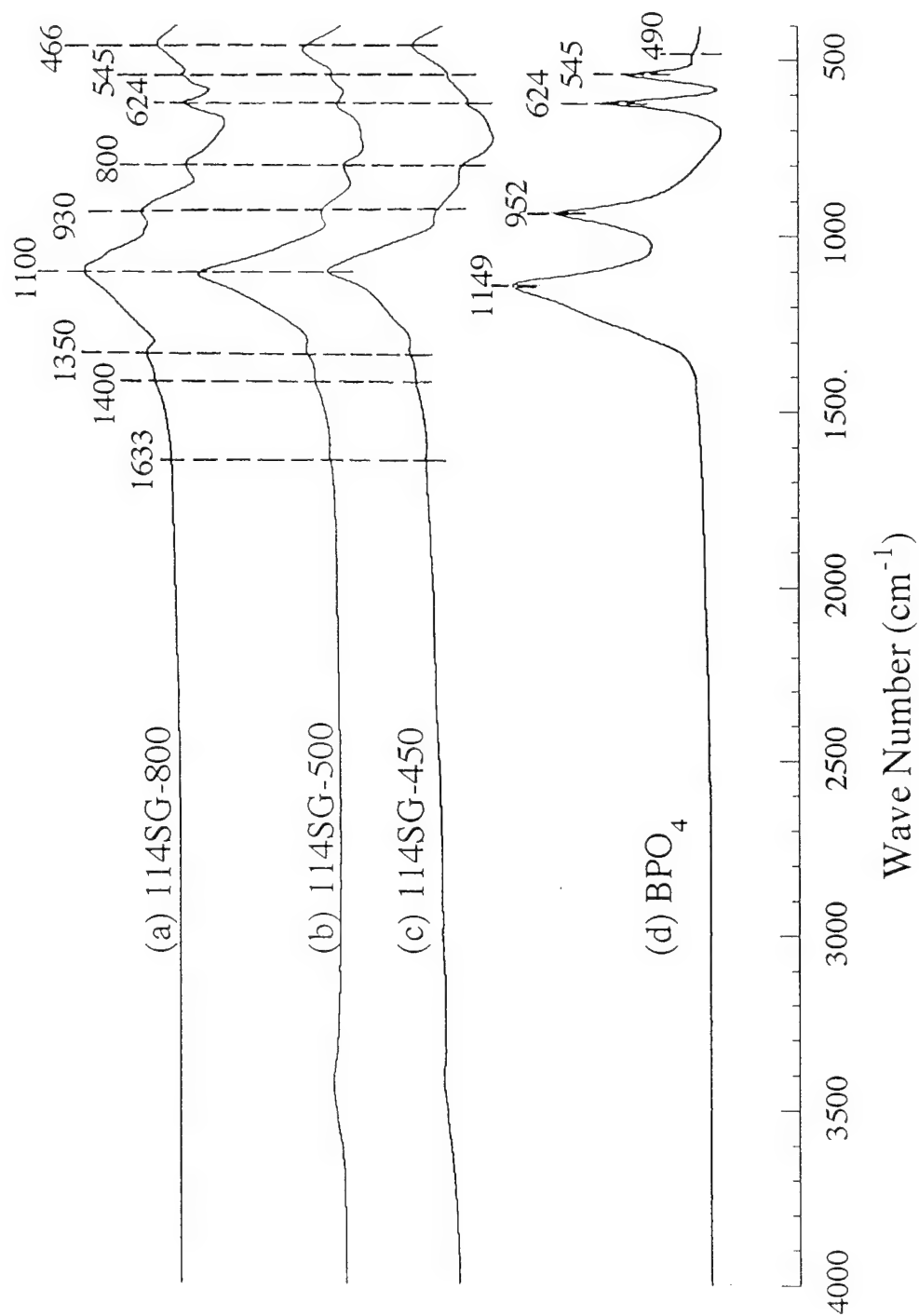


Figure II-8 Infrared absorption spectra collected on the MOSG derived heat-treated borophosphosilicate powders and heat-treated borophosphate gels; (a) 114SG-800, (b) 114SG-500, (c) 114SG-450 and (d) BPO<sub>4</sub>. See text for details on sample identification.

temperature. However, it is remarkable that this peak related to  $\text{BPO}_4$  phase (B-O-P linkage :  $624\text{ cm}^{-1}$ ) exists even in the gel sample heat-treated at  $450^\circ\text{C}$  (114SG-450) which is below the crystallization temperature ( $T_c=490^\circ\text{C}$ ). This suggests that the MOSG process does indeed allow for the formation of B-O-P linkages in the gel structure facilitating the crystallization of  $\text{BPO}_4$ . On the other hand, peaks related to the  $\text{CH}_3$  group ( $1193$ ,  $1450$  and  $2960\text{ cm}^{-1}$ ) almost disappear and the presence of only a small peak corresponding to C-O ( $1630\text{ cm}^{-1}$ ) vibration is seen after heat treatment at  $450^\circ\text{C}$ . This peak decreases with gradual increase in the heat-treatment temperature as expected, and is completely eliminated after heat-treatment at  $800^\circ\text{C}$ .

IR spectra obtained on the powders derived using the MOSP process corresponding to the  $\text{B}_2\text{O}_3:\text{P}_2\text{O}_5:\text{SiO}_2 = 1:1:4$  stoichiometry, which were heat-treated at  $450^\circ\text{C}$ ,  $500^\circ\text{C}$  and  $800^\circ\text{C}$ , respectively, are presented in Figure II-9. Similar to the gel powders derived using the MOSG process, the peak corresponding to B-O-P ( $624\text{ cm}^{-1}$ ) linkage is seen to appear as the crystalline  $\text{BPO}_4$  phase forms, and peaks related to carbon seem to disappear after heat-treatment. In addition, there is also a weak peak at  $670\text{ cm}^{-1}$  corresponding to B-O-Si vibrations, which is seen only at  $450^\circ\text{C}$  and  $500^\circ\text{C}$ . It should be noted that at  $500^\circ\text{C}$ , XRD data (see Figure 5(c)) for this glass indicates the presence of crystalline  $\text{Si}_3(\text{PO}_4)_4$ . Thus, combining the IR analyses with the XRD results, it can be concluded that at  $500^\circ\text{C}$ , in comparison to the MOSG derived samples, boron remains largely bonded to silicon in the glass phase. Subsequent heat treatment to  $800^\circ\text{C}$  leads to crystallization of  $\text{BPO}_4$  leaving behind the excess phosphorus probably bonded to silicon in the amorphous borophosphosilicate matrix.

Based on these observations, a number of structural differences in the gel powders can be highlighted. One of the distinct differences between the heat-treated gel powders synthesized using the MOSG and the MOSP processes is that the B-O-B linkage is seen to appear at  $1350\text{ cm}^{-1}$  only in the IR spectra of the samples obtained using the MOSG process. In addition, the B-O bond is seen as a shoulder at  $1400\text{ cm}^{-1}$  in the MOSG derived samples, while the MOSP derived samples do not show the presence of B-O-B linkage at  $1350\text{ cm}^{-1}$ . The peak corresponding to B-O-B linkage at  $1350\text{ cm}^{-1}$  appears in all heat-treated samples synthesized using the MOSG process and does not seem to change significantly with heat-treatment temperature. This result is related to the fact that the as-prepared gel powders derived from the MOSG process contain more unreacted B-OH groups compared to those synthesized using the MOSP process. In other words, the unreacted B-OH groups in the as-prepared powders derived using the MOSG process condense during the heat-treatments to result in B-O-B linkages in the glasses. The presence of these units could very

well reflect the microsegregation of boron oxide in these glasses. The absence of B-OH groups in the IR spectra of MOSP derived powders is probably due to the loss of boron occurring during extraction of the liquid after sol-precipitation.

Another important difference between MOSG and MOSP derived samples corresponding to the same stoichiometry of  $\text{B}_2\text{O}_3:\text{P}_2\text{O}_5:\text{SiO}_2=1:1:4$  is that the MOSG derived sample heat-treated at  $450^\circ\text{C}$  (below crystallization temperature,  $T_c = 490^\circ\text{C}$ ) shows the presence of B-O-P ( $624\text{ cm}^{-1}$ ) linkage which is related to the crystalline phase of  $\text{BPO}_4$ , while the MOSP derived sample heat-treated at the same temperature exhibits only weak absorption corresponding to B-O-Si ( $670\text{ cm}^{-1}$ ) without showing the presence of B-O-P linkages. Furthermore, the MOSG derived sample heat-treated at  $500^\circ\text{C}$  (just above the crystallization temperature) shows a much more intense peak corresponding to the B-O-P linkages in comparison with MOSP derived sample heat-treated at  $500^\circ\text{C}$  (refer to Figure II-8(b) and II-9(b)). This result is consistent with the X-ray data which show that the MOSG derived sample reveals more intense peaks corresponding to crystalline  $\text{BPO}_4$  phase than the MOSP derived sample heat-treated at  $500^\circ\text{C}$  (refer to Figs. II-5(c) and II-6(c)). Consequently, it can be concluded that the unreacted B-OH groups in the as-prepared powders of MOSG process not only result in the formation of B-O-B units leading to microsegregation but also react with unreacted P-OH groups to form B-O-P linkages during the heat-treatments even below the crystallization temperature of the  $\text{BPO}_4$  phase. Therefore, it can be concluded that the formation of B-O-P bonds due to the unreacted B-OH groups in the as-prepared powders derived using the MOSG process helps in the nucleation and crystallization of  $\text{BPO}_4$  phase just above its crystallization temperature. In addition, the presence of these linkages also contributes to the observed differences in the peak intensities corresponding to the crystalline  $\text{BPO}_4$  phase.

The precipitation reaction responsible for the MOSP process, on the other hand, leads to the separation of the condensed alkoxide units from solution. As a result, most of unreacted groups can be extracted and remain in solution during centrifugal separation. Hence, the MOSP process, while promoting loss of boron, leads to a gel with a lower boron content that remains largely bonded to silicon (B-O-Si linkages) in the glassy borophosphosilicate phase. Consequently, the excess P remains as crystalline  $\text{Si}_3(\text{PO}_4)_4$  and in the glass phase at  $500^\circ\text{C}$ , limiting the formation of B-O-P linkages in the as-prepared powders. Further heat treatment to  $800^\circ\text{C}$ , however, leads to dissolution of the  $\text{Si}_3(\text{PO}_4)_4$  phase and subsequently, the crystallization of  $\text{BPO}_4$ .

The other interesting aspect is the presence of the unknown absorption at  $545\text{ cm}^{-1}$  seen in the heat-treated samples of both the MOSG and MOSP derived gel powders containing B-O-P linkages as well as in the borophosphate gel powders heat-treated at  $800^\circ\text{C}$ . This absorption is also seen to

increase with corresponding increase in the heat treatment temperature. Although the peak at  $545\text{ cm}^{-1}$  occurs at a similar position corresponding to the B-OH vibration at  $560\text{ cm}^{-1}$ , its presence in heat-treated samples makes its assignment due to the hydroxide quite tenuous. This is mainly because its occurrence is seen only after crystallization of the  $\text{BPO}_4$  phase (along with the formation of B-O-P linkage at  $624\text{ cm}^{-1}$ ) in both MOSG and MOSP derived samples. Moreover, the as-prepared powders derived from the MOSP process to begin with, do not show a strong vibration corresponding to the presence of B-OH bonds. On heat treatment at  $800^\circ\text{C}$ , the wide band around  $3300$  to  $3600\text{ cm}^{-1}$  due to the presence of these unreacted groups are also eliminated. Thus if the absorption at  $545\text{ cm}^{-1}$  were to represent the B-OH linkage, it should decrease with temperature and disappear at  $800^\circ\text{C}$  wherein the wide band due to unreacted -OH groups have totally disappeared. Therefore, it can be deduced that this peak is related to the formation of the  $\text{BPO}_4$  phase since its presence is seen in the heat-treated samples of both MOSG and MOSP derived gel powders containing B-O-P linkage as well as in the borophosphate gel heat-treated at  $800^\circ\text{C}$ . Furthermore, the intensity of the peak is seen to increase with the crystallization of the  $\text{BPO}_4$  phase (compare IR spectra of 114SP-800 with 114SP-450 and 114SP-500 in Figure 8). All these aspects indicate consistently that the unknown absorption is indeed characteristic of the borophosphate phase.

Figure II-10 shows the IR spectra obtained from both, the MOSG and MOSP derived samples corresponding to the  $\text{B}_2\text{O}_3:\text{P}_2\text{O}_5:\text{SiO}_2=1:1:8$  stoichiometry heat-treated at  $800^\circ\text{C}$ . In comparison with the samples of  $\text{B}_2\text{O}_3:\text{P}_2\text{O}_5:\text{SiO}_2=1:1:4$  stoichiometry, the relative intensities of absorptions related to B or P (B-O at  $1400\text{ cm}^{-1}$ , B-O-P at  $624\text{ cm}^{-1}$ , etc.) are lowered due to the smaller amounts of  $\text{B}_2\text{O}_3$  and  $\text{P}_2\text{O}_5$  present in these samples. However, similar to the samples corresponding to  $\text{B}_2\text{O}_3:\text{P}_2\text{O}_5:\text{SiO}_2=1:1:4$  composition, only the MOSG derived sample shows the presence of the B-O-B linkage at  $1350\text{ cm}^{-1}$ . At the same time, the absorption centered at  $545\text{ cm}^{-1}$  is also lower in intensity in comparison to the  $\text{B}_2\text{O}_3:\text{P}_2\text{O}_5:\text{SiO}_2=1:1:4$  composition samples synthesized using both the MOSG and MOSP processes. The IR results obtained for gel powders corresponding to both  $\text{B}_2\text{O}_3:\text{P}_2\text{O}_5:\text{SiO}_2=1:1:4$  and  $1:1:8$  compositions imply that the microsegregation of boron oxide occurs during the heat-treatments of the MOSG derived samples due to the presence of unreacted B-OH groups in the as-prepared powders. Thus, the modified oxide sol-gel derived samples could lead to eventual segregation of  $\text{B}_2\text{O}_3$  and formation of the crystalline oxide as has been reported by Nogami and Moriya [7]. In this sense, the MOSG process therefore results in gels which could be considered to be inhomogeneous at the molecular level in contrast to the MOSP process. The MOSP process, on the other hand, leads to gels with

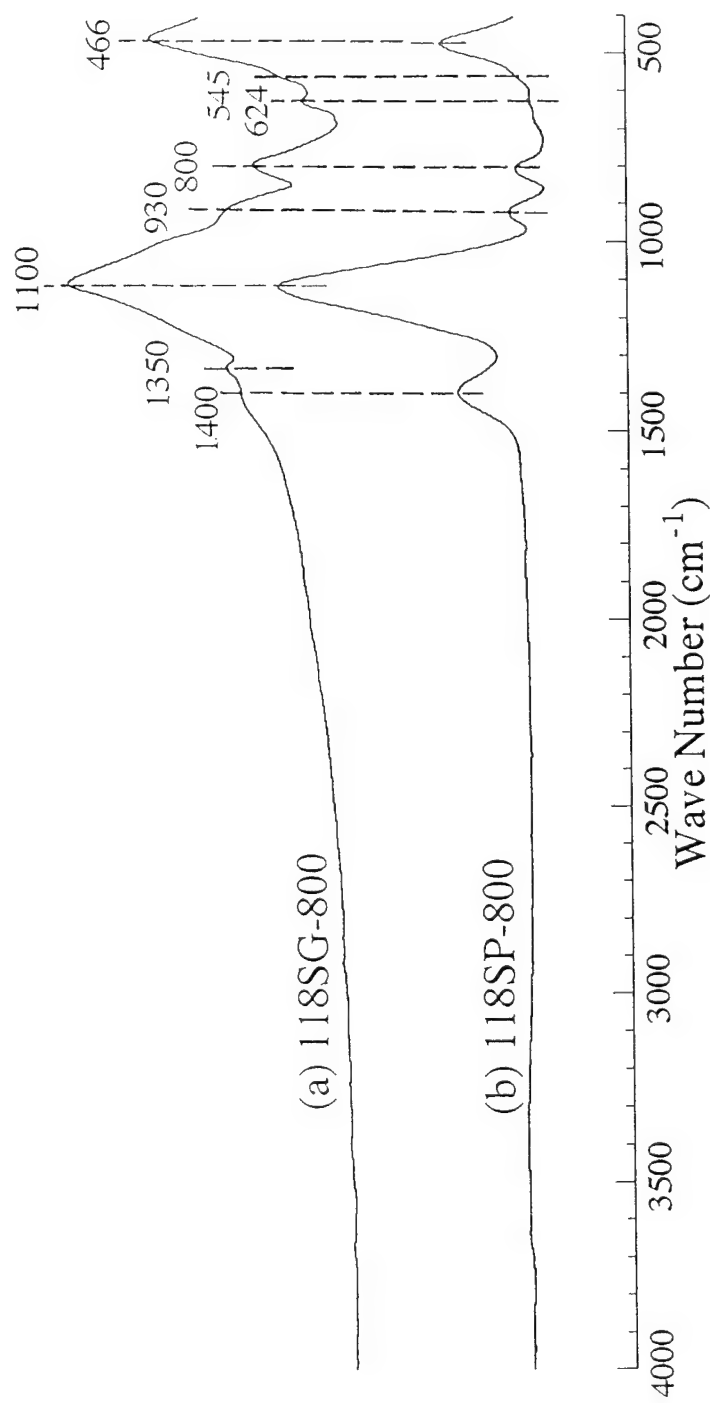


Figure II-10. Infrared absorption spectra collected on the heat-treated borophosphosilicate powders derived using the MOSG and MOSP processes with stoichiometric ratio of  $\text{B}_2\text{O}_3:\text{P}_2\text{O}_5:\text{SiO}_2=1:1:8$ ; (a) 118SG-800 and (b) 118SP-800. See text for sample details.



reduced C and B contents due to extraction of unreacted alkoxy and hydroxy complexes. The loss of boron and carbon renders the process truly beneficial since homogeneous gels can be synthesized which eventually lead to the formation of glass-ceramics containing  $\text{BPO}_4$  as the crystalline phase. The loss of boron could, however, be prevented by allowing the solution containing the initial components to react for a longer period of time prior to initiation of the precipitation reaction. It may be worthwhile to compare the structure of the gels at this stage with the MOSG derived gels for true molecular homogeneity.

### *II-2.3. Sintering Behavior*

Figure II-11 shows the morphology of as-prepared and heat-treated gels corresponding to the composition,  $\text{B}_2\text{O}_3:\text{P}_2\text{O}_5:\text{SiO}_2 = 1:1:4$ , derived using the MOSG process. Heat-treated gels show the porous nature (Figure II-11(b)), which could be expected because the glass transition temperature and the crystallization temperature of the  $\text{BPO}_4$  phase occur at very close temperature intervals, for this glass. Moreover, both of these processes overlap with the temperature range (400-700°C) most favored for carbon removal. One can therefore envisage the formation of porosity due to the loss of carbon from the softened gels. The sintered samples showed a fair amount of visible porosity mainly due to the entrapment of air and the formation of CO and  $\text{CO}_2$  from the reaction of carbon in the gels with oxygen. The loss of these gases becomes increasingly difficult due to the viscous nature of the gels. Even after considerable heat treatments, complete removal of the trapped bubbles is extremely difficult. The presence of porosity, although conducive to obtaining low dielectric constants, is deleterious to achieving good strength and mechanical integrity. Therefore, hot pressing experiments were conducted by pressing samples using a pressure of 4,500 psi at 1200°C for 1h in argon. The hot-pressed glass-ceramic was examined for its microstructure using SEM after the sample surface was etched with 1M HF acid. The analysis revealed an overetched specimen surface exhibiting small particles of crystallized boron phosphate in a dense glass matrix as shown in Figure II-12. The micrographs also reveal a noticeable decrease in porosity for the hot-pressed sample, which will provide for improved structural and mechanical properties.

The calcined heat-treated powders derived using the MOSP process were sintered at 1000°C for 72 h in air. Figure II-13 shows the micrographs obtained on over-etched surface of sintered sample derived using the MOSP process. The micrographs show the presence of small sub-micron sized (0.5  $\mu\text{m}$ ) crystallites embedded in a glass matrix. Energy-Dispersive X-ray Analysis (EDAX) was performed on the MOSP derived sintered sample and the X-ray traces collected are shown in Figure II-14. The traces clearly show the presence of a large amounts of silicon in the matrix and significant concentrations of phosphorus in the particles. These results suggest that the matrix

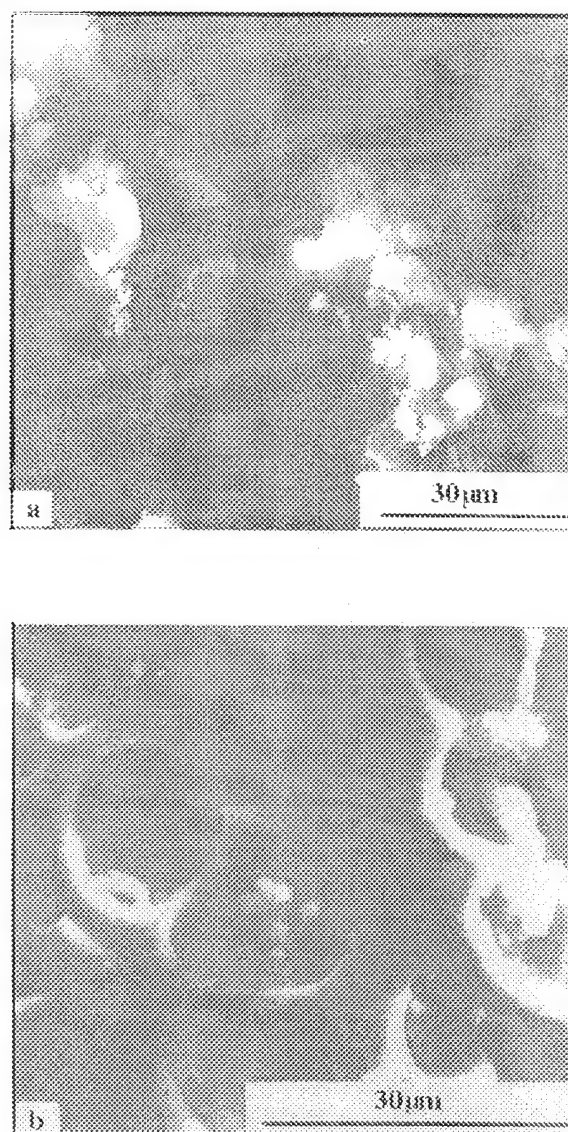


Figure II-11. Scanning electron micrographs showing the morphology of the (a) as-prepared and (b) heat-treated (at 800°C for 96 h) borophosphosilicate ( $\text{B}_2\text{O}_3\text{:P}_2\text{O}_5\text{:SiO}_2=1:1:4$ ) glass and glass-ceramic derived using the MOSG process. Note the porous microstructure of the heat-treated gels due to the simultaneous processes of loss of carbon and softening of the glass.

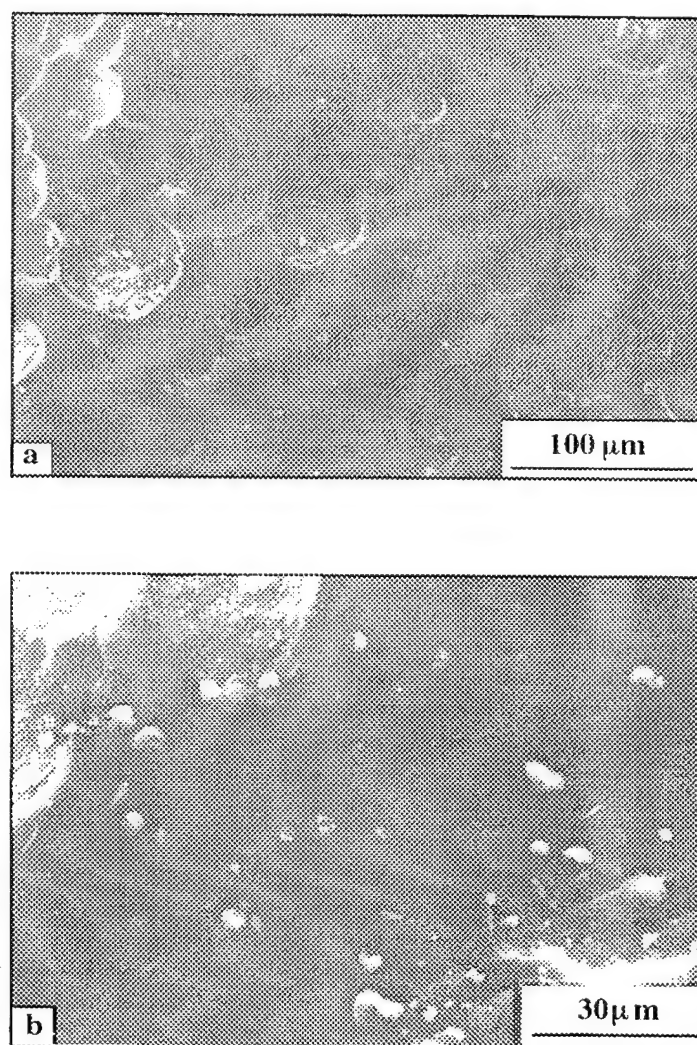


Figure II-12. Scanning electron micrographs showing the microstructure of the hot-pressed (1200°C, 4500 psi, 1h, in Ar) borophosphosilicate ( $\text{B}_2\text{O}_3\text{:P}_2\text{O}_5\text{:SiO}_2=1\text{:}1\text{:}4$ ) glass-ceramic derived using the MOSG process. The micrographs show the over-etched surface of the glass-ceramic containing  $\text{BPO}_4$  crystallites.

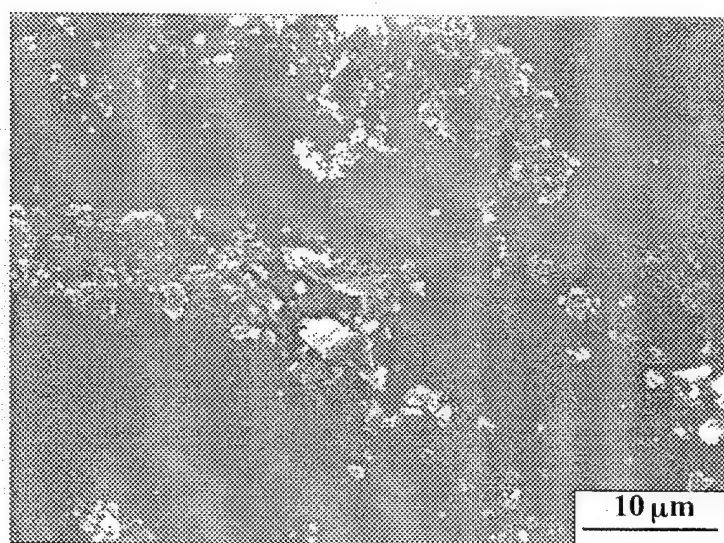
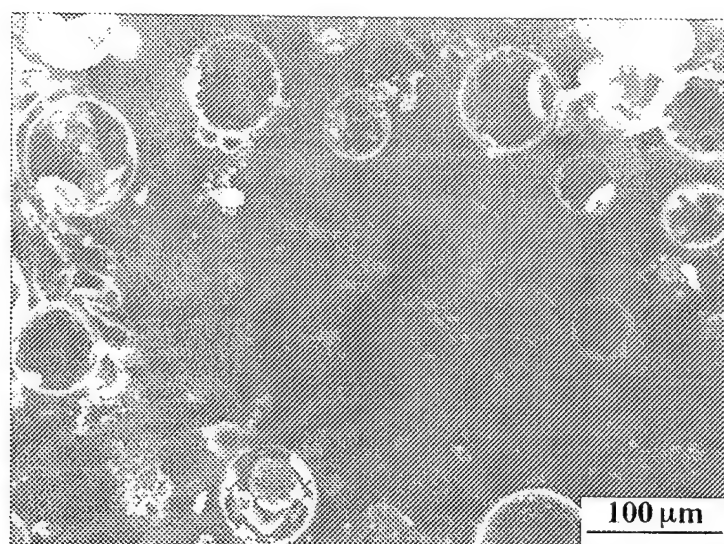


Figure II-13 Scanning electron micrographs showing the microstructure of a sintered borophosphosilicate ( $\text{B}_2\text{O}_3:\text{P}_2\text{O}_5:\text{SiO}_2=1:1:4$ ) sample derived using the MOSP process.

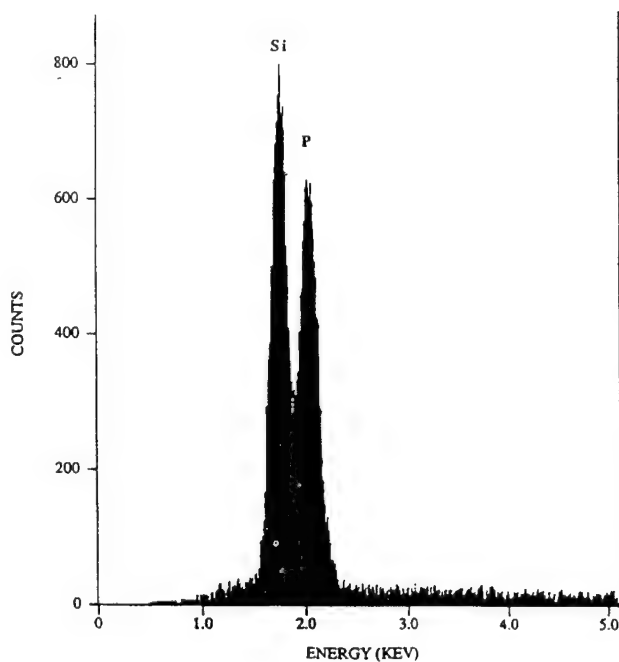
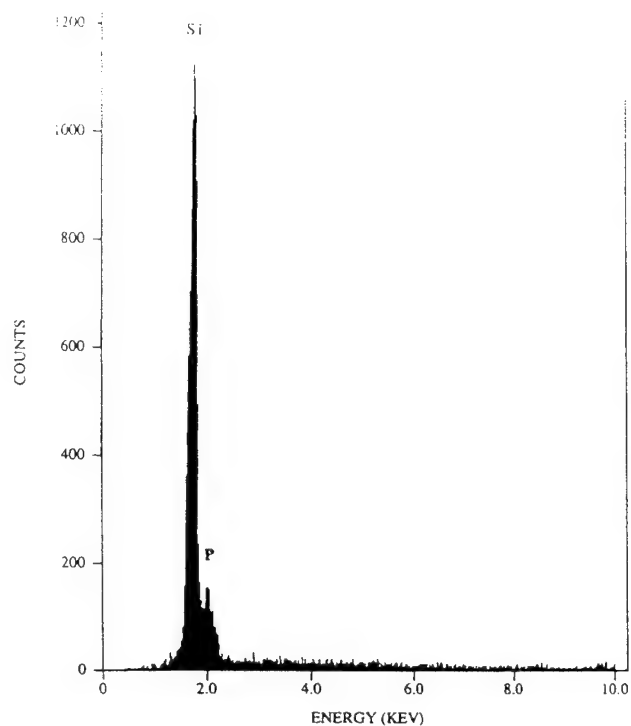


Figure II-14 Results of Energy-Dispersive X-ray Spectroscopy (EDAX) performed on (a) the matrix and (b) the particles of sintered borophosphosilicate ( $\text{B}_2\text{O}_3\text{:P}_2\text{O}_5\text{:SiO}_2=1\text{:}1\text{:}4$ ) glass-ceramic derived using the MOSP process. Note the ratio of Si:P in the matrix and the particles.

phase is essentially a borophosphosilicate glass with high silicon content, while the particles correspond to crystallized boron phosphate. EDAX analysis is, therefore, consistent with the X-ray diffraction results which showed crystalline  $\text{BPO}_4$  phase. The sintered sample also showed a small amount of visible porosity. However, the sintered glass-ceramic obtained using the MOSP process showed a significant reduction in porosity compared to the glass-ceramic produced via the MOSG process. This improvement is linked to the fact that many of the problems associated with the removal of carbon encountered in the MOSG experiments are avoided in the MOSP approach. The precipitation reaction forces the separation of the condensed alkoxide units from alcohol and water. As a result, the powders have a reduced amount of residual carbon as can be seen in the IR results and chemical analyses, which results in a much smaller volume fraction of bubbles caused by the formation and escape of carbon dioxide gas.

#### *II-2.4. Dielectric Properties*

Dielectric measurements were conducted on both the MOSG and MOSP derived sintered samples as well as the MOSG derived hot-pressed sample. The results of these dielectric measurements are shown in Table II-5. As can be seen, the samples exhibit dielectric values in the range of 3.86-4.36 and dissipation factors of 0.0007-0.0010 at a frequency of 1 MHz. Among the MOSG derived samples, sample 2 showed a much lower dielectric constant (3.94) as opposed to sample 1 even though it was sintered for a considerably longer time. This could be due to the fact that sample 2 have been prepared by sintering the cold-pressed dried gel powders using a pressure of 10,000 psi, while sample 1 had been prepared by sintering the isostatically cold-pressed dried gel powders using a higher pressure of 40,000 psi. The presence of a large amount of initial porosity in sample 2 combined with the viscous nature of the glass, makes it extremely difficult to eliminate the pores completely despite the long sintering time. Thus, although both samples had a fair amount of porosity, it can be expected that sample 2 is much more porous comparison with sample 1, which is reflected in its lower dielectric constant. On the other hand, measurements on the hot-pressed sample indicated dielectric values of 4.25 at 1 MHz with a dissipation factor of 0.0018. There seems to be no significant deviation in the dielectric constant values due to hot-pressing, although there is a significant reduction in porosity. Nevertheless, the dielectric constant of the densest sample obtained by hot pressing is less than 4.5, suggesting the potential of these materials as substrates in microelectronic packaging.

Sintered sample derived using the MOSP process exhibits a dielectric constant of 3.86 and a dissipation factor of 0.0007 both taken at a frequency of 1 MHz. Despite the reduced porosity in the samples, these values are lower than those obtained on the gels prepared using the MOSG process (3.94-4.36 and dissipation factors of 0.0007-0.0010 at 1 MHz). This reduction of

Table II-5 Dielectric constant and dissipation factor of sintered borophosphosilicate glasses and glass-ceramics synthesized using the MOSG and MOSP processes corresponding to the stoichiometry of  $B_2O_3:P_2O_5:SiO_2=1:1:4$

Sample	Sintering condition	Measured at 100 kHz		Measured at 1 MHz	
		Dielectric Constant	Dissipation Factor	Dielectric Constant	Dissipation Factor
1 (MOSG)	CIP (40,000psi) sintered in air 1000°C, 24 h 1100°C, 72 h	4.37	0.0015	4.36	0.0007
2 (MOSG)	Cold-pressed (10,000psi) sintered in air 1100 °C, 144 h	3.94	0.0019	3.94	0.0010
3 (MOSG)	Hot-pressed in Ar 1450 °C, 4,500psi	-	-	4.25	0.0018
4 (MOSP)	Cold-pressed (10,000psi) sintered in air 1000 °C, 72 h	3.86	0.0006	3.86	0.0007



dielectric constant values is a reflection of the difference in the volume fraction of the crystallized boron phosphate phase, and the corresponding larger volume fraction of the glassy phase in the MOSP derived powders. The reduction in the volume fraction of crystallized boron phosphate could occur due to either differences between the gel structures of MOSP and MOSG powders or the loss of boron and phosphorous as soluble hydrolyzed species in the filtrate.

### II-3. Conclusions

Borophosphosilicate glasses and glass-ceramics were synthesized using both modified oxide sol-gel (MOSG) and modified oxide sol-precipitation (MOSP) processes. The two approaches lead to gels and powders possessing different molecular structures. As a result, they display differences in their crystallization behavior. The as-prepared powders corresponding to the  $\text{B}_2\text{O}_3:\text{P}_2\text{O}_5:\text{SiO}_2=1:1:4$  and  $1:1:8$  stoichiometry, derived using the MOSG process contain more unreacted B-OH groups compared to those derived using the MOSP process. This is because the precipitation reaction forces the separation of the condensed alkoxide units from solution during centrifugation leaving most of the unreacted groups dissolved in solution. The presence of these unreacted B-OH groups in the as-prepared powders derived using the MOSG process undergo condensation during heat-treatments and cause microsegregation of boron oxide, while also forming B-O-P linkages below the crystallization temperature ( $T_c$ ) of  $\text{BPO}_4$ . The formation of these B-O-P linkages in the MOSG derived samples helps to nucleate  $\text{BPO}_4$  phase and leads to rapid crystallization of  $\text{BPO}_4$  in comparison to the MOSP derived samples. As a result, MOSG derived samples possess a larger amount of the crystalline  $\text{BPO}_4$  phase than the MOSP derived samples when heat-treated just above the crystallization temperature of  $490^\circ\text{C}$ .

The as-prepared gel powders synthesized using the MOSG and MOSP processes also differ in carbon contents. The precipitation process (MOSP) results in powders with much less carbon content, which causes a significant reduction in porosity compared to the glass-ceramics produced through the MOSG process. At the same line, there is loss of boron in the gel powders derived using the MOSP process. This is because the precipitation reaction forces the separation of the condensed alkoxide units from alcohol and water. This separation of solvent and residual alkoxy groups helps in preventing microsegregation of boron oxide and also results in glasses with reduced carbon content. Although the gel powders contain reduced amount of boron, it does not affect the crystallization of  $\text{BPO}_4$  at  $800^\circ\text{C}$ . Consequently, these gel powders lead to sintered glass-ceramics exhibiting  $\text{BPO}_4$  as the crystalline phase with reduced porosity. The increased ease of carbon removal from the as-prepared gel powders coupled with the reduced porosity seen in the pressurelessly sintered samples suggests that the MOSP process is quite attractive for processing oxide glasses and glass-ceramics in comparison to the MOSG process. However, the sintered



specimens prepared using both the MOSG and MOSP processes exhibited dielectric constants in the range of 3.86-4.36 at a frequency of 1 MHz, which is indicative of the excellent potential of these materials for use as substrates in electronic packaging.

## II-4. References

- [1] R.F. Field, Proc. Am. Soc. Test. Mater., 54 (1954) 456.
- [2] M.A. Subramanian, R.D. Shannon, B.H.T. Chai, M.M. Abraham, and M.C. Wintersgill, Phys. Chem. Miner., 16 (1989) 741.
- [3] J. C. Brinker and G.W.Scherer, Sol-Gel Science: The Physics and Chemistry of Sol-Gel Processing, (Academic Press, Boston, 1990).
- [4] C.J. Brinker and D.M. Haaland, J. Am. Ceram. Soc. 66 (1983) 758.
- [5] M. Prassas and L. L. Hench, in: Ultrastructure Processing of Ceramics, Glasses, and Composites, Eds. L.L. Hench and D.R. Ulrich (Willey, New York, 1984) p. 100.
- [6] A.D. Irwin, J.S. Holgren, T.W. Zerda and J. Jonas, J. Non-Cryst. Solids 89 (1987) 191.
- [7] M. Nogami and Y. Moriya, J. Non-Cryst. Solids 48 (1982) 359.
- [8] D.R. McKenzie, Thin Solid Films 108 (1983) 247.
- [9] F. Babonneau, L. Coury AND J. Livage, J. Non-Cryst. Solids 121 (1990) 153.
- [10] H.-X. Han, Solid State Commun. 65 (1988) 921.
- [11] T. Woignier, J. Phalippou and J. Zarzycki, J. Non-Cryst. Solids 63 (1984) 117.
- [12] N. H. Ray, Phys. Chem. Glasses 16 (1975) 75.
- [13] G. Sedmale, J. Vaivads, U. Sedmalis, V.O. Kabanov and O.V. Yanush, J. Non-Cryst. Solids 129 (1991) 284.
- [14] T. Izawa, N. Shibata and A. Takeda, App. Phys. Lett. 31 (1977) 33.

The above results show the potential of the modified oxide sol-gel and sol-precipitation processes for the synthesis of borophosphosilicate glasses and glass-ceramics. Both the processes result in glasses and glass-ceramics with low dielectric constant (3.86-4.36 at 1MHz). In order to lower the dielectric constant further, attempts were made to study the influence of incorporation of nitrogen into the glasses synthesized using above processes. The results of these studies are included in the following section.

(B) Effect of Incorporation of Nitrogen on the Structure and Dielectric Properties of Modified Oxide Sol-Precipitated Borosilicate Glasses and Glass-Ceramics

In this section the modified oxide sol-gel process was extended further towards the synthesis of low dielectric constant borosilicate glasses and glass-ceramics. Correspondingly, an attempt was made to incorporate nitrogen into the glass structure and understand its influence on the structure of the glass, its sinterability and dielectric properties.

### III-1. Experimental Procedures

#### III-1.1. Synthesis of Glasses

Borosilicate glasses were synthesized using the modified oxide sol-gel process described in the earlier section. Accordingly, commercially obtained boron oxide (99.98%, Johnson Matthey) and tetraethylorthosilicate (TEOS; 99.999%, Aldrich) were used as precursors. The alkoxide of boron was generated *in-situ* using ethanol. A typical procedure for synthesis of these glasses consisted of preparation of a clear solution of boron oxide in alcohol to which TEOS was added. The beaker was covered with parafilm, and the contents were stirred for 10 minutes until the boron oxide dissolved in alcohol. TEOS was then added to the beaker containing the solution of boron oxide in alcohol. Boron oxide and TEOS were selected in the stoichiometric ratio of  $B_2O_3 : SiO_2 = 1 : 6$ . The solution was continuously stirred for 15 minutes to obtain a clear sol. Water was then introduced to the resulting solution in two stages. The first stage was accompanied by addition of half of the total water for hydrolysis and stirring the solution for 45 minutes at 65°C. This was necessary to induce formation of borosiloxy chains. The second stage consisted of adding the remaining amount of water with sufficient ammonium hydroxide to induce a precipitation reaction. The solution was centrifuged to collect the precipitate which was then dried at 150°C for 24 hours in air to yield the xerogels. Figure III-1 shows the flow sheet highlighting the procedure that was used to synthesize borosilicate gel powders.

#### III-1.2. Heat-Treatment and Sintering

In order to investigate the effect of heat treatments on the structural and electrical properties of borosilicate glasses, the as-prepared powder was subjected to various heat treatment conditions in different atmospheres, as shown in Table III-1. As indicated in Table III-1, the as-prepared

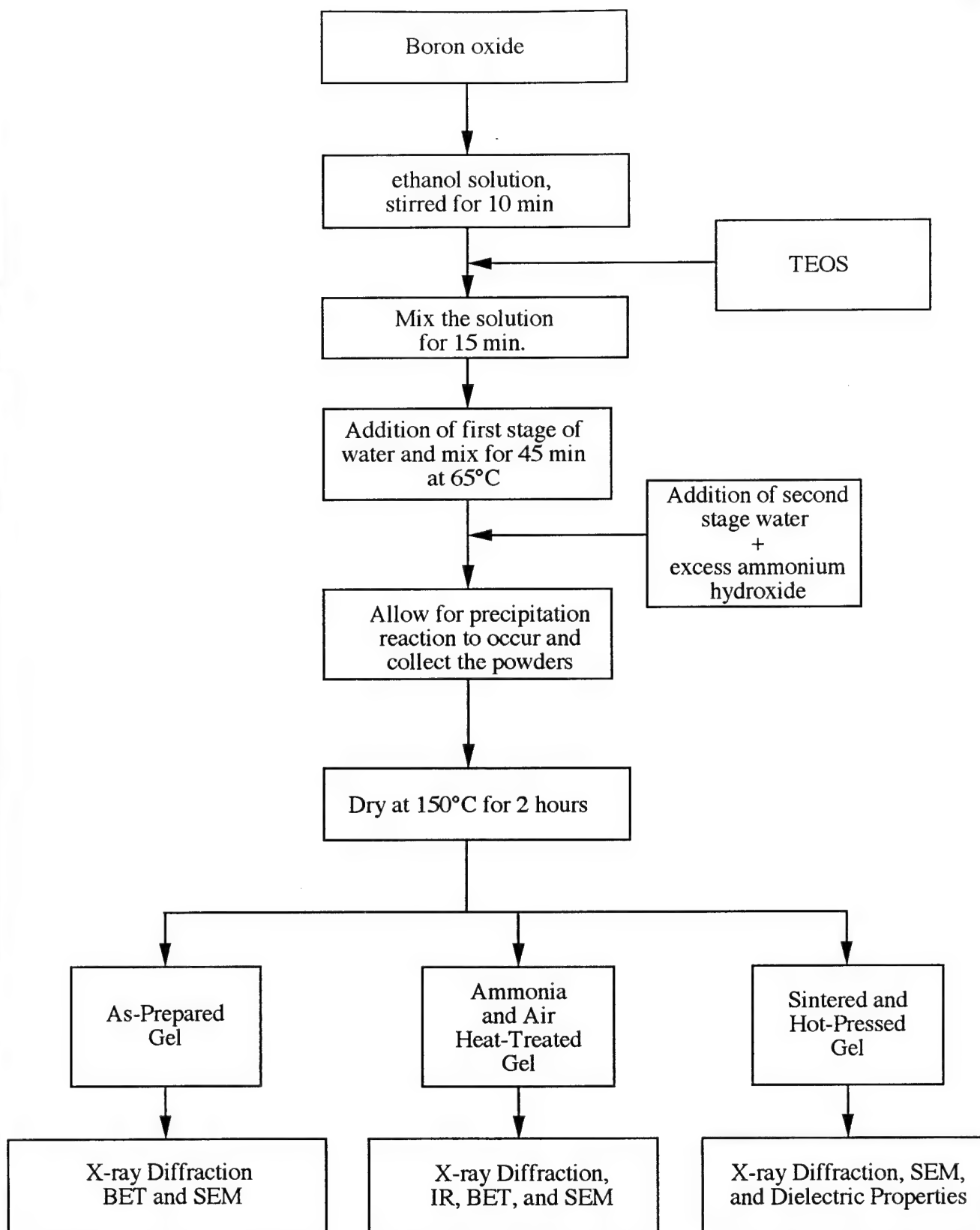


Figure III-1. Flow sheet showing the procedure followed for synthesizing borosilicate gel powders.

Table III-1. Schedule of heat treatments employed for the various gel samples

	Pre-calcination at 800°C (24 hours)	Ammonia treatment temperature (°C) (24 hours)
DAm 800	X	800
DAm 1000	X	1000
Air 800	O	X
AAm 800	O	800
AAm 1000	O	1000

X : not conducted

O : conducted

powders were either directly heat treated in ammonia, referred to as (DAm) in subsequent discussion, or calcined first in air followed by ammonia treatments, referred to as (AAm) hereon. The direct ammonia treatments were conducted both at 800°C and at 1000°C for 24 hours. These samples have been accordingly referred to as DAm 800 and DAm 1000, respectively, in the following sections. In the case of the samples that were calcined in air prior to ammonia treatments, the as-prepared gel powders were placed on a Pt foil and heat treated in air to 800°C for 24 hours. The calcined powders were then subjected to ammonia treatments at 800°C and 1000°C for 24 hours. Samples heat treated at 800°C are referred to as AAm 800, while those heat treated at 1000°C are referred to as AAm 1000 in the subsequent sections. Some of the as-prepared gel powders were only calcined in air at 800°C and were not subjected to any ammonia treatments. This was done mainly to compare the various structural effects due to nitridation. These samples will be referred to as Air 800 in the discussion to follow.

The heat-treated powders were cold-pressed into pellets using a pressure of approximately 10,000 psi ( $\approx 6.9 \times 10^7$  Pa). The cold-pressed pellets corresponding to DAm 800, DAm 1000, AAm 800, and AAm 1000 designations were then sintered in an ultrahigh-purity (UHP) nitrogen atmosphere at 1350°C for 12 and 48 hours, respectively, while the sample designated as Air 800 was sintered in air at 1000°C for 48 hours.

### III-1.3. Materials Characterization

X-ray Diffraction (Rigaku  $\theta/\theta$  Diffractometer) was used to characterize the as-prepared and heat-treated gels to identify the presence of any crystalline phases. A CamScan scanning electron microscope was used for conducting the SEM studies. The SEM analysis was performed on powders and sintered samples to observe the particle size and the sintered microstructure. Specific surface area was also measured using the Brunnauer-Emmett-Teller (BET) technique (Autosorb 1, Quantachrome Instruments). The molecular linkages of the various components in the heat-treated powders were investigated using a Fourier Transform Infrared (FTIR) Spectrometer (Galaxy Series FTIR 5000, ATI Mattson). Infrared spectra in the spectral range of 400 - 4000  $\text{cm}^{-1}$  were collected on the powders using the KBr technique. Dielectric measurements were also conducted on the sintered samples. Samples for dielectric measurements were prepared using the same procedure described in the previous section. Since the sintered samples always contain porosity, the pure dielectric constant of the matrix phase was determined using the logarithmic mixture rule [1].

$$\log \kappa = \sum_i v_i \log \kappa_i = (1 - v_{\text{pore}}) \log \kappa_{\text{glass}}$$

where ' $\kappa$ ' is the measured dielectric constant, ' $v_{\text{pore}}$ ' is the volume fraction of pores in the sintered glass, and ' $\kappa_{\text{glass}}$ ' is the pure dielectric constant of the glass.

The volume fractions of pores in the sintered glasses were very difficult to estimate in the absence of known values of density of these glasses. However, an approximate estimate was made based on the SEM micrographs of the sintered glasses using the linear intercept method. Finally, the powders were also chemically analyzed for H, C, and N content by Galbraith laboratories (Knoxville TN).

### III-2. Results and Discussion

Borosilicate gels were prepared using the modified oxide sol-gel process. The resultant gel powders and heat treated powders were first characterized for structure and morphology. Results of these studies are described and discussed below.

#### III-2.1. Characterization of As-Prepared and Heat-Treated Gel Powders

The color of the as-prepared gel powder was white. After direct ammonia heat treatments, the powders (DAm 800 and DAm 1000) appeared slightly gray in color, indicating the presence of residual carbon, while all gel powders subjected to air heat treatments (Air 800, AAm 800, and AAm 1000) prior to ammonia treatments retained the white color even after completion of the heat treatments. All the heat treated powders were subjected to X-ray diffraction analysis. Figure III-2 shows the X-ray diffraction patterns collected on the as-prepared and heat treated powders. The as-prepared powder (see Figure III-2(a)) shows the typical amorphous nature of the gel powders. This is reflective of the rapid condensation of the partially hydrolyzed alkoxy groups with minimum growth of the condensed oxide units. After heat treatments (see Figs. III-2(b-f)), all heat treated powders still appear amorphous, as exhibited by X-ray diffraction patterns.

The as-prepared and heat treated powders were also observed under the SEM to analyze the particle size and morphology. Figure III-3 shows the micrographs of all the powders. The as-prepared powders (see Figure III-3(a)) consist of agglomerates of very fine particles about 0.5  $\mu\text{m}$  in size. After direct heat treatments in ammonia, both DAm 800 and DAm 1000 (see Figs. III-3(b) and (c)) exhibit almost similar morphology, and particle sizes as the as-prepared gel powders. This suggests that the incorporation of nitrogen during direct ammonia treatments does not seem to result in significant growth of the particles.

After heat treatment in air (see Figure III-3(d) : Air 800), however, the particles have grown in size to about 1-1.5  $\mu\text{m}$ , and partial sintering of the particles seems to have occurred. Ammonia heat treatment of the previously air heat treated powders, namely, AAm 800 and AAm 1000, does not

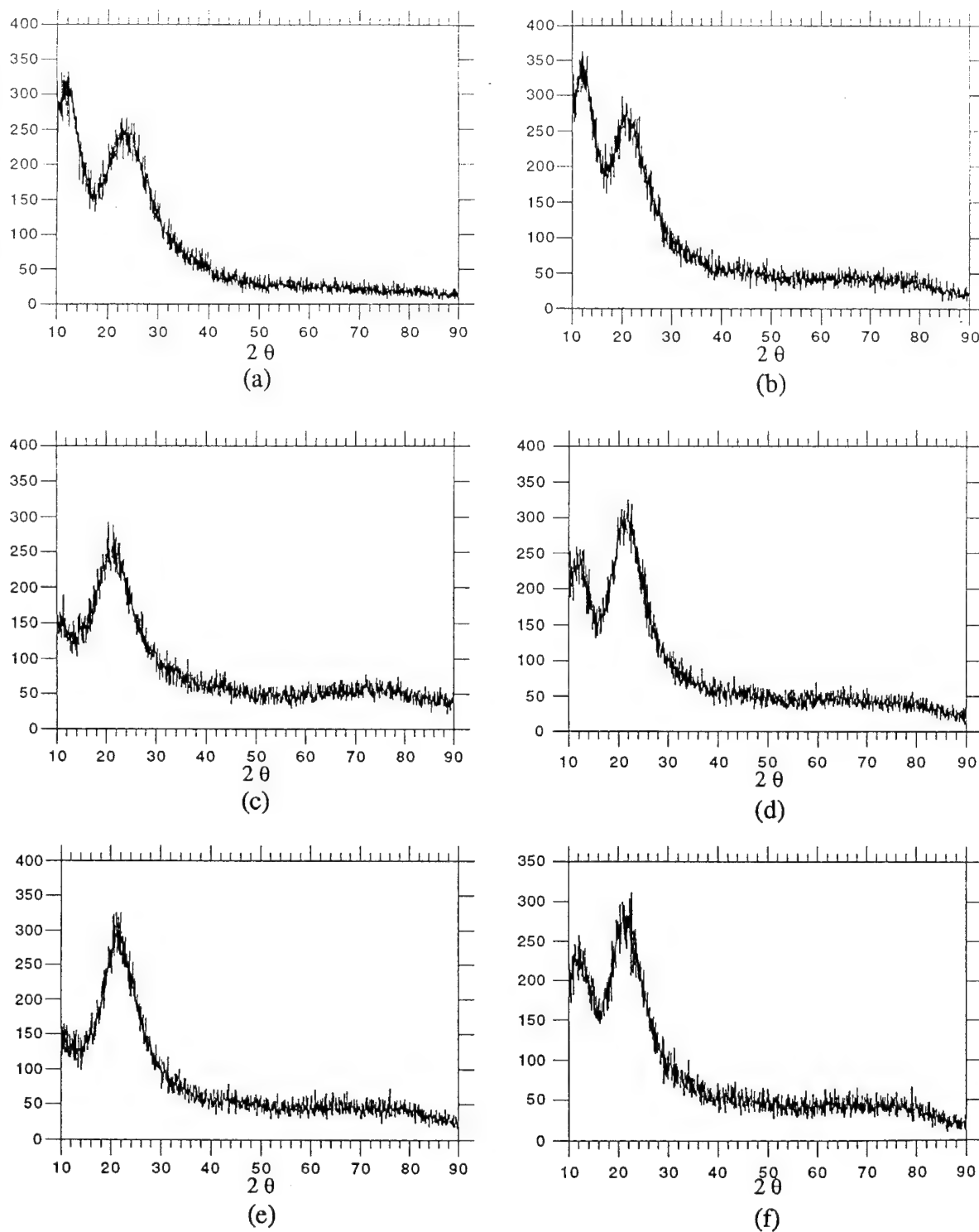


Figure III-2. X-ray diffraction patterns showing the crystalline phase in the as-prepared and heat treated gel powders: (a) as-prepared, (b) DAm 800, (c) DAm 1000, (d) Air 800, (e) AAm 800, and (f) AAm 1000.



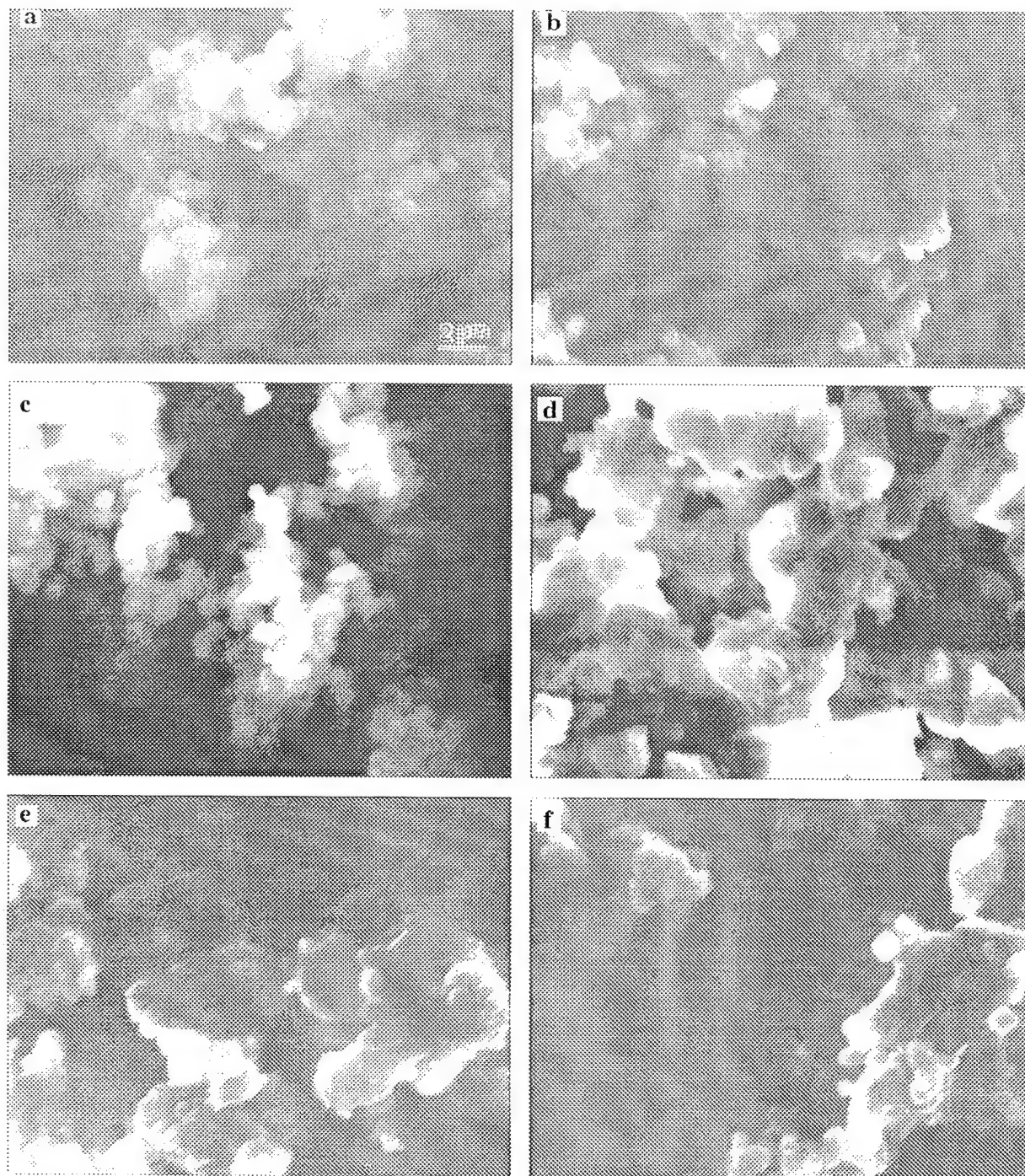


Figure III-3. SEM micrographs showing the morphology of the as-prepared and heat treated gel powders: (a) as-prepared, (b) DAm 800, (c) DAm 1000, (d) Air 800, (e) AAm 800, and (f) AAm 1000. (Note: The micron marker is the same for all the micrographs)

seem to cause any change in the morphology consistent with the earlier observation of gel powders directly treated in ammonia. Figure III-3(e) and (f) show the morphology of the AAm 800 and AAm 1000 gel powders. As can be seen, the powders seem to retain the same morphology and particle sizes of the gel samples Air 800 that were calcined in air. Specific surface area data, which are listed in Table III-2, are also consistent with SEM observation. Samples corresponding to DAm 800 ( $9.3825 \text{ m}^2/\text{g}$ ) and DAm 1000 ( $9.1848 \text{ m}^2/\text{g}$ ) exhibit specific surface areas similar to those of the as-prepared gel powders ( $9.8374 \text{ m}^2/\text{g}$ ). On the other hand, the calcined sample, Air 800, shows a much lower specific surface area ( $2.3517 \text{ m}^2/\text{g}$ ) than DAm 800, DAm 1000, and the as-prepared gel powders. Similarly, ammonia treatments of the calcined gel powders do not result in significant change in specific surface area (refer to specific surface area data for AAm 800 ( $2.1689 \text{ m}^2/\text{g}$ ) and AAm 1000 ( $2.1149 \text{ m}^2/\text{g}$ )). Thus, it can be seen that, in both cases, incorporation of nitrogen during heat treatment in ammonia does not seem to cause any change in the original particle size and morphology.

It is possible that oxygen→nitrogen exchange reaction occurs with nitrogen entering the oxide particles during ammonia heat treatment, forming the corresponding nitrides. This exchange reaction results in considerable shrinkage without causing any change in the morphology, while the low diffusivity of nitrogen at temperatures of  $800^\circ\text{C}$  and  $1000^\circ\text{C}$  results in practically no growth. Also, nitrogen being a smaller atom than oxygen, leads to the formation of a glass with a possible higher molar density. In order to investigate the nature of the incorporated nitrogen, FTIR was used to study the molecular structure of the gel powders.

### III-2.2. Structure of Heat Treated Glasses Using Infrared Spectroscopy

The IR spectra collected on Air 800 and AAm 800 samples, and the subtracted difference between these two spectra, are presented in Figure III-4. The boron-oxygen (B-O) stretching vibration ( $1405 \text{ cm}^{-1}$ ), silicon-oxygen (Si-O) stretching mode ( $1088 \text{ cm}^{-1}$ ), borosiloxo (B-O-Si) linkages ( $930$  and  $670 \text{ cm}^{-1}$ ), oxygen-silicon-oxygen (O-Si-O) bending ( $798 \text{ cm}^{-1}$ ), and silicon-oxygen-silicon (Si-O-Si) bending ( $466 \text{ cm}^{-1}$ ) modes are observed in the IR spectrum of the Air 800 powder [2-5]. The subtraction scale factor used in Figure III-4 was optimally chosen to almost cancel the Si-O stretching band, because it is known that the intensity of Si-O stretching band is much less sensitive to the local changes in the environment of the glass matrix such as those caused by the incorporation of nitrogen. The vibrational modes corresponding to other molecular linkages are more sensitive to these changes, mainly due to the big difference in the force constants [6]. The IR spectrum collected on AAm 800 and the corresponding differential spectra with Air 800

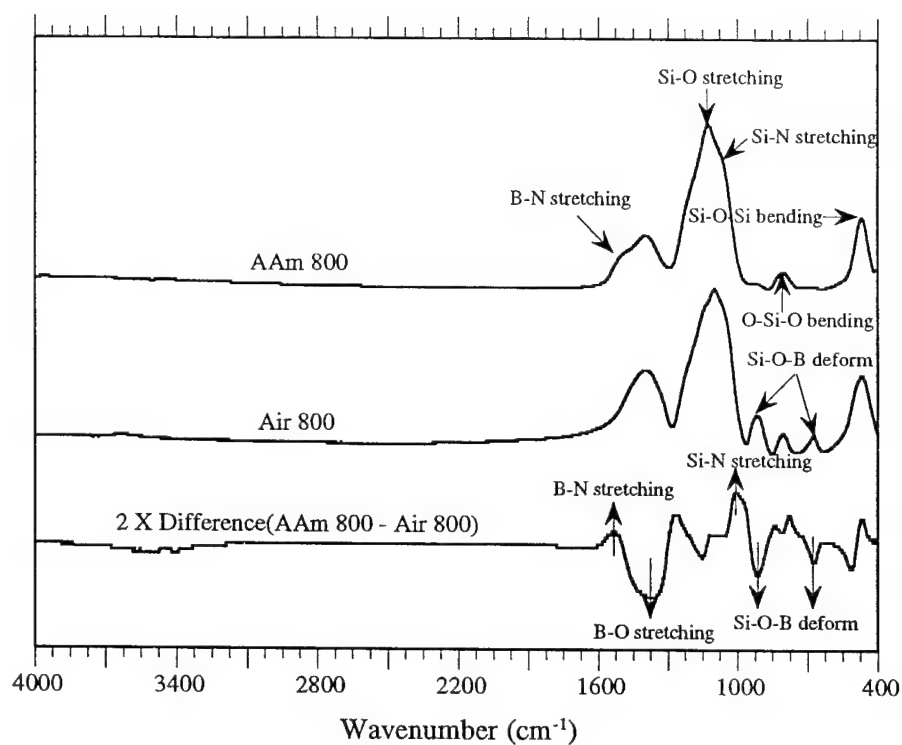


Figure III-4. Infrared absorption spectra collected on AAm 800, Air 800, and the difference between these two spectra (Scale of difference spectrum has been expanded by a factor 2). Please refer to the text for the assignment of the various molecular linkages.

reveal several different features. One of the most noticeable features is the appearance of boron-nitrogen (B-N) stretching band ( $1510\text{ cm}^{-1}$ ) and silicon-nitrogen (Si-N) stretching band ( $970\text{ cm}^{-1}$ ), which appear as shoulders because of the overlap with the strong Si-O stretching and B-O stretching bands [2, 3, 5]. Another important feature is the decrease in the intensity of the B-O stretching and the B-O-Si stretching modes. These features clearly imply that, during heat treatment in ammonia, the existing bridging oxygen bonds are broken, resulting in the replacement of oxygen with nitrogen, leading to the formation of new corresponding nitrogen linkages.

The increase in the intensities of O-Si-O and Si-O-Si bending modes and the broadening of the Si-O stretching vibration are strange occurrences seen in the IR spectra collected on the ammonia heat treated powders. It was reported by Brinker and Haaland [3] that the broadening of the Si-O stretching vibration may be due to a greater disorder or bond strain caused by the introduction of nitrogen into the network during ammonia heat treatment. Incorporation of nitrogen results in breakage of the Si-O-Si linkage wherein oxygen is replaced by the lighter element nitrogen. In fact, this should cause for a reduction in the intensity of the Si-O-Si and O-Si-O bending modes. However, it has been reported that bending modes of O-Si-O and Si-O-Si are dependent on bond angle distortion [3]. It is also known that the interactional force constants of the O-Si-O and Si-O-Si bending vibrations are 14 and 100 times smaller than the radial Si-O stretching force constant. Thus, these modes are more sensitive to changes in the local environment of the glass matrix than the stretching vibrational modes. Moreover, the stretching mode of Si-O was used as the scale factor and all the peaks were subtracted following normalization of the Si-O stretching frequency. The difference spectrum, therefore, demonstrates this greater sensitivity of the bending vibrations to local perturbations. The broadening of the Si-O stretching vibration could also be a reflection of the formation of Si-N linkages, which is seen on the low energy side of the Si-O stretching vibration.

Figure III-5 shows the IR spectra collected on AAm 800, DAm 800 powder samples, and the difference between these two spectra. In the case of DAm 800, an increase in intensities of B-N stretching and Si-N stretching bands and a slight decrease in the intensity of B-O stretching modes can be observed. It therefore implies that more nitrogen was introduced into DAm 800 gel samples during direct ammonia treatments than in the samples that were subjected to identical ammonia treatments after the initial air treatments (AAm 800). An explanation for this could be provided based on the gel morphology and gel structure. It should be noted that the DAm 800 powders were obtained after heat treating the as-prepared gels in ammonia at  $800^{\circ}\text{C}$ . On the other hand, the AAm 800 samples were generated by heat treating the gel powders in ammonia after initial calcination in air. The initial calcination treatment obviously results in particle growth and also partial sintering

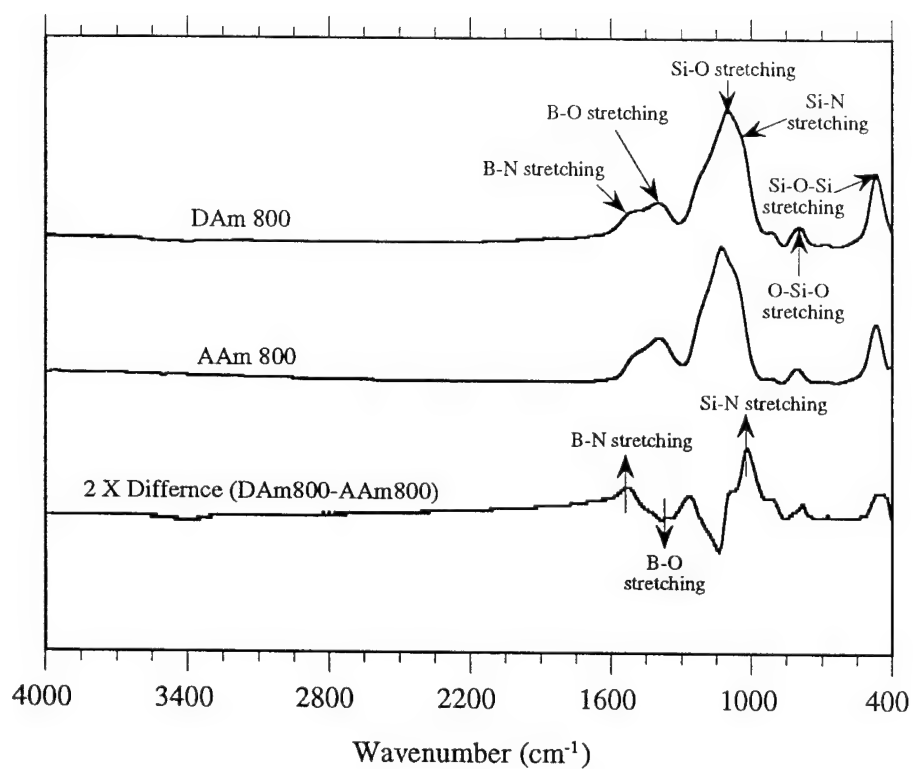


Figure III-5. Infrared absorption spectra collected on DAM 800, AAm 800, and the difference between these two spectra (Scale of difference spectrum has been expanded by a factor 2). Please refer to the text for the assignment of the various molecular linkages.

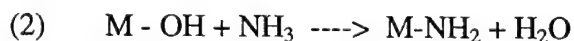
(see Figure III-3(d)). Consequently, there is a large reduction in specific surface area (refer to Table III-2). However, the DAm 800 samples were generated by heat treatment of the as-prepared gels, which have a larger specific surface area than the calcined gel powders. Thus, the DAm 800 powder is composed of more active surfaces and can be expected to contain more nitrogen, as indicated by the IR results in comparison to the AAm 800 sample following identical ammonia treatments.

Another explanation for this observation is the mechanism of incorporation of nitrogen itself. There are several mechanisms for incorporation of nitrogen that have been reported in the literature [7, 8]. In the case of systems containing strong Lewis acids such as boron and aluminum, the mechanism of incorporation of nitrogen is known to comprise chemical adsorption of ammonia to the Lewis acid metal sites at elevated temperatures as shown below [7]:

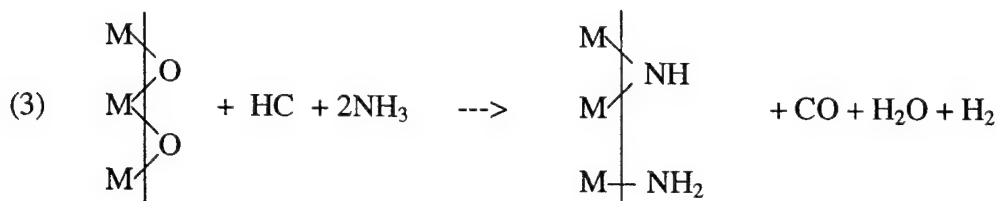


where 'M' is the metal .

In the case of silicon, nitridation may occur predominantly by attack of the silanol groups at the surface, which can be represented as [8]:



However, in the case of gels containing residual carbon resulting from unhydrolyzed alkoxy groups, ammonia helps to remove carbon via a reaction which can be represented generally as [7]:



This mechanism would be mainly responsible for breaking the oxygen linkages, thereby reducing the network. It is reported that this reaction is especially favored at high temperatures where ammonia is likely to be dissociated, creating a very reducing atmosphere. This reducing

Table III-2. Comparison of the specific surface area of the as-prepared and heat-treated gel powders

Sample	Specific surface area ( $\text{m}^2/\text{g}$ )
As-prepared	9.8374
DAm 800	9.3825
DAm 1000	9.1848
Air 800	2.3517
AAm 800	2.1689
AAm 1000	2.1149

environment is especially favorable for breaking the M-O-M linkages. Therefore, in the case of DAm 800 sample, since the as-prepared gel powders contain residual carbon before heat treatment, it is possible that all these mechanisms are prevalent. On the other hand AAm 800 powders contain very much less amount of residual carbon because of the prior calcination treatment in air. Hence, it is possible that only mechanism (1) and (2) are instrumental for incorporation of nitrogen into these powders. In summary, the reactive nature of the as-prepared gel and the presence of residual carbon could be both responsible for incorporation of larger amounts of nitrogen into DAm 800 powders and the consequent more intense B-N and Si-N vibrations seen in the IR spectra.

The IR spectra collected on AAm 800 and AAm 1000 samples, and the corresponding difference between these two spectra, are presented in Figure III-6. This Figure clearly shows the effect of heat treatment temperature on the incorporation of nitrogen. In the case of AAm 1000, significant increase in intensities of the B-N stretching and Si-N stretching bands is observed with corresponding decrease in the B-O stretching frequencies. Such behavior at high temperatures can easily be expected. At high temperature of 1000°C, ammonia can be expected to dissociate more easily, providing for easy cleavage of the M-O-M bonds, and consequently replacing the oxygen with nitrogen. Thus, more nitrogen can be expected to be introduced into the glasses at higher temperatures.

The nitrided gel samples were then sintered at different temperatures to observe the effect of nitrogen on densification. The resultant microstructure was also examined to analyze the effects of nitrogen on the sintering behavior. The results of these studies are discussed below.

### III-2.3. Sintering Behavior

The sintered samples were subjected to X-ray diffraction analyses, and the resultant X-ray diffraction patterns are shown in Figure III-7. As can be seen, all the nitrided gel powders sintered at 1350°C for 48 hours, except the DAm 1000 powders show the presence of cristoballite as the crystalline phase. The gel powders that were directly heat-treated in ammonia at 1000°C (DAm 1000) remain amorphous even after sintering at 1350°C for 48 hours (see Figure III-7(b)). An interesting observation is that the AAm 800 sample remains amorphous after sintering at 1200°C for 48 hours, even though cristoballite is the crystalline phase seen at 1350°C (see Figs. III-7(c) and (d)). At the same time, the XRD pattern corresponding to the same gel powders that were calcined in air at 800°C, designated as Air 800, on sintering at 1000°C for 48 hours, also shows cristoballite to be the crystalline phase (see Fig. III-7(f)). These results, therefore, show that incorporation of nitrogen tends to delay the crystallization and shifts the onset of crystallization to higher temperatures (compare XRD patterns of AAm 800 at 1200°C, 1350°C, and Air 800 at 1000°C). Similar observations can also be seen on the gel samples designated DAm 800 and DAm



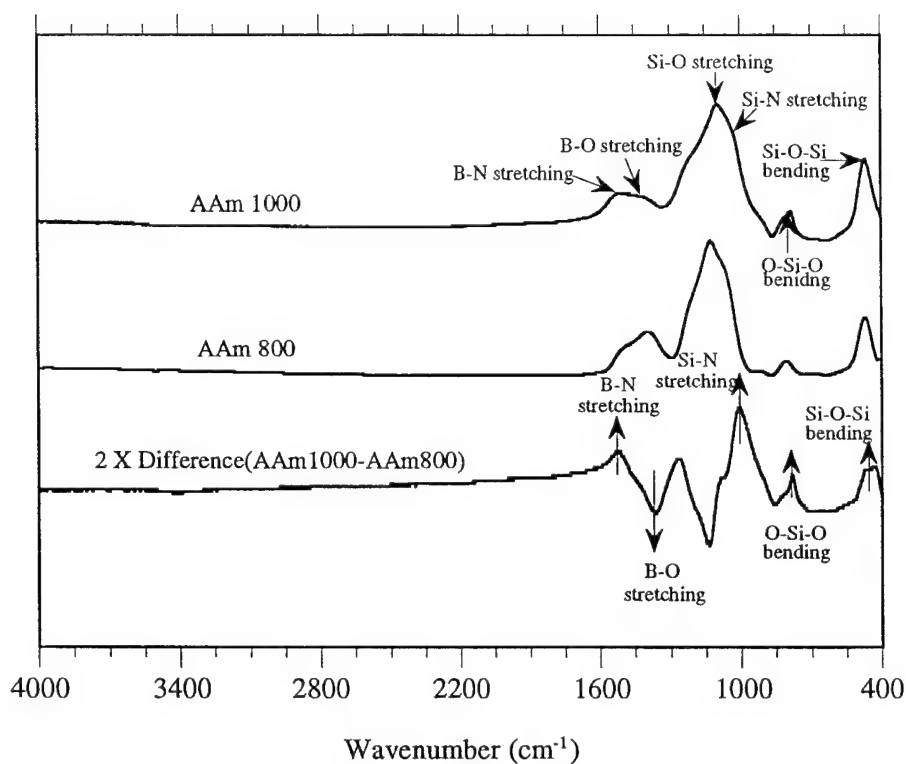


Figure III-6. Infrared absorption spectra collected on AAm 1000, AAm 800, and the difference between these two spectra (Scale of difference spectrum has been expanded by a factor 2). The assignment of the different molecular linkages can be found in the text.

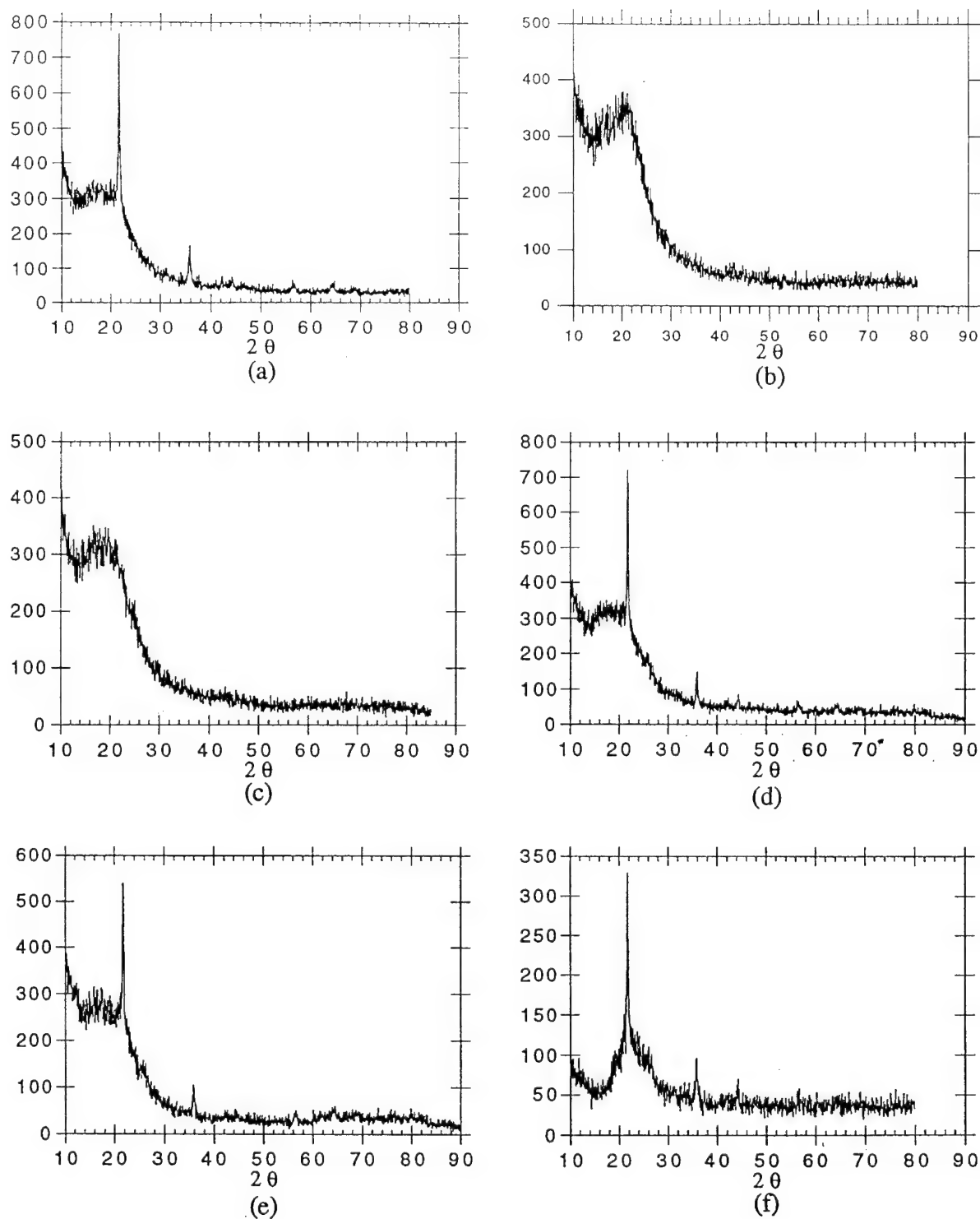
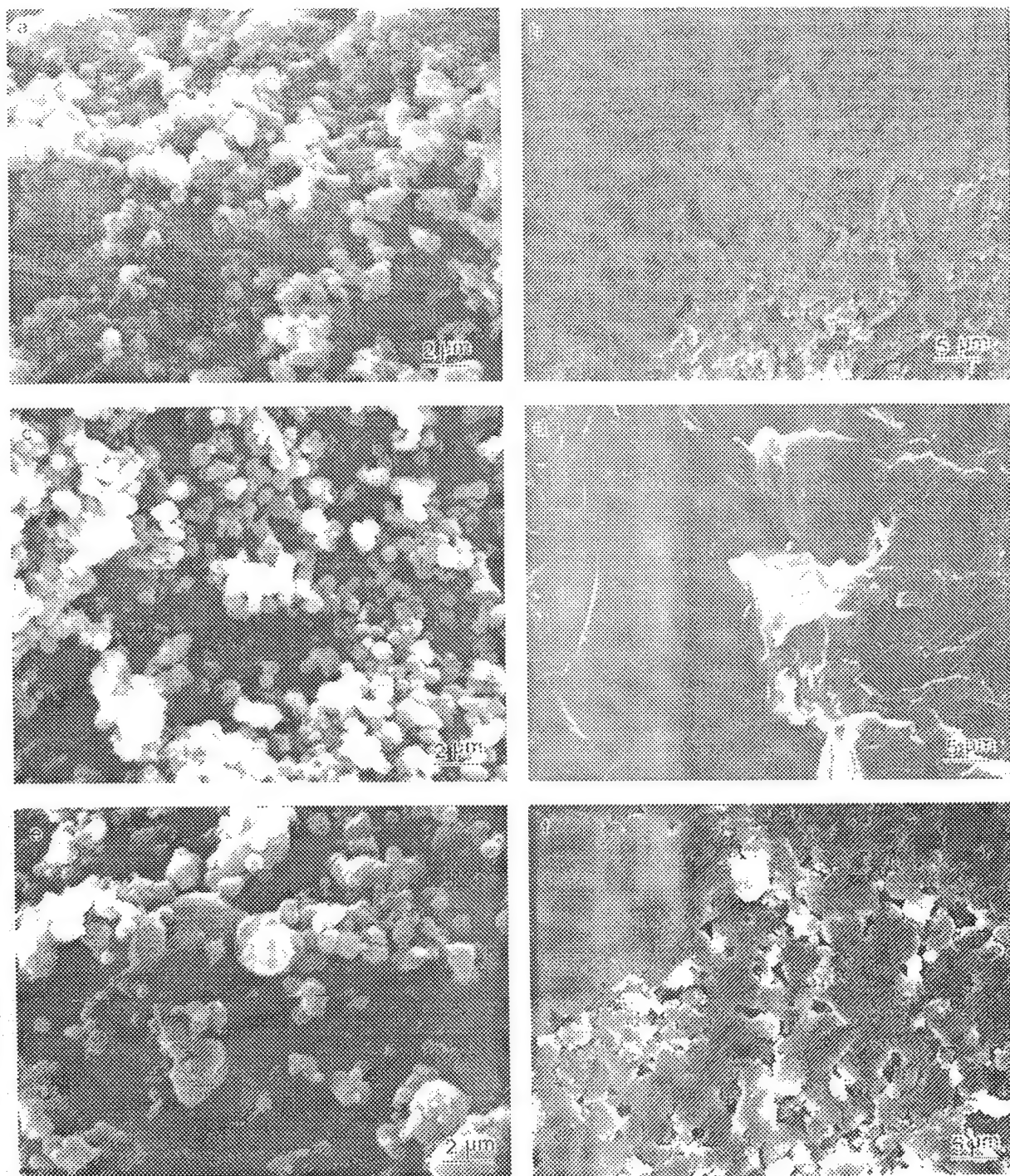


Figure III-7. X-ray diffraction traces showing the crystalline phase in the sintered samples : (a) DAM 800 sintered at 1350°C for 48 hours, (b) DAM 1000 sintered at 1350°C for 48 hours, (c) AAm 800 sintered at 1200°C for 48 hours, (d) AAm 800 sintered at 1350°C for 48 hours, (e) AAm 1000 sintered at 1350°C for 48 hours, and (f) Air 800 sintered at 1000°C for 48 hours.

1000 which have been directly heat treated in ammonia (see Figs. III-7(a) and (b)). The DAm 1000 powders remain amorphous even after sintering at 1350°C for 48 hours. Thus, the higher nitridation temperature leads to incorporation of more nitrogen into the gel, prolonging the crystallization of cristoballite.

The exact reason for the crystallization of cristoballite is still not clear and will involve detailed structural analysis to be conducted on the gels and the nitrided powders. However, based on the IR and XRD data, it can be speculated that the synthesized borosilicate gel structure consists of a random arrangement of silicon-oxygen tetrahedra. On heat treatment, there is rearrangement of the silicon-oxygen environment, which results in freezing the metastable, higher energy, and high temperature phase of crystalline silicate, which is cristoballite. Incorporation of nitrogen breaks the silicon-oxygen environment, resulting in exchange of oxygen. As a result, it could be possible that much higher temperatures are required to rearrange the silicon around the remaining oxygen in the presence of the less mobile nitrogen, to form the desired cristoballite phase.

Figs. III-8 and III-9 show the fracture surfaces of DAm 800, DAm 1000, AAm 800, and AAm 1000 samples after sintering at 1350°C for 12 hours and 48 hours, respectively. The SEM micrographs shown in Figs. III-8(d) and III-9(c) indicate viscous sintering to be the mechanism responsible for densification of AAm 800 sample. The fracture surfaces corresponding to DAm 800 (Figs. III-8(a) and (b)) and AAm 1000 (Figs. III-8(e) and (f)) sintered for 12 hours at 1350°C, however, show only partial sintering to have occurred near the surface of the bulk sample (see Figs. III-8(b) and (f)). Complete densification seems to occur when the samples are sintered at 1350°C for 48 hours (see Figs. III-9(a) and (d)). The fracture surfaces of these samples, shown in Figs. III-8(b), 8(f), 9(a), and 9(d), once again indicate viscous sintering to be the mechanism responsible for densification. The gel powders directly treated in ammonia at 1000°C, DAm 1000, did not show any indication of densification even after soaking the compacts at 1350°C for 48 hours (see Figs. III-8(c) and III-9(b), which represent images taken at both the surface and the center region of the fracture surface). This sintering behavior is clearly an indication of the effect of incorporation of nitrogen. As can be seen from the XRD data shown in Figs. III-7(c) and (d), nitridation tends to prolong the crystallization of cristoballite from the oxynitride glass matrix. There also appears to be an optimum nitrogen content that prevents the crystallization of cristoballite and the contribution to slow diffusion rates, limiting the densification. However, all the nitrided samples contain significant amounts of oxygen to provide adequate diffusion and thereby lead to viscous sintering. On the other hand, the directly nitrided gel powder at 1000°C, DAm 1000, contains significant amounts of nitrogen to introduce substantial covalent character, limiting its diffusion. As a result, these powders do not show any signs of densification even after



**Figure III-8.** SEM micrographs showing the morphology of the fracture surfaces of the samples sintered at 1350°C for 12 hours: (a) the middle region of DAM 800 bulk sample, (b) near the surface of DAM 800 bulk sample, (c) DAM 1000 (see text for details), (d) AAm 800 (refer to text for details), (e) the middle region of AAm 1000 bulk sample, and (f) near the surface of AAm 1000 bulk sample.

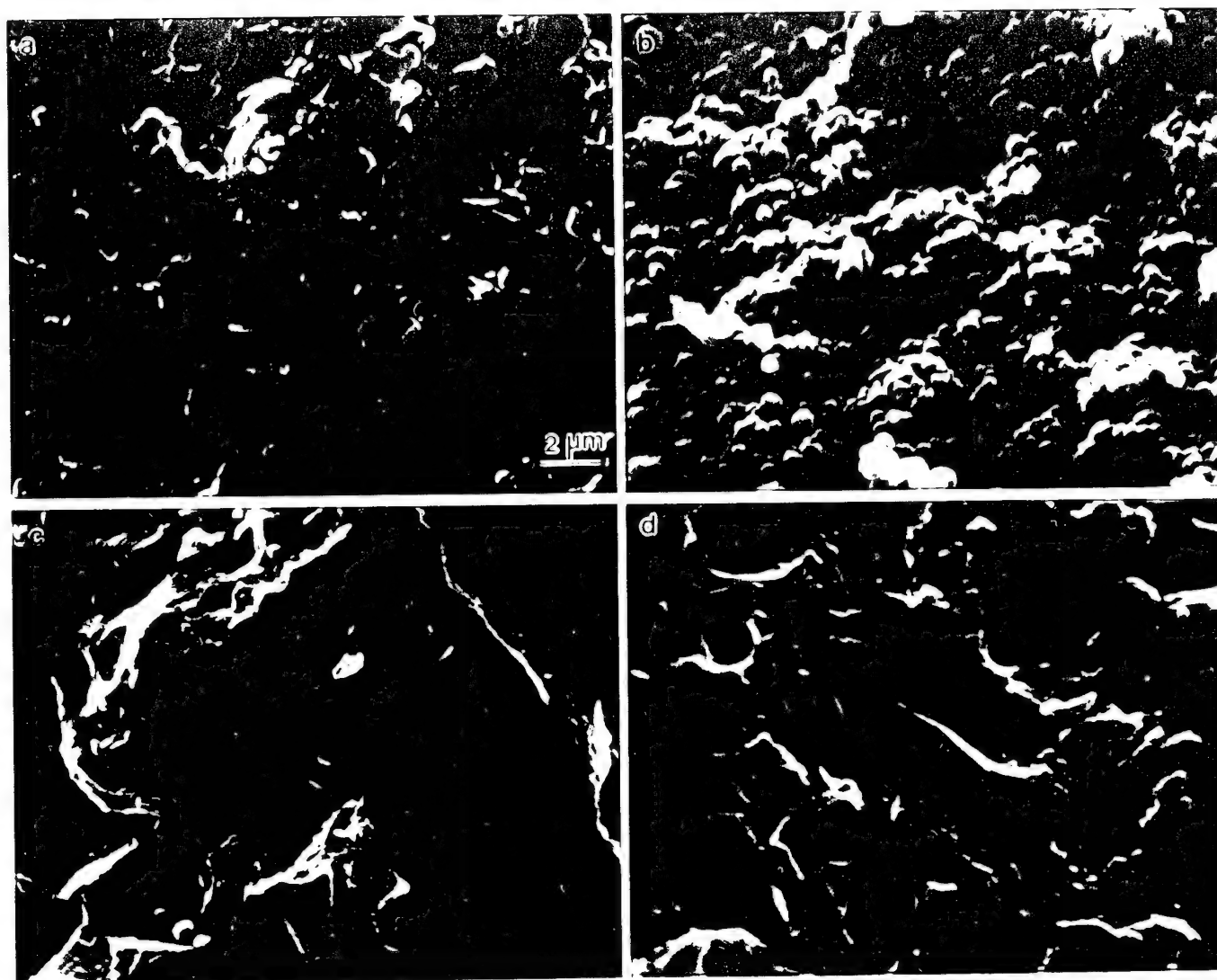


Figure III-9. SEM micrographs showing the morphology of the fracture surfaces of the samples sintered at 1350°C for 48 hours : (a) DAm 800, (b) DAm 1000, (c) AAm 800, and (d) AAm 1000.

prolonged heat treatments at 1350°C for 48 hours. Hot-pressing would therefore be needed to initiate sintering of these nitrided gel powders. In order to correlate the IR results and the above sintering behavior, chemical analysis was therefore conducted on the gel powders to estimate the nitrogen contents.

Results of chemical analyses of the samples are presented in Table III-3. All the heat-treated samples show significantly reduced amounts of carbon and hydrogen ( $< 0.5$  wt%). The nitrogen content, as expected, is the highest in the high-temperature directly nitrided sample, DAm 1000 (6.63 wt%), and the lowest in AAm 800 sample (2.04 wt%). The nitrogen contents are similar for the directly nitrided DAm 800 (3.57 wt%) and for samples calcined in air prior to nitridation, AAm 1000 (3.67 wt%). The high nitrogen content in the DAm 1000 sample provides significant covalent character to the glass, thereby rendering the powders unsinterable at 1350°C even after soaking the powder compacts at 1350°C for 48 hours. The replacement of oxygen with nitrogen also makes crystallization extremely difficult in this case. Similarly, AAm 800 powders were most easily sintered. On the other hand, DAm 800 and AAm 1000 samples have intermediate nitrogen content, and hence they revealed only partial sintering at 1350°C when held for an insufficient period of 12 hours. At the same time, the AAm 800 sample was completely sintered when kept at 1350°C for 12 hours, and revealed signs of classical viscous sintering at 1350°C when heated for a sufficient period of 48 hours. The chemical analysis results are also consistent with the IR data in which DAm 800 and AAm 1000 samples showed significant increase in intensities of B-N stretching and Si-N stretching bands and a corresponding decrease in B-O stretching band.

Thus, nitridation seems to alter the structure of the gels and also affects the sintering behavior. In order to investigate the effect of nitridation on the electrical properties, the sintered samples were evaluated for their dielectric behavior at 1 MHz. These results are discussed below.

#### III-2.4. Dielectric Properties

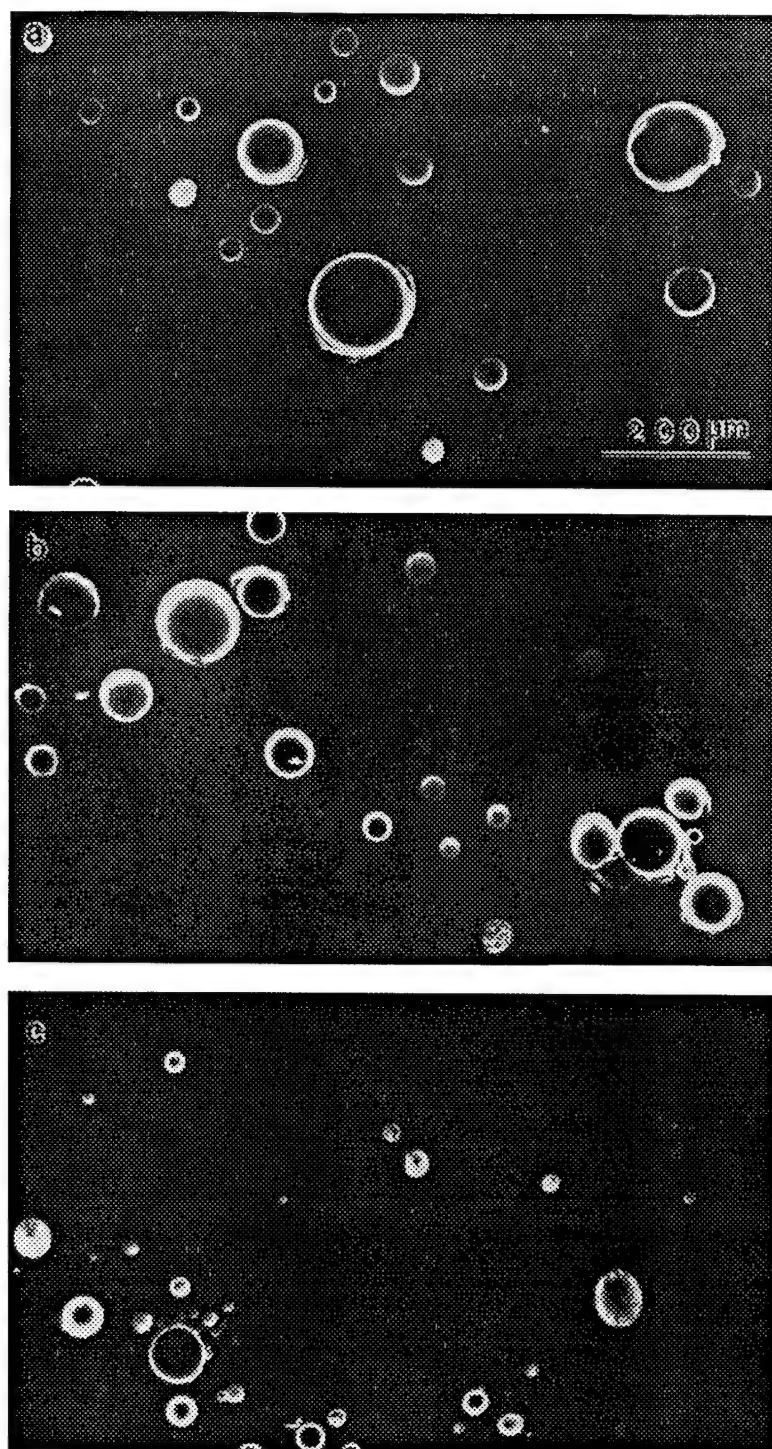
Figure III-10 shows SEM micrographs of the polished surface of sintered Air 800, AAm 800, and AAm 1000 samples. As can be seen, all the samples seem to contain varying amounts of porosity. However, the polished surface of the sintered DAm 800 sample did not seem to reveal any visible pores when observed under the SEM. This could be possible since calcination of the gels in air leads to softening of the glass. Removal of carbon tends to occur under these conditions, leading to porosity. However, the direct nitridation treatment, such as in the DAm 800 samples, results in incorporation of nitrogen while shifting the softening point to higher temperatures. It is therefore possible that these samples contain no obvious macropores, but the presence of micropores can never be discounted. Hence, it was assumed that this sample is relatively dense with almost no porosity. Since the sintered samples contain varying amounts of porosity, the

Table III-3. Chemical analyses of the as-prepared and heat-treated gel powders

Sample	Carbon*	Hydrogen*	Nitrogen*	Boron*	Silicon*
As-prepared	0.62	1.40	<0.5	4.28	26.26
DAm 800	<0.5	<0.5	3.57		
DAm 1000	<0.5	<0.5	6.63		
AAm 800	<0.5	<0.5	2.04		
AAm 1000	<0.5	<0.5	3.67		

\* All the analyses are in wt%





**Figure III-10. SEM micrographs showing the polished surfaces of the samples : (a) AAm 800 sintered at 1350°C for 48 hours, (b) AAm 1000 sintered at 1350°C for 48 hours, (c) Air 800 sintered at 1000°C for 48 hours. (Note: All the micrographs are obtained from the middle region of the bulk samples)**



measured dielectric values would be representative of the matrix phase and the included porosity. In order to estimate the intrinsic dielectric constant of the oxynitride phase, it is necessary to know the volume fraction of porosity in the sintered samples. With no knowledge of the true density of the oxynitride phase and its exact structure, it was decided to use the linear intercept method to estimate the percentage of porosity from the SEM micrographs of the sintered samples. An estimation of volume fraction of pores using the above approach, however, is a realistic approximation. This is so since we assume the oxynitride phase to be homogeneous as suggested by the IR and XRD results, and it is possible that the porosity is also uniformly dispersed in the matrix. It is therefore fair to assume that the present approximation will not be far from depicting a realistic condition and, in fact, represents a more conservative situation as opposed to the case of having pockets of open porosity concentrated at certain regions.

Table III-4 shows the volume fractions estimated from the SEM micrographs shown in Fig. III-10, using the linear intercept method. These values, combined with the measured and calculated dielectric constants using the logarithmic mixture rule, are also shown in Table III-4. From Table III-4, the effect of nitrogen on the dielectric constant can be easily seen by comparing the values for the nitrified samples after calcination (AAm 800 and AAm 1000) with the unnitrified Air 800 sample. As can be seen, with increasing nitrogen content there is a slight decrease in the dielectric constant, as expected. This is mainly because replacement of oxygen with the lighter element, nitrogen, reduces the total number of electrons per unit volume, thereby decreasing the electronic polarization, which is important for the dielectric constant at high frequency of 1 MHz. It is interesting to note, however, that despite the nitrogen content of DAm 800 being similar to that of AAm 1000, the DAm 800 sample exhibits a lower dielectric constant. This is probably because of the assumption that this sample is devoid of any pores, since none were visible under the SEM. Nevertheless, all the samples exhibit dielectric constants less than 5, which is lower than most of the oxide based counterparts. Thus, it can be seen that nitridation of sol-precipitated glasses at moderate temperatures leads to oxynitride glasses with lower dielectric constant ( $< 5$ ). Moreover, it is also known that the oxynitride glasses and glass-ceramics are stronger than the corresponding oxides. Therefore, incorporation of moderate amount of nitrogen can be used to obtain high strength glasses with lower dielectric constants.

### III-3. Conclusions

An economical modified oxide sol-precipitation process has been used to synthesize borosilicate glasses that have been subjected to direct nitridation and nitridation after an initial calcination treatment. Ammonia heat treatments of initially calcined samples show an increase in B-N and Si-N bonds, with a corresponding decrease in B-O-Si bonds. Despite identical ammonia

Table III-4. Estimated volume fraction and measured dielectric constant of sintered samples

	Measured dielectric constant ( $\kappa_m$ )	Volume fraction (%)	Dielectric constant ( $\kappa'$ )	Loss tangent
DAm 800	3.872	100.0	3.872	0.00415
AAm 800	3.677	92.9	4.062	0.00400
AAm 1000	3.686	94.0	4.006	0.00395
Air 800	3.694	92.7	4.094	0.00360

heat treatment condition, there was a significant difference in the structure as revealed by the IR analyses. Direct-ammonia-treated samples showed an increase in B-N and Si-N linkages with a slight decrease in the B-O bond compared to samples treated in ammonia after the initial air heat treatment. This suggests that more nitrogen is incorporated during direct ammonia treatments due to the finer particle size and the operating nitridation mechanisms. Crystallization and sintering behavior was also significantly affected by introduction of nitrogen. Incorporation of nitrogen increases the glass transition temperature while correspondingly increasing the crystallization temperature. At the same time, with increasing nitrogen contents there is more covalent character introduced, which makes sintering extremely difficult. Similarly, incorporation of nitrogen lowered the dielectric constants, although by moderate amounts. Nevertheless, all the samples showed values much less than 5, suggesting the potential of these glasses for application in microelectronic packaging and as dielectric materials in VLSI circuit technology.

### III-4. References

- [1] W.D. Kingery, H.K. Bowen, and D.R. Uhlmann, Introduction to Ceramics, 2nd ed., Chap.18. John Wiley & Sons, New York, 1976
- [2] P.N. Kumta and M.A. Sriram, J. Mater. Sci. A, 28 (1993) 1097.
- [3] C. J. Brinker and D. M. Haaland, J. Am. Ceram. Soc., 66 (1983) 758.
- [4] J. Wong and C.A. Angell, Glass Structure by Spectroscopy, Chap. 7, Marcel Dekker, New York, 1976.
- [5] P.S. Peercy, H.J. Stein, B.L. Doyle, and V.A. Wells, in Proc. 7th Intl. Conf. on Chemical Vapor Deposition, Vol. 79-3., T.O. Sedgewick and Hans Lydtin Eds., The Electrochemical Society, Princeton, NJ, pp. 199-208 (1979).
- [6] J. Bock and G-J Su, J. Am. Ceram. Soc., 53 (1970) 69.
- [7] B.A. Morrow and I.A. Cody, J. Phys. Chem., 80 (1976) 1996.
- [8] H.O. Mulfinger, J. Am. Ceram. Soc., 49 (1966) 462.